Review

Spin structure of the nucleon—status and recent results

S.E. Kuhn [a,*], J.-P. Chen [b], E. Leader [c]

[a] *Department of Physics, Old Dominion University, Norfolk, VA 23529, USA*
[b] *Thomas Jefferson National Accelerator Facility, Newport News, VA 23606, USA*
[c] *Department of Physics, Imperial College, London SW7 2AZ, UK*

A B S T R A C T

After the initial discovery of the so-called "spin crisis in the parton model" in the 1980s, a large set of polarization data in deep inelastic lepton–nucleon scattering was collected at labs like SLAC, DESY and CERN. More recently, new high precision data at large x and in the resonance region have come from experiments at Jefferson Lab. These data, in combination with the earlier ones, allow us to study in detail the polarized parton densities, the Q^2 dependence of various moments of spin structure functions, the duality between deep inelastic and resonance data, and the nucleon structure in the valence quark region. Together with complementary data from HERMES, RHIC and COMPASS, we can put new limits on the flavor decomposition and the gluon contribution to the nucleon spin. In this report, we provide an overview of our present knowledge of the nucleon spin structure and give an outlook on future experiments. We focus in particular on the spin structure functions g_1 and g_2 of the nucleon and their moments.

© 2009 Elsevier B.V. All rights reserved.

Contents

* Corresponding author.
  E-mail address: Kuhn@jlab.org (S.E. Kuhn).

1. Introduction

The measurement of a spin dependent observable is generally a daunting task, but with rich rewards, because spin seems to have a scalpel-like ability to expose weaknesses and failures of theories. Witness the switch from S, T to $V - A$, which led to the Weinberg–Salam electroweak theory, or the demise of Regge poles, which had successfully described hadronic cross-sections and shrinking diffraction peaks, or the spin crisis in the parton model of deep inelastic scattering, supposedly resolved by an anomalous gluon effect, now shown to be untenable, and, most recently, the realization that some of the information, gathered for 40 years on the fundamental electromagnetic form factors of the nucleon, is unreliable.

In this review we attempt to survey the tremendous experimental and theoretical effort, mainly involving studies of polarized lepton–hadron scattering and polarized proton–proton reactions, that has led to our present knowledge of the internal spin structure of the nucleon,

Deep inelastic lepton–hadron scattering (DIS) has played a seminal role in the development of our present understanding of the sub-structure of elementary particles. The discovery of Bjorken scaling in the late 1960s [1] provided the critical impetus for the idea that elementary particles contain point-like constituents and for the subsequent invention of the Parton Model. DIS continued to play an essential role in the long period of consolidation that followed, in the gradual linking of partons and quarks, in the discovery of the existence of missing constituents, later identified as gluons, and in the wonderful confluence of all the different parts of the picture into a coherent dynamical theory of quarks and gluons— Quantum Chromodynamics (QCD). Polarized DIS, involving the collision of a longitudinally polarized lepton beam with a longitudinally or transversely polarized target, provides a complementary and equally important insight into the structure of the nucleon.

At first sight the theoretical treatment of the polarized case seems to mimic the unpolarized case, with the structure functions $F_{1,2}(x)$ replaced by the polarized structure functions $g_{1,2}(x)$, and with parton densities $q(x)$ replaced by polarized densities $\Delta q(x)$. But it turns out that the polarized case is much more subtle: there is an anomalous gluon contribution to $g_1(x)$, and $g_2(x)$ has no interpretation at all in purely partonic language.

The latter insights were mainly inspired by the unexpected results of the European Muon Collaboration (EMC) measurement of $g_1(x)$ in 1988 [2]. The first excitement caused by this experiment was its indication of the failure of a sum rule due to Ellis and Jaffe based on the assumption that the contribution from strange quarks to g_1 is negligible [3]. It was soon realized, however, that there were more profound ramifications, which led to an intense scrutiny of the theory, since they implied a "spin crisis in the parton model" [4]— the spins of the quarks seemed to provide only a tiny fraction of the spin of the nucleon, in contrast to the situation in simple-minded constituent quark models of hadrons, where the quark spins account for a very large fraction of the proton spin. The crisis was believed to be resolved via a large polarized gluon contribution.

Of course the parton model predates QCD. In the more general field-theoretic framework we know that Bjorken Scaling [5], i.e. the fact that structure functions and parton densities depend only on x, cannot hold exactly, and these functions have a Q^2 dependence which can be calculated perturbatively in QCD, resulting in some of the most stringent tests of the validity of the theory. Moreover, because of the unfortunate need to renormalize the theory, the parton densities lose their simple physical meaning, and their actual functional form depends upon the renormalization scheme employed.

At present the situation, as will be discussed, is full of interest.

- Measurements of the polarized gluon density suggest that it is much too small to resolve the spin crisis [6,7]. This almost certainly implies that the partons possess orbital angular momentum, and it appears possible to estimate this, at least for the quarks, via a study of deeply virtual Compton scattering on protons [8].
- More precise data expected from the COMPASS experiment at CERN and the *pp* program at RHIC will allow further scrutiny of the validity of the above conclusion.
- There are now significant measurements of $g_2(x)$ which can be used to test the Wandzura–Wilczek approximation [9], the Burkhardt–Cottingham sum rule [10], and the Efremov–Leader–Teryaev sum rule [11].
- Measurements at Jefferson Laboratory are probing the hitherto inaccessible region of large *x*, where there are intriguing predictions about the behavior of the ratios $\Delta q(x)/q(x)$, as well as the region of low Q^2, where higher twist effects are important and where the issue of "duality" between the resonance and deep inelastic regions can be studied.
- By combining DIS data with the growing reservoir of data on semi-inclusive DIS (SIDIS) it should become possible to learn about the polarized sea densities $\Delta \bar{u}$ and $\Delta \bar{d}$ and to resolve the present disagreement between DIS and SIDIS about the sign of the strange quark density $\Delta s(x) + \Delta \bar{s}(x)$.

The aim of this review is phenomenological, i.e., it tries to strike a reasonable balance between theory and experiment. The theoretical treatment is thus conventional QCD and does not address interesting, and sometimes profound, matters like the Chern–Simons current and non-perturbative effects such as instantons, axial ghosts, and the U(1) problem. These are discussed in detail in the review of Anselmino, Efremov and Leader [12], and in the review of Bass [13], who also examines the consequences of a fixed pole in the virtual-photon Compton amplitude.
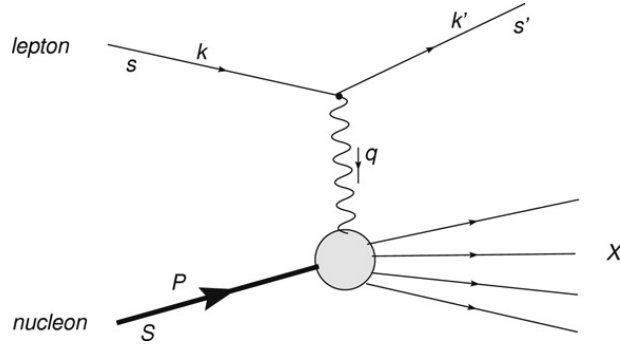
Fig. 1. Feynman diagram for deep inelastic lepton–hadron scattering.

1.1. Definitions and formalism

Consider the inelastic inclusive scattering of polarized leptons on polarized nucleons. We denote by m the lepton mass, k (k') the initial (final) lepton 4-momentum and s (s') its covariant spin 4-vector, such that $s \cdot k = 0$ ($s' \cdot k' = 0$) and $s \cdot s = -1$ ($s' \cdot s' = -1$); the nucleon mass is M and the nucleon 4-momentum and spin 4-vector are, respectively, P and S. Assuming, as is usually done, one photon exchange (see Fig. 1), the differential cross-section for detecting the final polarized lepton in the solid angle $d\Omega$ and in the final energy range (E', $E' + dE'$) in the laboratory frame, $P = (M, \mathbf{0})$, $k = (E, \mathbf{k})$, $k' = (E', \mathbf{k'})$, can be written as

$$\frac{d^2\sigma}{d\Omega \, dE'} = \frac{\alpha^2}{2Mq^4} \frac{E'}{E} L_{\mu\nu} W^{\mu\nu} \tag{1}$$

where $q = k - k'$ and α is the fine structure constant.

The leptonic tensor $L_{\mu\nu}$ (summed over the unobserved final lepton spin) is given by

$$L_{\mu\nu}(k, s; k') = \sum_{s'} [\bar{u}(k', s') \, \gamma_\mu \, u(k, s)]^* [\bar{u}(k', s') \, \gamma_\nu \, u(k, s)] \tag{2}$$

and can be split into symmetric (S) and antisymmetric (A) parts under μ, ν interchange:

$$L_{\mu\nu}(k, s; k') = 2\{L_{\mu\nu}^{(S)}(k; k') + \mathrm{i} L_{\mu\nu}^{(A)}(k, s; k')\} \tag{3}$$

where

$$L_{\mu\nu}^{(S)}(k; k') = k_\mu k'_\nu + k'_\mu k_\nu - g_{\mu\nu}(k \cdot k' - m^2)$$

$$L_{\mu\nu}^{(A)}(k, s; k') = m \, \varepsilon_{\mu\nu\alpha\beta} \, s^\alpha \, q^\beta. \tag{4}$$

The unknown hadronic tensor $W_{\mu\nu}$ describes the interaction between the virtual photon and the nucleon and depends upon four scalar structure functions, the unpolarized functions $F_{1,2}$ and the spin-dependent functions $g_{1,2}$ (ignoring parity-violating interactions). These must be measured and can then be studied in theoretical models, in our case in the QCD-modified parton model. They can only be functions of the scalars q^2 and $q \cdot P$. Usually people work with

$$Q^2 \equiv -q^2 \quad \text{and} \quad x_{Bj} \equiv Q^2/2q \cdot P = Q^2/2M\nu \tag{5}$$

where $\nu = E - E'$ is the energy of the virtual photon in the lab frame. x_{Bj} is known as "x-Bjorken", and we shall simply write it as x. We also refer to the invariant mass of the (unobserved) final state, $W = \sqrt{(P+q)^2} = \sqrt{M^2 + 2M\nu - Q^2}$.

Analogous to Eq. (3) one has

$$W_{\mu\nu}(q; P, S) = W_{\mu\nu}^{(S)}(q; P) + \mathrm{i} \, W_{\mu\nu}^{(A)}(q; P, S). \tag{6}$$

The symmetric part, relevant to unpolarized DIS, is given by

$$W_{\mu\nu}^{(S)}(q; P) = 2 \left[\frac{q_\mu q_\nu}{q^2} - g_{\mu\nu} \right] F_1(x, Q^2) + \frac{2}{M\nu} \left[P_\mu - \frac{P \cdot q}{q^2} q_\mu \right] \left[P_\nu - \frac{P \cdot q}{q^2} q_\nu \right] F_2(x, Q^2). \tag{7}$$

The antisymmetric part, relevant for polarized DIS, can be written as

$$W_{\mu\nu}^{(A)}(q; P, s) = 2 \, \varepsilon_{\mu\nu\alpha\beta} \, q^\alpha \left\{ M^2 S^\beta G_1(\nu, Q^2) + \left[M\nu S^\beta - (S \cdot q) P^\beta \right] G_2(\nu, Q^2) \right\} \tag{8}$$

or, in terms of the scaling functions $g_{1,2}$

$$g_1(x, Q^2) = M^2 \nu G_1(\nu, Q^2), \qquad g_2(x, Q^2) = M\nu^2 G_2(\nu, Q^2), \tag{9}$$

$$W_{\mu\nu}^{(A)}(q; P, s) = \frac{2M}{P \cdot q} \, \varepsilon_{\mu\nu\alpha\beta} \, q^\alpha \left\{ S^\beta g_1(x, Q^2) + \left[S^\beta - \frac{(S \cdot q) P^\beta}{(P \cdot q)} \right] g_2(x, Q^2) \right\}. \tag{10}$$

Note that these expressions are electromagnetic gauge-invariant:

$$q^\mu W_{\mu\nu} = 0. \tag{11}$$

In the Bjorken limit, or deep inelastic regime,

$$-q^2 = Q^2 \to \infty, \qquad \nu = E - E' \to \infty, \qquad x \text{ fixed} \tag{12}$$

the structure functions $F_{1,2}$ and $g_{1,2}$ are known to approximately scale, i.e., vary very slowly with Q^2 at fixed x—in the simple parton model they scale exactly; in QCD their Q^2 evolution can be calculated perturbatively.

Differences of cross-sections with opposite target spins are given by

$$\left[\frac{d^2\sigma}{d\Omega \, dE'}(k, s, P, -S; k') - \frac{d^2\sigma}{d\Omega \, dE'}(k, s, P, S; k') \right] = \frac{\alpha^2}{2Mq^4} \frac{E'}{E} \, 4L_{\mu\nu}^{(A)} \, W^{\mu\nu(A)}. \tag{13}$$

After some algebra (for a detailed derivation see [12]), one obtains from Eqs. (13) and (10) expressions for the following polarized cross-section differences (note that here, and in the following, we have included the lepton mass terms that are usually ignored):

- For the lepton and target nucleon polarized longitudinally, i.e. along or opposite to the direction of the lepton beam, the cross-section difference under reversal of the nucleon's spin direction (indicated by the double arrow) is given by

$$\frac{d^2\sigma^{\overleftarrow{\Rightarrow}}}{dx\,dy} - \frac{d^2\sigma^{\overrightarrow{\Rightarrow}}}{dx\,dy} = \frac{16\pi\alpha^2}{Q^2} \left[\left(1 - \frac{y}{2} - \frac{y^2(M^2x^2 + m^2)}{Q^2} \right) g_1 - \frac{2M^2x^2y}{Q^2} g_2 \right]. \tag{14}$$

- For nucleons polarized transversely in the scattering plane, one finds

$$\frac{d^2\sigma^{\to\Uparrow}}{dx\,dy} - \frac{d^2\sigma^{\to\Downarrow}}{dx\,dy} = -\frac{16\alpha^2}{Q^2} \left(\frac{2Mx}{Q} \right) \sqrt{1 - y - \frac{M^2x^2y^2}{Q^2}} \left[\frac{y}{2} \left(1 + \frac{2m^2y}{Q^2} \right) g_1 + g_2 \right]. \tag{15}$$

Here we have used

$$y \equiv \frac{\nu}{E} = \frac{P \cdot q}{P \cdot k}. \tag{16}$$

In principle, these two independent observables allow measurement of both g_1 and g_2 (as has been done at SLAC and in Jefferson Lab's Halls A and C), but the transverse cross section difference is generally smaller because of kinematic factors and therefore more difficult to measure. Only in the past few years has it been possible to gather precise information on g_2, which turns out to be usually smaller than g_1 in DIS.

Since experimental results are often presented in the form of asymmetries, which are the ratios of cross-section differences to the unpolarized cross-section, we comment here briefly on the latter. The unpolarized cross-section is given by

$$\frac{d^2\sigma_{unpold}}{dx\,dy} = \frac{4\pi\alpha^2}{x\,y\,Q^2} \left\{ xy^2 \left(1 - \frac{2m^2}{Q^2} \right) F_1 + \left[1 - y - \frac{M^2x^2y^2}{Q^2} \right] F_2 \right\}. \tag{17}$$

It is a non-trivial task to obtain separate information on F_1 and F_2 and usually data are presented for F_2 and R where

$$R \equiv [1 + \gamma^2] \left(\frac{F_2}{2xF_1} \right) - 1 \tag{18}$$

and

$$\gamma^2 = \frac{4M^2x^2}{Q^2}. \tag{19}$$

For a longitudinally polarized target the measured asymmetry is

$$A_\parallel \equiv \frac{d\sigma^{\overleftarrow{\Rightarrow}} - d\sigma^{\overrightarrow{\Rightarrow}}}{2 \, d\sigma_{unpold}} \tag{20}$$

and for a transversely polarized target the measured asymmetry is

$$A_\perp \equiv \frac{d\sigma^{\rightarrow\Uparrow} - d\sigma^{\rightarrow\Downarrow}}{2d\sigma_{unpold}}. \tag{21}$$

It is customary to introduce the (virtual) photon–nucleon asymmetries $A_{1,2}$,

$$A_1 = \frac{g_1 - \gamma^2 g_2}{F_1} \tag{22}$$

and

$$A_2 = \gamma\left[\frac{g_1 + g_2}{F_1}\right]. \tag{23}$$

From Eqs. (14), (15) and (17), it follows that

$$A_\parallel = D\left(A_1 + \eta A_2\right) \tag{24}$$

and

$$A_\perp = d(A_2 - \xi A_1) \tag{25}$$

where

$$D = \frac{y[(1+\gamma^2 y/2)(2-y) - 2y^2 m^2/Q^2]}{y^2(1 - 2m^2/Q^2)(1+\gamma^2) + 2(1+R)(1 - y - \gamma^2 y^2/4)} \tag{26}$$

$$d = \left[\frac{[1+\gamma^2 y/2(1+2m^2 y/Q^2)]\sqrt{1 - y - \gamma^2 y^2/4}}{(1 - y/2)(1+\gamma^2 y/2) - y^2 m^2/Q^2}\right] D \tag{27}$$

$$\eta = \gamma\frac{[1 - y - y^2(\gamma^2/4 + m^2/Q^2)]}{(1 - y/2)(1+\gamma^2 y/2) - y^2 m^2/Q^2} \tag{28}$$

$$\xi = \gamma\frac{1 - y/2 - y^2 m^2/Q^2}{1+\gamma^2 y/2(1+2m^2 y/Q^2)}. \tag{29}$$

Measurements of both $A_\perp$ and $A_\parallel$ yield the values of g_1 and g_2 directly (given a parametrization of R and F_1), but in practice the majority of experiments in the past have only measured $A_\parallel$. These experiments have been interpreted as measurements of g_1, neglecting or correcting for g_2. Although it turns out that g_2 is small, there is no *a priori* reason for this, so it is safer to neglect some quantity for which we know an upper bound, e.g. we could utilize $|A_\perp| \leq 1$, but a better approach is to utilize the (virtual) photon–nucleon asymmetries. The point is that there exists a restrictive bound on A_2 (for the history of this see [14,15]):

$$|A_2| \leq \sqrt{R(1+A_1)/2}. \tag{30}$$

Replacing g_2 in terms of g_1 and A_2 yields

$$\frac{A_\parallel}{D} = (1+\gamma^2)\left[\frac{g_1}{F_1}\right] + (\eta - \gamma)A_2, \tag{31}$$

where $\eta - \gamma$ is typically very small. Most experiments either use a parametrization for A_2 or neglect the A_2 terms in Eqs. (24) and (31) altogether, leading to the approximations

$$A_1 \approx \frac{A_\parallel}{D} \approx (1+\gamma^2)\left[\frac{g_1}{F_1}\right] \tag{32}$$

to evaluate g_1 and then utilize the bound Eq. (30) to estimate the error involved.

Strictly speaking, all of the above, from Eq. (7) onwards, applies only to a spin 1/2 target. For targets with higher spin, like the deuteron, the hadronic tensor contains many more structure functions. But in all the practical cases of interest the target nucleus may be considered as a weakly bound system of essentially independent nucleons, with a small correction for binding effects, and the nuclear asymmetries are then expressed in terms of the asymmetries on protons and neutrons. For a detailed analysis of this issue, and formulae relating measured asymmetries on deuterium and on ^{3}He to the nucleon structure functions, see Section 2.1.4 of [12]. For the more general theory of DIS on spin 1 targets, see [16,17].

Note that in the above we have kept terms of order M^2/Q^2 and smaller. They are sometimes necessary in order to extract the correct experimental values of the structure functions from the measured asymmetries. However, very often, the QCD analysis of the structure functions is carried out at *leading twist* only, ignoring higher twist terms, i.e. of order M^2/Q^2. This is clearly inconsistent in those cases, for example the Jefferson Lab experiments, where the above terms are important.

1.2. Experiments

When Bjorken proposed his famous sum rule [5] 40 years ago, he considered it "useless" since the experimental technology needed to test it appeared far from reach. It required substantial advances in both polarized target and polarized beam technology before the first double-polarization lepton scattering experiment could begin [18]. The first round of experiments at SLAC [18–21] using polarized electrons impinging on a polarized proton target seemed to confirm the expectations of the naive quark parton model (namely, that most of the proton spin was carried by its quark helicities). However, the range in x covered was rather limited, and the data had large errors and were taken at fairly low Q^2. Nevertheless, these experiments started the exploration of the nucleon spin structure, not only in the DIS region, but also in the region of the nucleon resonances [20].

The EMC collaboration [2] used the (naturally polarized) muon beam at CERN, with much higher beam energy, together with a large polarized proton target, to extend the covered range down to significantly lower $x \approx 0.01$. Together with the earlier SLAC data, their results seemed to indicate that little to none of the proton spin was due to the helicities of the quarks. This violated the Ellis–Jaffe sum rule [3] within the simple quark–parton picture assuming that SU(3) is a good symmetry and the strange (sea) quark contribution to the nucleon spin could be ignored. The final data from the EMC experiment are published in [22].

This puzzling result spurred the rapid development of several new experiments that had the goal to verify the data on the proton with greater precision and, most importantly at the time, test the Bjorken sum rule [5] by probing the spin structure of the neutron as well. This last goal required the use of targets containing polarized neutrons, for which two very different technologies were developed.

One possibility is to use polarized deuterons as a target composed of equal amounts of polarized protons and neutrons, from which neutron information can be extracted by comparison with pure proton targets (taking nuclear binding effects like the deuteron D-state into account). This method follows closely the example of polarized proton target technology, which typically involves chemical compounds (like alcohols or ammonia) rich in hydrogen (either ^{1}H for protons or ^{2}H = D for deuterons) which are seeded with paramagnetic centers (with unpaired electrons), cooled to cryogenic temperatures (1 K or lower) and immersed in a strong magnetic field (usually several T). The unpaired electrons are polarized to nearly 100% in the field, and this polarization is transferred to the hydrogen nuclei via the process of Dynamic Nuclear Polarization
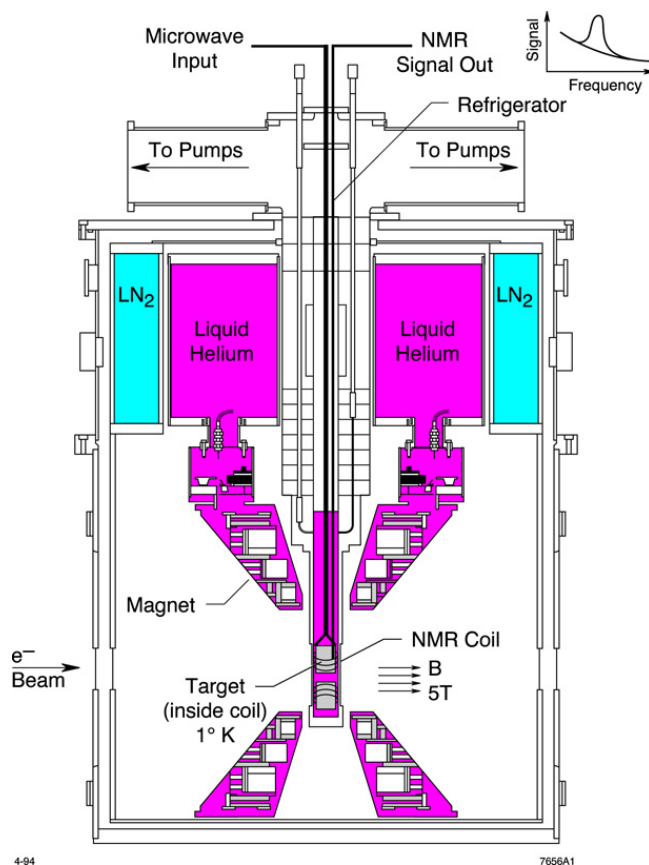
Fig. 2. Typical solid state polarized proton or deuteron target for electron scattering experiments. The cell containing the frozen ammonia (^{15}N$\vec{\text{H}}_3$ or ^{15}N$\vec{\text{D}}_3$) is at the center of a Helmholtz-type magnet generating a homogeneous field of about 5 T. A ^{4}He evaporation refrigerator (a liquid helium bath in a low-pressure environment) cools the target material to about 1 K. 140 GHz microwaves irradiate the target material to dynamically polarize the hydrogen nuclei. The polarization is measured by a resonant NMR circuit (the obtained signal vs. frequency is sketched in the top right). Polarized targets for muon beams are typically much longer and can be cooled to lower temperatures.

Fig. 3. Typical gaseous ^{3}He target for electron scattering experiments. The glass cell containing pressurized ($\approx$ 10 atm) ^{3}He gas is at the center of a Helmholtz magnet generating a homogeneous field of 25 G. The cell is connected to a second, heated volume where the ^{3}He is polarized by spin-exchange collisions with alkali atoms, the latter being pumped by high-intensity lasers. The polarization is measured either via an NMR circuit (consisting of RF drive coils and NMR signal pickup coils) or using the EPR method.
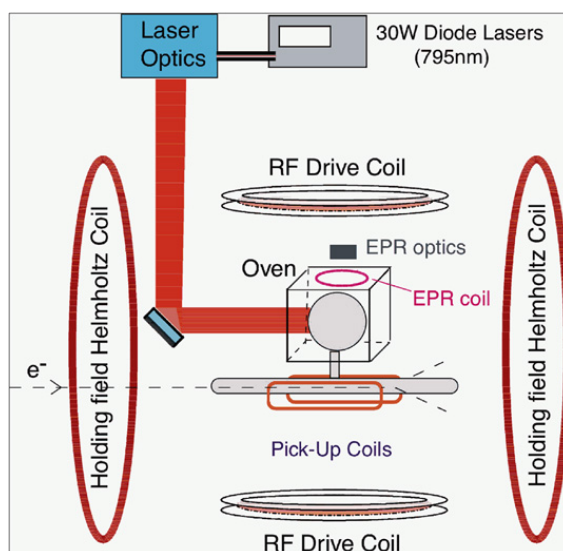
(DNP), by employing microwave radiation of the proper frequency to induce coupled electron–nucleon spin transitions. This technique typically achieves a proton polarization of 80%–90% and a deuteron polarization of 30%–50%, both of which can be measured using a Nuclear Magnetic Resonance (NMR) system. Fig. 2 shows an example of such a target. In the case of deuteron targets, one can also use ^{6}LiD compounds, where both the lithium nucleus and the deuteron are polarized to increase the fraction of events from polarized nucleons (the so-called dilution factor).

A complementary approach uses polarized ^{3}He nuclei to gain information on the neutron, since to first order the ^{3}He nucleus can be considered as a bound state of a proton–proton pair (with their spins anti-aligned) and an unpaired neutron carrying almost all of the nuclear spin. Again, nuclear corrections to this picture are important, but the advantage is that one does not have to subtract a large contribution from polarized protons to extract the neutron results. The most widely used version of this target uses a glass vessel containing pressurized ^{3}He gas mixed with a trace amount of an alkali atom vapor (typically rubidium) that can be electron-spin polarized via optical pumping with circularly polarized laser light. The ^{3}He nuclei are polarized through spin exchange collisions with the alkali atoms. A typical example is shown in Fig. 3. Polarizations of up to nearly 50% have been achieved in these targets, which can withstand much larger beam currents than the solid-state DNP targets. As an example, the polarized ^{3}He target used in JLab Hall A [23], with a 15 µA electron beam on an 40 cm long, 10 atm ^{3}He target, achieved a luminosity of 10^{36} cm^{-2} s^{-1}. Recently, a new development of a hybrid technique [24], using a mixture of rubidium and potassium atoms, has significantly increased the spin-exchange efficiency and, in turn, increased the target polarization up to 60% for the high density target. Further improvement to over 70% polarization has been achieved for this target by using recently available narrow-width lasers. The high luminosity and high polarization allow measurements of the spin structure functions with very high statistical precision. The target polarization is measured with both NMR and EPR (electron para-magnetic resonance) methods to a precision of 3%. Since the holding field is low, it is relatively easy to point the polarization in any direction in the horizontal plane using two pairs of Helmholtz coils. At Jefferson Lab, the addition of a new pair of vertical coils recently allowed the target also to be polarized along the vertical direction, enabling the study of transverse spin.

The successor collaboration to EMC at CERN, called SMC (Spin Muon Collaboration), used large dynamically polarized cryogenic deuteron [25] and proton [26] targets to extract information on the neutron and to improve on the statistics and the kinematic reach of the EMC result. They also pioneered the use of semi-inclusive data, where a leading hadron is identified in coincidence with the scattered lepton, to get more information on the contribution of various quark flavors to the nucleon spin [27]. The complete data set collected by the SMC resulted in precise inclusive results both at the highest momentum transfer Q^2 [28] and at the lowest quark momentum fraction x accessible to fixed target experiments [29].

The E142 collaboration at SLAC was the first to use a ^{3}He gas target with high luminosity to directly access the neutron spin structure functions g_1^n and g_2^n [30,31]. Together with the EMC and SMC experiments, the results showed that the Bjorken sum rule including perturbative QCD (pQCD) corrections appeared to be valid. E142 was followed by a series of additional experiments at SLAC that used all three nuclear targets, proton, deuteron and ^{3}He, to accumulate a highly precise data set on spin structure functions in the deep inelastic region. Instrumental for achieving ever higher precision was a significant improvement in the polarization (to over 80%) and intensity of available electron beams from strained GaAs cathodes irradiated with circularly polarized laser light. By using several electron beam energies and a set of up to 3 spectrometers, the E143 [32–34] and the E155 [35,36] collaborations collected data on the proton and the deuteron over
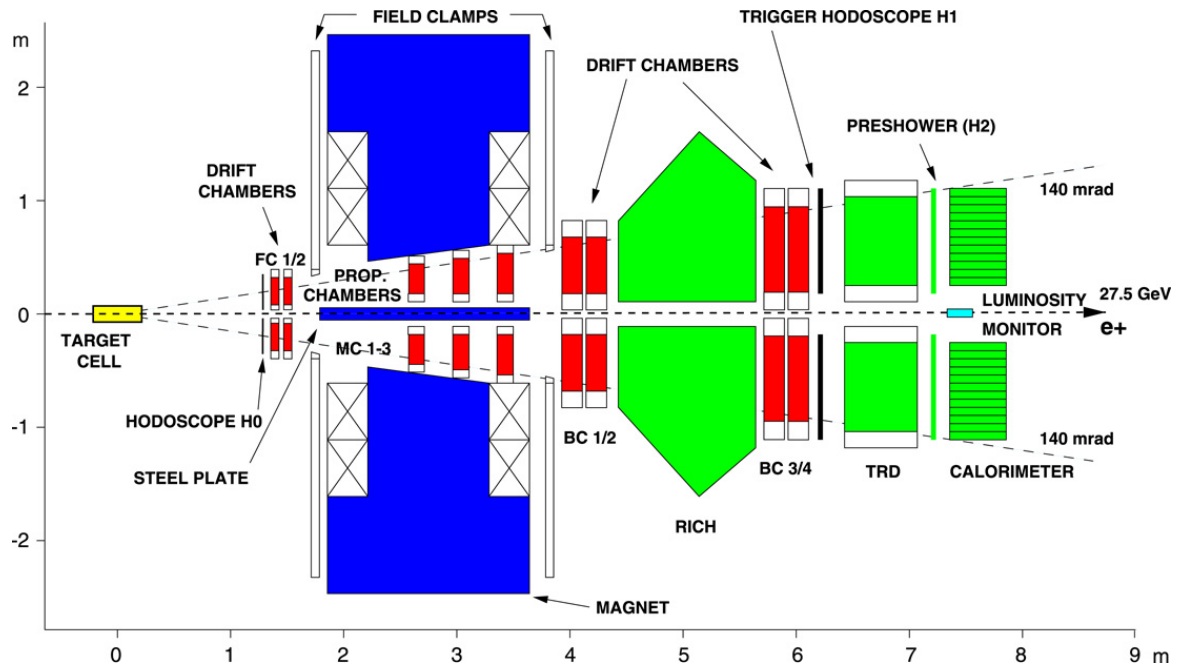
Fig. 4. Layout of the HERMES experiment at HERA/Desy (Hamburg, Germany). The stored electron or positron beam traverses an open storage cell fed by an atomic beam source with polarized H, D or ^{3}He. The scattered leptons (and leading hadrons) are detected in a large acceptance spectrometer consisting of wire chambers, scintillator hodoscopes, ring-imaging Cherenkov (RICH) and transition–radiation (TRD) detectors, and an electromagnetic calorimeter.

a wide range of momentum transfer Q^2 at several values of x, which were used to study scaling violations for polarized structure functions. The E154 collaboration [37,38] added more neutron data at similar kinematics, using a polarized ^{3}He target. The E143 collaboration also published the first precision results at lower Q^2 and in the nucleon resonance region ($W \leq 2$ GeV) [39]. The spin structure functions $g_2^{p,n,d}$ were measured with high precision by rotating the target polarization for all 4 experiments from a longitudinal to a perpendicular orientation to the beam [34,40,41].

The most innovative approach to measuring DIS structure functions came from the HERMES collaboration (see Fig. 4) which used positrons or electrons circulating in one of the HERA rings at DESY together with internal low-density gas targets fed directly from atomic beam sources [42,43]. The target atoms are polarized using hyperfine transitions induced by radio frequency fields and Stern–Gerlach type separation with magnetic sextupoles. The atomic beam is injected into a thin, windowless tube through which the beam circulates. This method yields a pure polarized target without any dilution from unpolarized materials. The polarization of the beam is accomplished by utilizing the Sokolov–Ternov effect (the spontaneous vertical polarization through spin-dependent synchrotron radiation of leptons in a storage ring). Spin rotators turn the polarization into the longitudinal direction at the target. The scattered electrons, as well as hadrons produced in coincidence, were detected by a large acceptance forward spectrometer. This setup allowed the HERMES collaboration not only to independently measure the inclusive spin structure functions g_1 and g_2 (for final results see [44]), but also semi-inclusive structure functions for flavor-tagging [45]. In addition, they collected a large data set on related reactions of interest, from Deeply Virtual Compton Scattering (DVCS) [46] and transverse spin structure functions [47] to a first direct measurement of the gluon polarization [48].

After the shutdown of the HERA ring, there are now three laboratories left where experiments studying the spin structure of the nucleon continue: CERN, with the SMC-successor experiment "COMPASS"; BNL (on Long Island, NY) with the polarized proton–proton collision program at RHIC; and the Thomas Jefferson National Accelerator Facility ("Jefferson Lab" or JLab) in Newport News, VA, with an ongoing program of electron scattering in all 3 experimental halls.

The COMPASS experiment (see Fig. 5) uses the secondary (naturally polarized) muon beam at CERN together with large polarized deuteron and hydrogen targets to extend the kinematic reach and precision of SMC, and, as its main purpose, to extract information on the gluon polarization. This latter goal has been pursued by measuring both the production of hadron pairs with high transverse momentum [6] and by detecting charmed mesons in the final state (which are predominantly produced via photon–gluon fusion). Indirect information on the gluon contribution to the nucleon spin also comes from NLO analyses of inclusive DIS data, where the large kinematic lever arm offered by COMPASS makes an important contribution. First results on the deuteron have been published [49–51] and the COMPASS experimental program will continue in the foreseeable future.

Another novel approach to studying the spin structure of the nucleon uses high-energy collisions of counter-circulating proton beams in the Relativistic Heavy Ion Collider (RHIC) at Brookhaven National Lab (BNL, Long Island, NY). Polarized protons are injected into a series of accelerators that finally fill both RHIC rings, where energies up to 100 GeV (250 GeV in the future) can be reached (see Fig. 6). Siberian snakes rotate the proton spins to avoid depolarizing resonances, while spin rotators can select the desired spin direction at the interaction points.
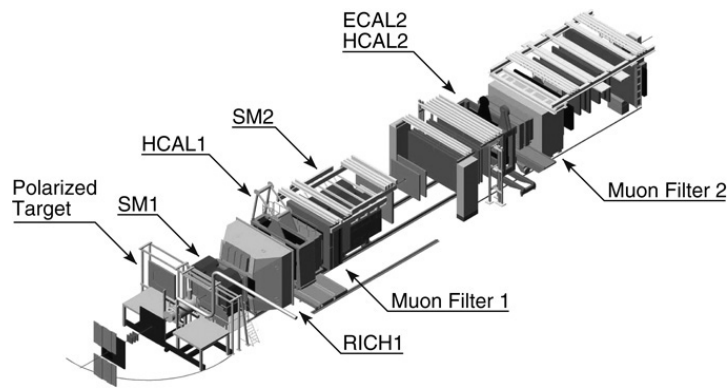
Fig. 5. Layout of the COMPASS experiment at CERN (Geneva, Switzerland).
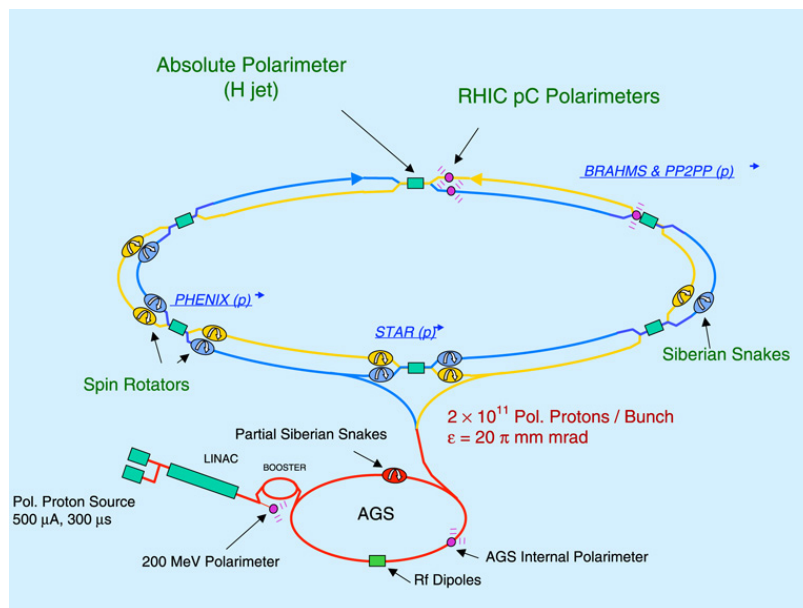

Fig. 6. Layout of the RHIC accelerator complex at BNL (Long Island, NY).

At present, there are two large experiments (PHENIX and STAR) that use polarized proton collisions to study the gluon helicity contribution ΔG to the nucleon spin. The observables used so far include meson production with high transverse momentum p_T as well as jet production, both probing the gluons through quark–gluon and gluon–gluon interactions in the initial state. First results from these experiments have been published [52–55] and will be discussed in Section 2.3. By orienting the proton spins perpendicular to the beam direction, both experiments can also study reactions sensitive to transverse spins.

Finally, for the last 10 years a large program using electron scattering to study the spin structure of nucleons has been underway at Jefferson Lab (JLab). This program has utilized the highest polarization electron beams (over 85%) with energies from 0.8 GeV to close to 6 GeV and all three species of polarized targets (p, d and ^{3}He) to study spin-dependent structure functions both in the DIS regime as well as in the nucleon resonance region (and even on nuclei). This program is ongoing in all three experimental halls and will be continued once the energy upgrade to 12 GeV of the JLab accelerator is completed in 2014. In the following we give some of the experimental details for all three halls; the results achieved so far will be discussed in the relevant sections 2.3–4.

The spin structure program in JLab's Hall A is focussed on the neutron, using a polarized ^{3}He target (Fig. 3) as an effective polarized neutron target. The target polarization direction can be oriented longitudinal or transverse to the beam direction. Measurements of polarized cross-sections and asymmetries in the two orthogonal directions allow a direct extraction of g_1, g_2, A_1 and A_2. A series of high precision experiments [56–65] measured g_1 and g_2 in a wide range of kinematics, from very low $Q^2 (\approx 0.01$ GeV^2) up to 5 GeV^2 and from the elastic peak to the DIS region ($W \approx 3$ GeV). A pair of High Resolution Spectrometers (HRS) are used to detect the scattered electrons. The HRS have angular acceptances of ≈ 6 msr and momentum acceptances of $\approx 9\%$. Their angular range is 12.5°–160° and can reach as low as 6° with the addition of a septum magnet. The high luminosity of 10^{36} cm^{-2} s^{-1} allowed for precision measurements at numerous HRS momentum and angular settings to cover a wide swath in the (Q^2, W)-plane. The electron detector package consists of vertical drift chambers (for momentum analysis and vertex reconstruction), scintillation counters (for data acquisition trigger), gas Cherenkov counters
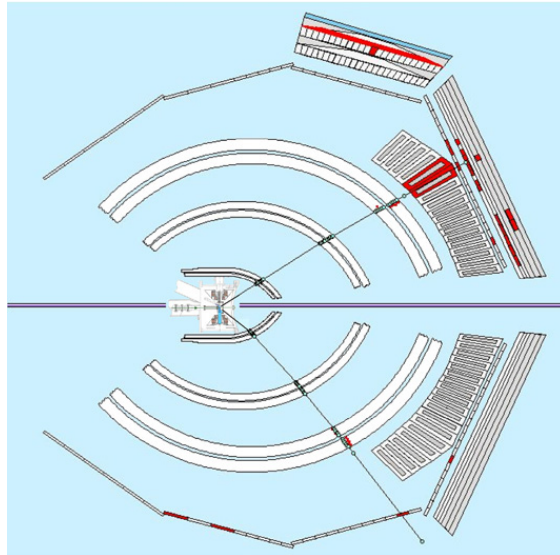
Fig. 7. Schematic of the CEBAF Large Acceptance Spectrometer (CLAS) with the polarized target at its center. Charged particle tracks are measured with three layers of drift chambers, while electrons (track in upper half) can be identified using a set of Cherenkov counters, time-of-flight scintillators and a electromagnetic calorimeter.

and lead–glass shower calorimeters (for particle identification). The HRS optical property and acceptance have been carefully studied. Absolute cross sections are measured to a level of 2%–3% precision. Asymmetries are measured to a level of 4%–5% precision, mostly due to the uncertainties from the beam and target polarization measurements. The spin structure functions g_1 and g_2 are extracted using polarized cross section differences in which contributions from unpolarized materials, such as target windows and nitrogen, cancel. Corrections for the two protons in ^{3}He are still needed since they are slightly polarized due to the D state (8%) and S′ state (1.5%) of the ^{3}He wave function [66]. Corrections for binding and Fermi motion are applied using state-of-the-art ^{3}He calculations [67,68]. Uncertainties due to the nuclear corrections have been studied [67]. In the region of DIS and for the extraction of moments, the uncertainties are usually small, typically less than 5%.

The EG1–EG4 series of experiments in JLab's Hall B (see Fig. 7) has as its goal to map out the asymmetry A_1 and the spin structure function g_1 of both nucleons over the largest, continuous kinematic range accessible. It makes use of the CEBAF Large Acceptance Spectrometer (CLAS) in Hall B that covers an angular range of about 6° to over 140° in polar angle and nearly 2π in azimuth [69]. Because of the open geometry and the toroidal magnetic field (maintained by 6 superconducting coils evenly distributed in azimuth), one can simultaneously detect scattered electrons over a wide kinematic range, as well as secondary produced hadrons (nucleons, pions and kaons) for semi-inclusive or exclusive channels. By combining runs with several different beam energies from 1 to 6 GeV, a continuous coverage in Q^2 from 0.015 to 5 GeV^2 and in final state mass W, from the elastic peak ($W = 0.94$ GeV) to the DIS region ($W \approx 3$ GeV), has been achieved. Inclusive results from the EG1 experiment have been published [70–73].

The relatively low luminosity limit of this open detector (about 10^{34} cm^{-2} s^{-1}) is rather well matched to the luminosity limits typical for solid state, dynamically polarized targets. EG1–EG4 took data on both hydrogen (^{15}NH$_3$) and deuterium (^{15}ND$_3$). So far, only targets polarized along the beam direction have been utilized (because of the difficulty to combine a large transverse magnetic field with the open geometry of CLAS), which necessitates (minor) corrections of the measured asymmetries for the unobserved contribution from A_2 (see Eq. (31)). A fit to the world data on A_2 and on unpolarized structure functions R and F_1 [74,75] is used to extract the desired spin structure function information from the measured asymmetries. In addition to the structure function $g_1(x, Q^2)$, the CLAS data have also yielded new results on resonance excitation and decay (via exclusive π^+, π^0 and π^- channels) [76,77], on deeply virtual Compton scattering [78], and on single and double spin asymmetries in semi-inclusive hadron production [79].

The first experiment completed in Hall C used a standard DNP ammonia target (^{15}NH$_3$ and ^{15}ND$_3$) and the existing high momentum spectrometer (HMS) for a detailed look at the resonance region at intermediate $Q^2 \approx 1.3$ GeV^2. This is the only experiment at JLab on the proton and the deuteron where both longitudinal and transverse double spin asymmetries were measured, allowing an unambiguous separation of the structure functions A_1 and A_2 or g_1 and g_2 up to a final state missing mass of $W \approx 2$ GeV. First results have been published [80].

2. Spin-dependent parton density functions

2.1. The simple parton model

The parton model was invented [81] long before QCD to explain the fact that the unpolarized structure functions $F_{1,2}$ apparently scale, i.e., do not decrease with Q^2, in contrast to the elastic form factors which decrease rapidly [1]. The partons
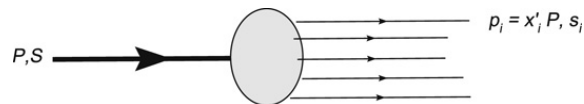
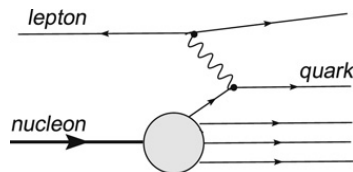**Fig. 8.** The nucleon viewed as a collinear beam of partons.

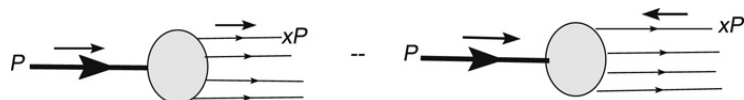**Fig. 9.** Parton model description of DIS.

Fig. 10. Visualization of the longitudinally polarized parton density $\Delta q(x)$. The upper arrows show the spin direction.

were conceived of as effectively massless, point-like constituents of the nucleon, which interact electromagnetically like leptons, and it was argued that a nucleon, in a frame where it is moving very fast, could be viewed as a "beam" of collinear partons, as shown in Fig. 8. The partons are characterized as having momentum $\boldsymbol{p} = x'\boldsymbol{P}$ and covariant spin vector s.

The interaction with the hard photon is then visualized as in Fig. 9, in which the lepton–quark scattering is treated analogously to elastic lepton–lepton scattering. Requiring the final quark to be on mass shell, i.e. $(p + q)^2 = 0$, selects the value $x' = x$.

For *unpolarized* DIS one finds the scaling result expressed in terms of the number density $q(x)$ of quarks and $\bar{q}(x)$ of antiquarks

$$F_1(x, Q^2) = \frac{1}{2} \sum_j e_j^2 \left[q_j(x) + \bar{q}_j(x) \right] \tag{33}$$

where the sum is over flavors j, e_j is the charge of the quark, and the Callan–Gross relation [82] yields

$$F_2(x) = 2xF_1(x). \tag{34}$$

For *longitudinally polarized* DIS one obtains

$$g_1(x) = \frac{1}{2} \sum_j e_j^2 \left[\Delta q_j(x) + \Delta \bar{q}_j(x) \right] \tag{35}$$

with

$$\Delta q(x) = q_+(x) - q_-(x) \tag{36}$$

where $q_{\pm}(x)$ are the number densities of quarks whose spin orientation is parallel or antiparallel to the longitudinal spin direction of the proton (see Fig. 10). In terms of these, the usual (unpolarized) parton density is

$$q(x) = q_+(x) + q_-(x). \tag{37}$$

Concerning the second spin structure function, there are many different, inconsistent results for $g_2(x)$ in the literature. In fact there is no unambiguous way to calculate g_2 in the simple parton model. For an explanation of the problem see Section 3.4 of [12].

The only reliable result is the Wandzura–Wilczek relation [9]

$$g_2(x) \simeq -g_1(x) + \int_x^1 \frac{g_1(x')}{x'} \, dx' \tag{38}$$

which was originally derived as an approximation in an operator product expansion approach, but which has recently been shown to be derivable directly in the simple parton model [83]. It is discussed further in Sections 2.6 and 3.

Let us rewrite the expression for g_1, Eq. (35), in terms of linear combinations of quark densities which have specific transformation properties under the group of flavor transformations $SU(3)_F$:

$$\Delta q_3 = (\Delta u + \Delta \bar{u}) - (\Delta d + \Delta \bar{d}) \tag{39}$$

$$\Delta q_8 = (\Delta u + \Delta \bar{u}) + (\Delta d + \Delta \bar{d}) - 2(\Delta s + \Delta \bar{s}) \tag{40}$$

$$\Delta \Sigma = (\Delta u + \Delta \bar{u}) + (\Delta d + \Delta \bar{d}) + (\Delta s + \Delta \bar{s}). \tag{41}$$

These transform respectively as the third component of an isotopic spin triplet, the eighth component of an $SU(3)_F$ octet, and a flavor singlet. Then

$$g_1(x) = \frac{1}{9}\left[\frac{3}{4}\Delta q_3(x) + \frac{1}{4}\Delta q_8(x) + \Delta\Sigma(x)\right]. \tag{42}$$

Taking the first moment of this yields, for protons,

$$\Gamma_1^p \equiv \int_0^1 g_1(x)\mathrm{d}x = \frac{1}{9}\left[\frac{3}{4}a_3 + \frac{1}{4}a_8 + a_0\right] \tag{43}$$

where

$$a_3 = \int_0^1 \mathrm{d}x\,\Delta q_3(x)$$

$$a_8 = \int_0^1 \mathrm{d}x\,\Delta q_8(x)$$

$$a_0 = \Delta\Sigma \equiv \int_0^1 \mathrm{d}x\,\Delta\Sigma(x). \tag{44}$$

Now the hadronic tensor $W^{\mu\nu}$ is given by the Fourier transform of the nucleon matrix elements of the commutator of electromagnetic currents $J_\mu(x)$:

$$W_{\mu\nu}(q; P, S) = \frac{1}{2\pi}\int \mathrm{d}^4 x\, \mathrm{e}^{iq\cdot x}\langle P, S|[J_\mu(x), J_\nu(0)]|P, S\rangle. \tag{45}$$

In hard processes, $x^2 \simeq 0$ is important, so we can use the Wilson Operator Product Expansion (OPE). This gives moments of $g_{1,2}$ in terms of hadronic matrix elements of certain operators multiplied by perturbatively calculable Wilson coefficient functions. This is discussed in more detail in Section 3.1. The a_i in Eq. (44) turn out to be hadronic matrix elements of an octet of quark $SU(3)_F$ axial-vector currents $J_{5\mu}^j$ ($j = 1, \ldots, 8$) and a flavor singlet axial current $J_{5\mu}^0$ (see Eqs. (82), (84) and (85)). The octet of currents is precisely the one that controls the weak decays of the neutron and of the octet hyperons, which implies that the values of a_3 and a_8 are *known* from β-decay measurements:

$$a_3 \equiv g_A = 1.2670 \pm 0.0035 \qquad a_8 = 0.585 \pm 0.025. \tag{46}$$

Hence a measurement of Γ_1, Eq. (43), can be considered as giving the value of the flavor singlet a_0.

It should be noted that the connection with hadronic matrix elements of local operators is strictly only valid if the moments include the elastic contribution, which appears as a delta-function at $x = 1$. However in *deep* inelastic scattering the elastic contribution is completely negligible, so the experimentally tabulated moments do not include an elastic term, as can be seen in the discussion of the extrapolation to $x = 1$ given in Sections 2.4 and 2.5. However, in dealing with inelastic scattering at low Q^2, especially in the resonance region, it is important to distinguish between moments including the elastic contribution, for which the notation will remain Γ and those not including an elastic contribution which will be denoted $\bar{\Gamma}$.

Now we can put the startling result of the European Muon Collaboration [2] into context: Knowing the values of a_3 and a_8, the EMC measurement implied

$$a_0^{EMC} \simeq 0. \tag{47}$$

But in the naive parton model

$$a_0 = \Delta\Sigma = a_8 + 3(\Delta s + \Delta\bar{s}) \tag{48}$$

where $\Delta\Sigma$ is given by Eq. (41).

In 1974 Ellis and Jaffe [3] had suggested that one could ignore the contribution from the strange quarks, i.e., from $\Delta s + \Delta\bar{s}$, implying that

$$a_0 \simeq a_8 \simeq 0.59. \tag{49}$$

Thus the EMC result Eq. (47) is in gross contradiction with Ellis–Jaffe. It was this contradiction which at first aroused interest in the EMC result, but it was soon realized that their result had far more serious consequences.

Consider the physical significance of $\Delta\Sigma(x)$. Since $q_\pm(x)$ count the number of quarks of momentum fraction x with spin component $\pm\frac{1}{2}$ along the direction of motion of the proton (say the z-direction), the total contribution to J_z coming from the spin of a given flavor quark is

$$\langle S_z\rangle = \int_0^1 \mathrm{d}x\left\{\left(\frac{1}{2}\right)q_+(x) + \left(\frac{-1}{2}\right)q_-(x)\right\}$$

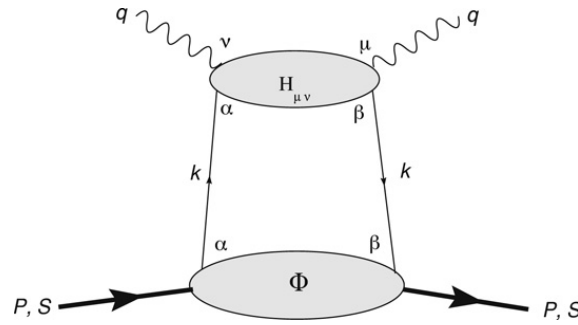$$= \frac{1}{2}\int_0^1 \mathrm{d}x\,\Delta q(x). \tag{50}$$

Fig. 11. QCD generalization of parton model.

It follows that

$$a_0 = 2\langle S_z^{quarks} \rangle \tag{51}$$

where $\langle S_z^{quarks} \rangle$ is the contribution to J_z from the spin of all quarks and antiquarks.

Naively, in a non-relativistic constituent model one would have expected all of the proton spin to be carried by the spin of its quarks. In a more realistic relativistic model one expects $2\langle S_z^{quarks} \rangle \approx 0.6$, which, as first noted by Sehgal [84], is actually close to the value obtained by neglecting the strange contribution in Eq. (48), but quite far from the EMC value Eq. (47) for a_0.

It was this discrepancy between the contribution of the quark spins to the angular momentum of the proton, as measured in DIS and as computed in both non-relativistic and relativistic constituent models of the proton, that was termed a "spin crisis in the parton model" [4]. It should be noted, however, that Thomas and co-workers have developed a constituent model, a more sophisticated version of the *Cloudy Bag* model, in which the nucleon is visualized as made up of valence quarks and a pion cloud, and the wave function includes the effect of single gluon exchange between the valence quarks. The pion cloud and the strength of the one gluon exchange were treated phenomenologically, determined from fits to various different static properties of the hadron octet and decuplet, and it was not clear if, or to what extent, double counting was taking place. However, lattice studies of the mass-splitting between the Δ and the nucleon [85] suggest that the pion cloud contributes very little to the splitting and thus allows a fairly reliable estimate of the value of the phenomenologically determined gluon coupling strength. It then turns out that the contribution of the quark spins to the angular momentum of the proton, in its rest frame, is $\Delta \Sigma \approx 0.35$, which is not too far from most recent experimental results. Thus in this approach there is no significant "spin crisis". For a review of this work see [86].

2.2. The parton model in QCD

The parton model is a heuristic picture, much like the impulse approximation in nuclear physics, and predates QCD. Once QCD is accepted as the theory of strong interactions, with quark and gluon fields as the fundamental fields, there will be interaction-dependent modifications of the simple parton model formulae for DIS. The theory is invariant under color gauge transformations, but the physical content of individual Feynman diagrams does depend upon the gauge, and it turns out that a parton-like picture emerges in the light-cone gauge $A_+ = 0$ where A^μ is the gluon vector potential. The description of nucleon structure becomes much more complicated, involving a set of twelve functions, and the parton model number densities $q(x)$, $\Delta q(x)$ (and the analogue for transversely spinning nucleons $\Delta_T q(x)$, which is not relevant for the longitudinal spin structure) are only the principal, so-called "leading twist" members of this set. In this review, we shall only deal with $q(x)$ and $\Delta q(x)$. The reaction is visualized as in Fig. 11, where the top "blob" involves a hard interaction (the photon is highly virtual) and the bottom "blob" involves non-perturbative soft interactions.

The main impact of the QCD interactions will be twofold:

(1) to introduce a mild, calculable logarithmic Q^2 dependence in the parton densities
(2) to generate a contribution to g_1 arising from the polarization of the gluons in the nucleon

We shall not go into the technical details, but simply indicate the physical source of these effects.

(1) *QCD corrections and evolution*

In Fig. 12 we show the Born term for the interaction of the virtual photon with a quark (the hard blob), and the simplest correction terms, a vertex correction and a diagram where a gluon is radiated from the active quark before it interacts with the photon.

Unfortunately these correction terms are infinite. The infinity is caused by collinear divergences which occur because of the masslessness of the quarks and which are removed by a process known as factorization. In this process the reaction is factorized (separated) into a hard and soft part and the infinity is absorbed into the soft part, which in any case cannot be calculated and has to be parametrized and studied experimentally.
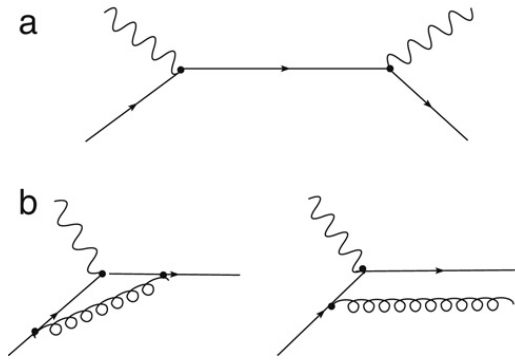
Fig. 12. Example of QCD correction terms (b) to the Born approximation (a).

The point at which this separation is made is referred to as the *factorization scale* μ^2. Schematically, one finds terms of the form $\alpha_s \ln \frac{Q^2}{m_q^2}$ which one splits as follows

$$\alpha_s \ln \frac{Q^2}{m_q^2} = \alpha_s \ln \frac{Q^2}{\mu^2} + \alpha_s \ln \frac{\mu^2}{m_q^2} \tag{52}$$

and one then absorbs the first term on the right hand side into the hard part and the second into the soft part. μ^2 is an arbitrary number, like the renormalization scale, and, in an exact calculation, physical results cannot depend on it. However it does mean that what we call the parton density has an extra label μ^2 specifying our choice. Moreover, since we never calculate to all orders in perturbation theory, it can make a difference what value we choose. It turns out that an optimal choice is $\mu^2 = Q^2$, so the parton densities now depend on both x and Q^2 i.e. we have $q(x, Q^2)$ and $\Delta q(x, Q^2)$, and perfect Bjorken scaling is broken. But the variation with Q^2 is gentle (logarithmic), and can be calculated via what are called the *evolution equations* which will be discussed later.

It turns out to be crucial in handling these divergences to use the technique of *dimensional regularization*, which is straightforward in the unpolarized case, but which runs into ambiguities in the polarized case. As a consequence there are several different factorization schemes in use and it is crucial, when presenting results on the parton densities, to specify which scheme is being utilized.

At present there are three schemes in use:

(i) The Vogelsang, Mertig and van Neerven scheme [87,88], $\overline{MS} - MNV$ (usually just abbreviated as $\overline{MS}$). In this scheme a_3 and a_8 are independent of Q^2.

(ii) The *AB* scheme of Ball, Forte and Ridolfi [89], which, in addition, has the first moment

$$\Delta \Sigma = \int_0^1 dx \, \Delta \Sigma(x, Q^2) \tag{53}$$

independent of Q^2.

(iii) The JET scheme of Carlitz, Collins and Mueller [90], Anselmino, Efremov and Leader [12] and Teryaev and Müller [91], and which is identical to the Chiral Invariant scheme of Cheng [92]. In this scheme a_3 and a_8 are independent of Q^2 as is $\Delta \Sigma$, but it can be argued that the JET scheme is superior to the others in that *all* hard effects are included in $H_{\mu\nu}$ (see Fig. 11).

Of course, if one could work to all orders in perturbation theory it would make no difference which scheme one used, but given that we work to leading order (LO), next to leading order (NLO), and in some cases to NNLO, the choice of scheme can be of importance.

For the polarized densities the evolution equations are

$$\frac{d}{d \ln Q^2} \Delta q(x, Q^2) = \frac{\alpha_s(Q^2)}{2\pi} \int_x^1 \frac{dy}{y} \{\Delta P_{qq}(x/y) \, \Delta q(y, Q^2) + \Delta P_{qG}(x/y) \, \Delta G(y, Q^2)\} \tag{54}$$

$$\frac{d}{d \ln Q^2} \Delta G(x, Q^2) = \frac{\alpha_s(Q^2)}{2\pi} \int_x^1 \frac{dy}{y} \{\Delta P_{Gq}(x/y) \, \Delta q(y, Q^2) + \Delta P_{GG}(x/y) \, \Delta G(y, Q^2)\}, \tag{55}$$

where $\Delta G(x)$ is analogous to $\Delta q(x)$

$$\Delta G(x) = G_+(x) - G_-(x). \tag{56}$$

The ΔP are the polarized *splitting functions* and are calculated perturbatively

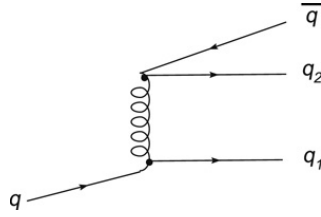$$\Delta P(x) = \Delta P^{(0)}(x) + \frac{\alpha_s}{2\pi} \Delta P^{(1)}(x) \tag{57}$$

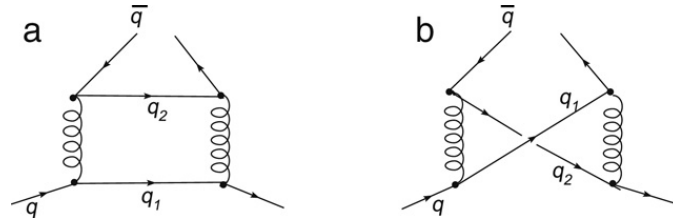**Fig. 13.** NLO amplitude for the $q \to \bar{q}$ transition.

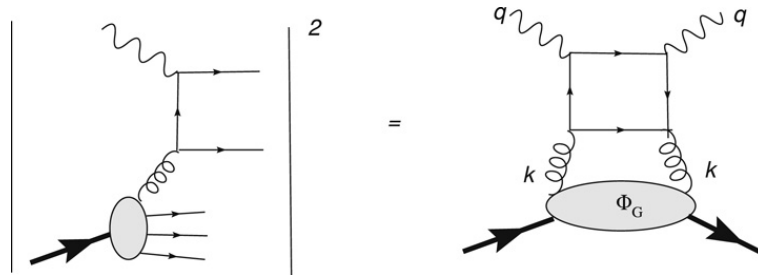**Fig. 14.** NLO contributions to the splitting function for a $q \to \bar{q}$ transition.

Fig. 15. QCD diagram leading to the anomalous gluon contribution.

where the superscripts (0) and (1) refer to LO and NLO contributions. For details about these the reader is referred to [87]. A pedagogical introduction to scheme dependence can be found in Section 11.8 of [93]. For a more complete set of relations between the densities and Wilson coefficients in the various schemes, see [94].

Note that in LO flavor combinations like $q_f - q_{f'}$ (e.g., $u(x) - d(x)$) and valence combinations like $q_f - \bar{q}_f$ (e.g., $u(x) - \bar{u}(x)$) are *non-singlet* and evolve in the same way, without the ΔG term in Eq. (54). (There is no splitting in LO from a q to a $\bar{q}$, nor from, say, a u to a d.) However, in NLO flavor non-singlets like $u(x) - d(x)$ and charge-conjugation non-singlets like $u(x) - \bar{u}(x)$ evolve differently. The origin of this difference can be seen in Figs. 13 and 14. Fig. 13 shows an NLO amplitude for a quark to split into a $\bar{q}$.

Fig. 14 shows two possible contributions to $\Delta P_{q\bar{q}}$ from taking the modulus squared of this amplitude. In (a) the contribution is pure flavor singlet and involves only gluon exchange, whereas in (b) the contribution is non-singlet. However, if we try to do something similar for a flavor changing splitting function e.g. ΔP_{du} we find that we cannot construct the non-singlet diagram.

The expression for $g_1(x, Q^2)$ now becomes

$$
g_1(x, Q^2) = \frac{1}{2} \sum_{flavors} e_q^2 \left\{ \Delta q(x, Q^2) + \Delta \bar{q}(x, Q^2) + \frac{\alpha_s(Q^2)}{2\pi} \right.
$$

$$
\left. \times \int_x^1 \frac{dy}{y} \{ \Delta C_q(x/y) \left[\Delta q(y, Q^2) + \Delta \bar{q}(y, Q^2) \right] + \Delta C_G(x/y) \, \Delta G(y, Q^2) \} \right\} \tag{58}
$$

where ΔC_G and ΔC_q are Wilson coefficients evaluated from the hard part calculated beyond the Born approximation. Note that very often the evolution equations are written using the *convolution notation*, for example,

$$
\Delta C_q \otimes \Delta q \equiv \int_x^1 \frac{dy}{y} \, \Delta C_q(x/y) \, \Delta q(y). \tag{59}
$$

(2) *The gluon contribution to g_1*

Fig. 15 demonstrates a NLO gluon-initiated contribution to DIS.

In the Bjorken limit, for the longitudinal polarized case, this turns out to involve the gluonic version of the famous Adler [95], and Bell and Jackiw [96] anomalous triangle diagram shown in Fig. 16. The net result is that there is an anomalous
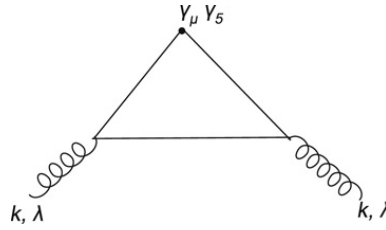
Fig. 16. Feynman diagram responsible for the anomaly.

gluonic contribution to the flavor singlet a_0 [90,97–99]

$$a_0^{gluons}(Q^2) = -3\frac{\alpha_s(Q^2)}{2\pi}\int_0^1 dx\,\Delta G(x, Q^2)$$

$$\equiv -3\frac{\alpha_s(Q^2)}{2\pi}\,\Delta G(Q^2).\tag{60}$$

Note that the factor 3 corresponds to the number of *light* flavors i.e. u, d, s. Heavy flavors do not contribute.
So, there exists potentially a *gluonic* contribution to the first moment of g_1:

$$\Gamma_1^{gluons}(Q^2) = -\frac{1}{3}\frac{\alpha_s(Q^2)}{2\pi}\,\Delta G(Q^2)!\tag{61}$$

This result is of fundamental importance. It implies that the simple parton model formula Eq. (44) for a_0 (and hence for Γ_1^p) in terms of the Δq_f could be considered as incomplete. Instead,

$$a_0 = \Delta\Sigma - 3\frac{\alpha_s}{2\pi}\,\Delta G.\tag{62}$$

However, it should be noted that there is a subtlety concerning Eq. (62). It turns out that the result actually depends on the factorization scheme utilized. Eq. (62) is correct in the AB and JET schemes, but the gluon contribution to a_0 is zero in the $\overline{MS}$ scheme. Now the spin crisis emerged from comparing the size of $\Delta\Sigma$ with what would be expected if the quark spins dominated the nucleon's angular momentum. But in NLO, in the $\overline{MS}$ scheme, $\Delta\Sigma$ varies with Q^2, so one could argue that it cannot be directly interpreted as the spin contribution of the quarks. It is the invariant AB or JET value of $\Delta\Sigma$ which should be interpreted directly as a spin.

The fundamental conclusion is that the small measured value of a_0 does not necessarily imply that the physically meaningful, invariant $\Delta\Sigma$ is small. This discovery was hailed as a resolution of the spin crisis. We shall see later that this seems to be a false hope.

2.3. Experimental determination of polarized parton densities

From the discussion in the previous two sections, it is clear that the bulk of information on polarized parton densities in the nucleon comes from charged lepton scattering experiments in the deep inelastic (DIS) region, with final state masses larger than $W = 2$ GeV and momentum transfers in excess of $Q^2 = 1$ GeV^2. As described in Section 1.2, a vast amount of data on the inclusive spin structure function $g_1(x, Q^2)$ has been accumulated by lepton scattering experiments at SLAC, CERN, DESY and Jefferson Lab. The Particle Data Group's compilation [100] of these data plotted vs. x are shown in Fig. 17 on the left side, while the right side displays the Q^2 dependence of $g_1^p(x, Q^2)$ for several fixed x bins. The observed mild violation of scaling is sensitive to the polarized gluon density (see Sections 2.2 and 2.5). In Section 2.4 we highlight in particular the new data taken at high values of x, where valence quarks dominate the measured spin structure functions. In that region, valence parton densities can be uniquely determined from DIS data on the proton and the neutron.

Inclusive data alone, however, are not able to distinguish the contributions from quark and antiquark densities. One approach to gather additional information has been to use semi-inclusive lepton scattering (SIDIS), where in addition to the scattered lepton one detects a leading hadron (typically a pion or kaon) in the final state. Struck quarks of different flavors have varying probabilities to produce those final state hadrons, as expressed through the various fragmentation functions. These are principally extracted from e^+e^- collision experiments, and still have considerable uncertainties (in particular for kaons). By comparing the asymmetries of semi-inclusive π^+, π^- and K^+, K^- production from protons and neutrons, one can try to separate out the contributions from all quark flavors. This approach was pioneered by the SMC collaboration [27] and the most detailed data set stems from the HERMES collaboration [45,102], as shown in Fig. 18. The COMPASS collaboration has also measured semi-inclusive channels [51].

While the virtual photon in deep inelastic lepton scattering couples directly to the quarks (via their electric charges), gluons can only be probed indirectly in this reaction. Their main influence is in the gentle (logarithmic) evolution of the quark densities with Q^2 (see the r.h.s. of Fig. 17), as outlined in Section 2.2. The resulting violation of Bjorken scaling can be
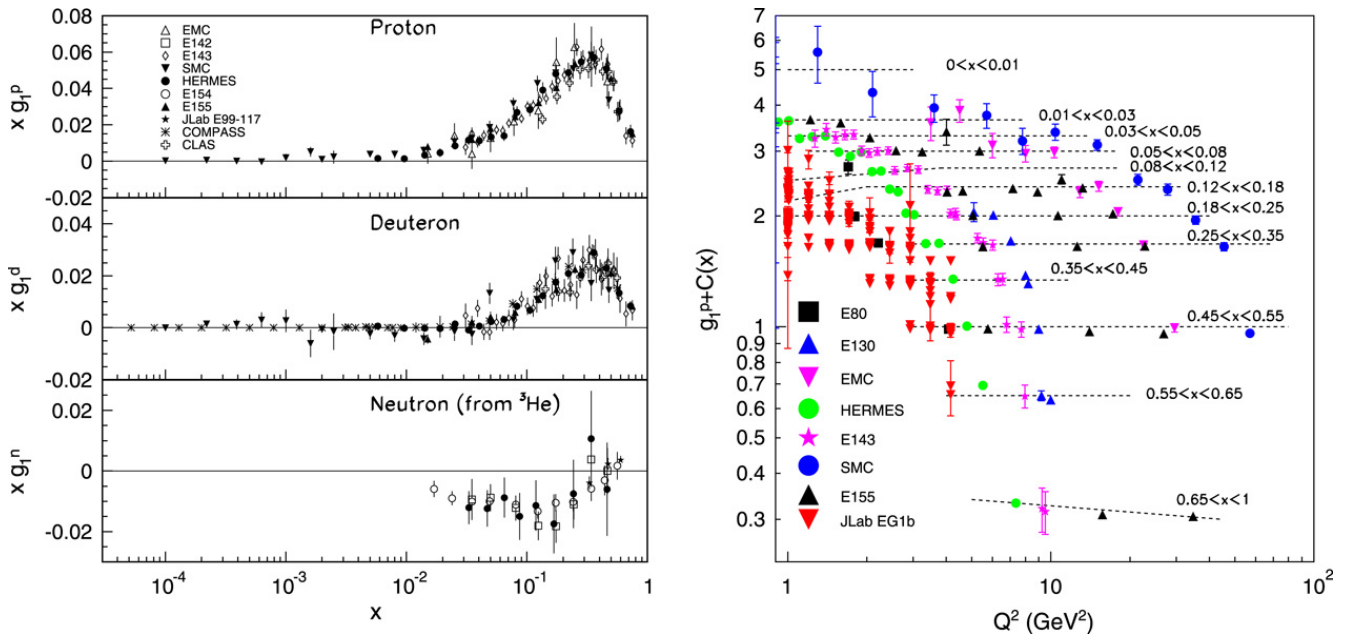
Fig. 17. World data on the polarized structure function $xg_1(x)$ for the proton, deuteron and neutron in the DIS region ($W > 2$ GeV), taken by different experiments, at several different values of Q^2, as compiled by the Particle Data Group [100] (left panel). The proton data are also shown versus Q^2, for several bins in x [101] (right panel; the dashed lines just connect the data to guide the eye). Note that much of the data at very small x is for $Q^2 < 1$ GeV^2.
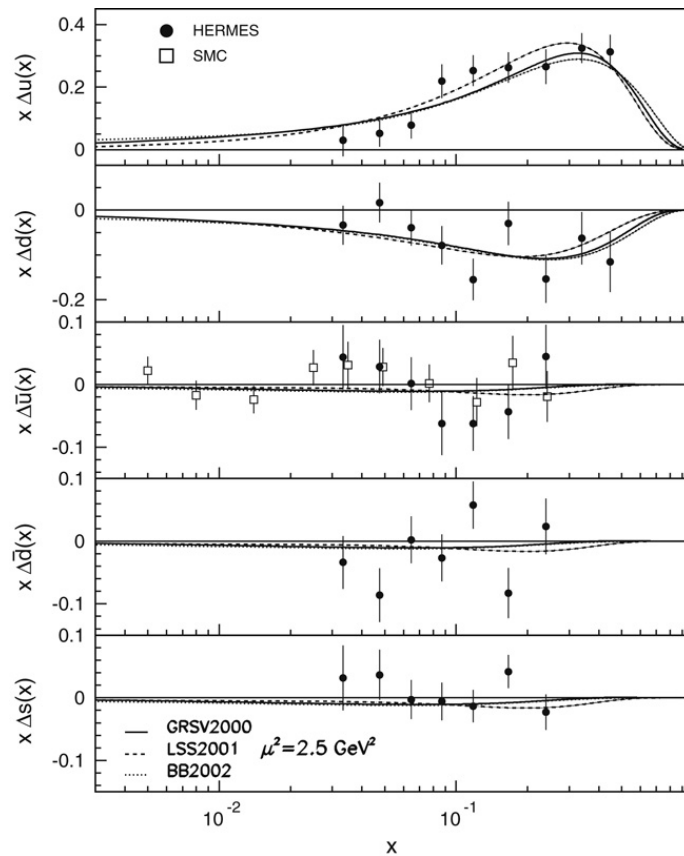
Fig. 18. World data on polarized parton densities $\Delta q(x)$ extracted from semi-inclusive DIS data, as compiled by the Particle Data Group [100].

exploited to extract the contribution of gluons to the nucleon momentum and spin. This has been spectacularly successful in the case of unpolarized DIS, where (thanks to the existence of the lepton–nucleon collider HERA) the range of Q^2 that has been accessed experimentally exceeds 5 orders of magnitude for some (fixed) values of x. The situation is much more difficult in the case of polarized structure functions; so far, only fixed target experiments have measured double spin observables in lepton–nucleon scattering. The highest Q^2 available are of order 100 GeV^2 (using the muon beam at CERN). Recent data from
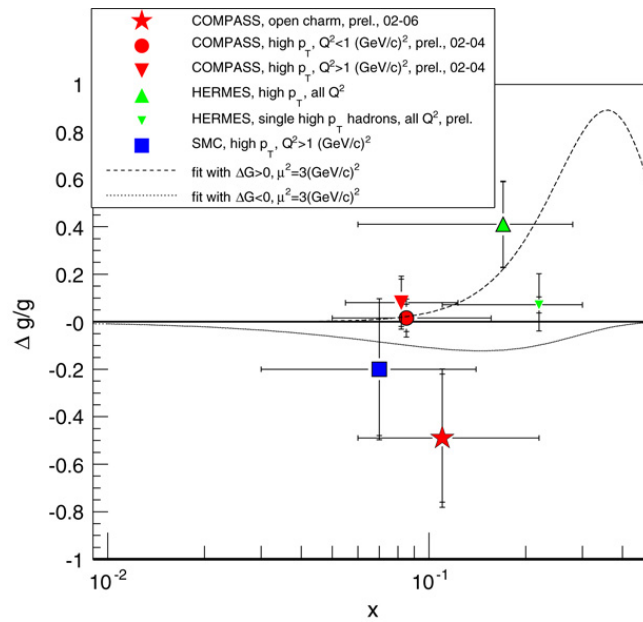
Fig. 19. Results (some preliminary) on the gluon polarization $\Delta G/G$ extracted (at leading order) from photon–gluon fusion processes. (Data compiled by the COMPASS collaboration [103]).

COMPASS [49] have dramatically improved the precision of g_1 at relatively high Q^2 for the deuteron which is an isoscalar target and therefore more sensitive to gluon contributions. For the maximum lever-arm in Q^2, it is important to push for high precision at both extremes of the Q^2 range. In this context, new deuteron results from Jefferson Lab [72] play an important role.

For a direct approach, it is highly desirable to measure observables that are more closely linked to the polarized gluon density in the nucleon, e.g. virtual or real photon–gluon fusion (see Fig. 15) in semi-inclusive lepton scattering or photon absorption, with two quarks in the final state stemming from the splitting of a gluon. In order to distinguish this process from the more copious direct quark diagrams, one has to select either events in which the final state hadrons or jets carry large transverse momentum p_T or where the final state quark has a heavy flavor (e.g., charm) unlikely to stem from the nucleon itself. This approach has been used by HERMES and COMPASS and was to be employed by the (unfortunately terminated) SLAC experiment E161.

The existing results (including preliminary data) are shown in Fig. 19. The new HERMES data point (inverted triangle) is extracted from high-p_T virtual photon production of a single hadron, while the COMPASS data points come from high-p_T hadron pairs or jets and from open charm production data (D^0 and D^*; indicated by the star symbol in Fig. 19). These data put some restrictions on the magnitude of the polarized gluon density $\Delta G(x)$ in the moderate x region to which they are sensitive but still have rather large statistical errors. Also, at present no NLO analyses of these data exist, and backgrounds from "ordinary" SIDIS processes as well as "resolved photon" contributions have to be taken into account.

An alternate route has been employed in the polarized proton collision program at BNL, using the Relativistic Heavy Ion Collider (RHIC). One selects final state signatures like hadrons, jets or even direct photons with large transverse momentum that indicate an underlying hard interaction between two constituents from the two colliding protons. The cross section for the production of this final state can be expressed as a convolution of the parton densities of the two initial protons with the hard parton–parton scattering cross section and the final state fragmentation function (see, e.g., [104]). There is good agreement between the NLO pQCD predictions and data for the unpolarized cross section [54], suggesting that pQCD can be applied reliably to such reactions.

For the double spin asymmetry, one divides the cross section difference for opposite proton spins by the sum. The result depends on products of polarized parton densities; depending on the kinematics one is mostly sensitive to quark–quark, quark–gluon or gluon–gluon subprocesses. While this quadratic dependence does not allow a "naive" direct extraction of polarized parton distributions (not even in LO), the observed asymmetry can be compared to predictions from parametrizations of quark and gluon densities. Fig. 20 shows the preliminary results from PHENIX (π^0 production, [105]) and STAR (jet production, [106]) for the double spin asymmetry A_{LL} versus transverse momentum p_T, compared with several model calculations based on the GRSV parametrization [108] of polarized parton densities. One clearly can see a preference for the curves labeled "$\Delta G = 0$" while some of the more extreme possibilities ($\Delta G = \pm G$) can be excluded. However, depending on the particular overall shape of the polarized gluon distribution with x, non-zero values of the overall first moment of ΔG are not excluded.

The most comprehensive analysis of all DIS, SIDIS and pp data so far has been conducted by de Florian, Sassot, Stratmann and Vogelsang [104]. The authors find good agreement between all data sets, which together yield a preference for the integral over $\Delta G(x)$ from $x = 0.05$ to $x = 0.2$ to be close to zero. For a definite answer on the question "what is the
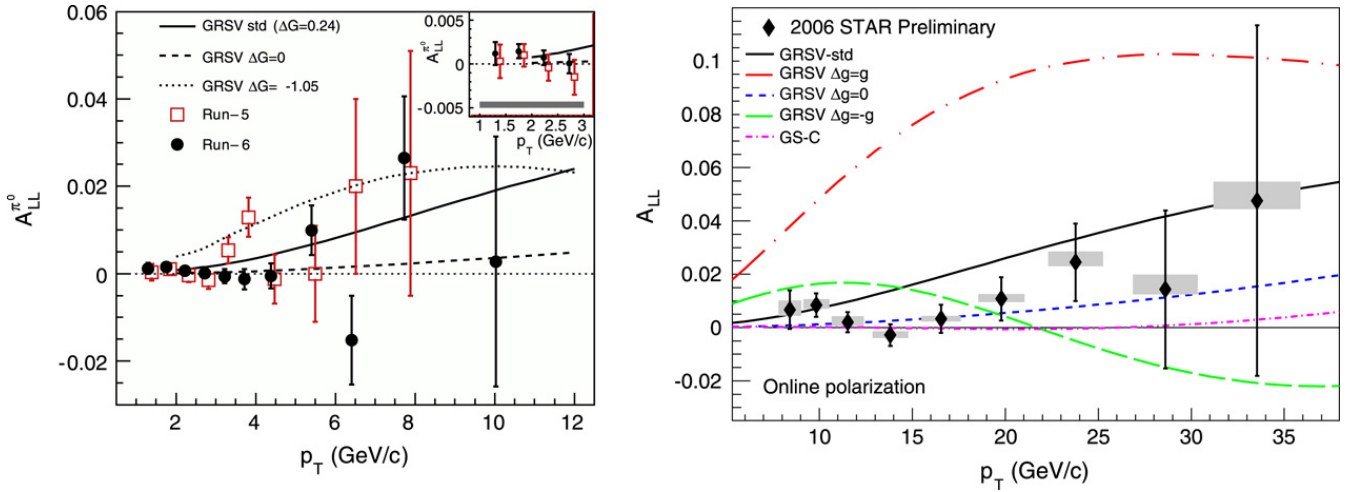
Fig. 20. Double spin asymmetries in high $p_T \pi^0$ production (PHENIX [105], left panel) and jet-production (STAR preliminary [106], right panel) from proton–proton collisions at 200 GeV center-of-mass energy at mid-rapidity. The various curves shown are the NLO pQCD predictions from several versions of the polarized gluon density parametrizations from Vogelsang et al. [107].

contribution ΔG to the nucleon spin" we need additional data that can better constrain the higher and lower x region, to pin down both the shape and overall magnitude of $\Delta G(x)$. These data will be forthcoming from future experiments at JLab (precision measurements of DIS on the deuteron, both at 6 GeV and at 12 GeV beam energy) and the continuation of the COMPASS experiment at CERN, as well as higher precision data for different center-of-mass energies and different final state channels from RHIC.

In Section 2.5, we survey the status of the polarized parton densities extracted from all the data described above.

2.4. Measurements of spin structure in the valence region

The properties of nucleon structure functions in the high-x region are of special interest, because this is where the valence quark contributions are expected to dominate. With minimal sea quark and explicit gluon contributions, it is a clean region to test our understanding of nucleon structure. Relativistic constituent quark models [109,86] should be applicable in this region and perturbative QCD [110] can be used to make predictions in the large x limit.

To first approximation, the constituent quarks in the nucleon are described by SU(6) wave functions with orbital angular momentum of zero. SU(6) symmetry leads to the following predictions [111]:

$$d(x)/u(x) = 1/2; \quad \Delta u(x)/u(x) = 2/3; \quad \Delta d(x)/d(x) = -1/3; \quad A_1^p(x) = 5/9; \quad \text{and} \quad A_1^n(x) = 0. \tag{63}$$

Relativistic Constituent Quark Models (RCQM) with broken SU(6) symmetry, e.g., the hyperfine interaction model [109], lead to a dominance of 'quark–diquark' configurations with the spectator-diquark spin $S = 0$ at high x. This implies that as $x \to 1$:

$$d/u \to 0; \quad \Delta u/u \to 1; \quad \Delta d/d \to -1/3; \quad A_1^p \to 1; \quad \text{and} \quad A_1^n \to 1. \tag{64}$$

In these RCQM models, relativistic effects lead to a non-zero quark orbital angular momentum and reduce the valence quark contributions to the nucleon spin from 1 to 0.6–0.75.

Another approach is leading-order pQCD [110], which assumes the quark orbital angular momentum to be negligible and leads to hadron helicity conservation. For a nucleon with helicity $+1/2$

$$q_{\pm}(x) \to (1-x)^{2n-1+(1\mp1)} \tag{65}$$

as $x \to 1$, where $n = 2$ is the number of spectators. The exponent for q_+ is therefore 3, while the strength of q_- is suppressed by an extra factor of $(1-x)^2$ at large x. This, plus SU(6), leads to:

$$d/u \to 1/5; \quad \Delta u/u \to 1; \quad \Delta d/d \to 1; \quad A_1^p \to 1; \quad \text{and} \quad A_1^n \to 1 \tag{66}$$

in agreement with [112]. Eq. (65) cannot hold at all Q^2, since evolution causes the power of $(1-x)$ to grow like $\log\log Q^2$ at large Q^2, but Eq. (66) should hold at all Q^2.

Not only are the limiting values at $x = 1$ important, but also the behavior as x approaches 1, which is sensitive to the dynamics in the valence quark region. A new approach [113] in pQCD, including quark orbital angular momentum (and therefore not requiring hadron helicity conservation), shows a different behavior at large x region while keeping the same limiting values at $x = 1$. In particular, the approach of $\Delta d/d$ towards unity only sets in at a significant larger x than predicted by hadron helicity conservation (see below).
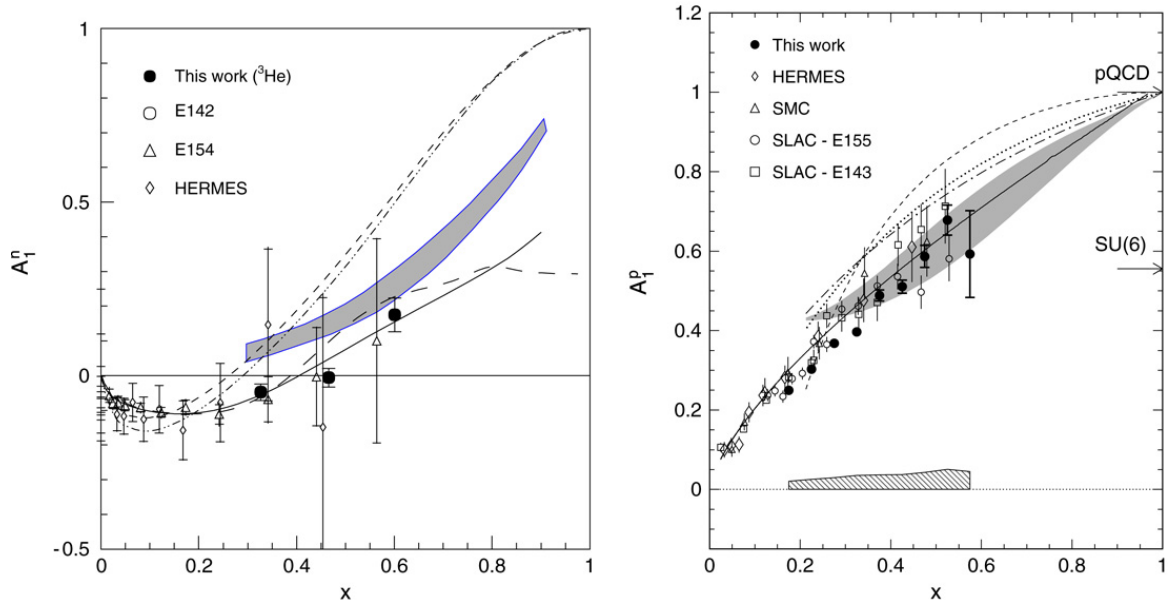
Fig. 21. A_1^n (left panel) and A_1^p (right panel) results from JLab Hall A E99-117 [61,62] and CLAS EG1b [72] experiments (filled circles), compared with the world data and theoretical predictions (see text for details).

Experimentally, it is difficult to access the high-x region because most high-energy experiments so far lacked the necessary luminosity and fine-enough resolution in x. This situation has dramatically changed with the advent of the high-current, moderate energy continuous electron beam at Jefferson Lab.

JLab Hall A experiment E99-117 [61,62] measured the neutron asymmetry A_1^n with high precision in the x region from 0.33 to 0.61 (Q^2 from 2.7 to 4.8 GeV^2). Asymmetries from inclusive scattering of a highly polarized 5.7 GeV electron beam on a high pressure (>10 atm) (both longitudinally and transversely) polarized ^{3}He target were measured. Parallel and perpendicular asymmetries were extracted. After taking into account the beam and target polarizations and the dilution factor, they were combined to form $A_1^{^3\mathrm{He}}$. Using a recent model [68], nuclear corrections were applied to extract A_1^n. The results on A_1^n are shown in the left panel of Fig. 21. The experiment greatly improved the precision of data in the high-x region, providing the first evidence that A_1^n becomes positive at large x, a clear evidence for SU(6) symmetry breaking. The results are in good agreement with the LSS 2001 pQCD fit to previous world data [114] (solid curve) and the statistical model [115] (long-dashed curve). The trend of the data is consistent with the RCQM [109] predictions (the shaded band). The data disagree with the predictions from the leading-order pQCD models [110] (short-dashed and dash-dotted curves). These data provide crucial input for the global fits to the world data to extract the polarized parton densities and the extractions of higher-twist effects.

New results for A_1^p and A_1^d from the Hall B EG1b experiment [72] are also available. The data cover the Q^2 range of 1.4–4.5 GeV^2 for x from 0.2 to 0.6 with an invariant mass larger than 2 GeV. The results on A_1^p are shown in the right panel of Fig. 21. The precision of the data improved significantly over that of the existing world data. Similar data also exist on the deuteron and once again exhibit a trend to exceed the asymmetries predicted by SU(6) (Eq. (63)) at large x. In addition to the prediction by the RCQM model [109] (again indicated by the shaded band), several curves based on different scenarios of SU(6) symmetry breaking as presented in the paper by Close and Melnitchouk [116] are also shown in the right panel of Fig. 21. These scenarios are based on duality arguments and include final state helicity-1/2 dominance (dashed curve), spin-1/2 dominance (dotted) and symmetric wave function suppression (dash-dotted), which is closest to the data.

The polarized quark distribution functions $\Delta u/u$ and $\Delta d/d$ in the high-x region were first extracted, in the leading-order approximation, from the Hall A neutron data and the world proton data (left panel of Fig. 22) [61,62]. A recent leading-order extraction used the CLAS EG1b proton and deuteron data [72] as well. The results are shown in the right panel of Fig. 22, along with predictions from leading-order pQCD [110] (dashed curves) and a pQCD fit (solid line) including quark orbital angular momentum contributions [113]. The results of $\Delta d/d$ are in significant disagreement with the predictions from the leading-order pQCD model assuming hadron helicity conservation. Data agree better with the fit including quark-orbital angular momentum contributions, suggesting that the quark orbital angular momentum may play an important role in this kinematic region.

2.5. Status of polarized parton densities

From measurements of $g_1(x, Q^2)$ at various values of x and Q^2, one can, in principle, via Eq. (58), extract the quark and gluon polarized parton densities. We shall first consider general issues related to the determination of the parton densities and then discuss what is known about the densities themselves.
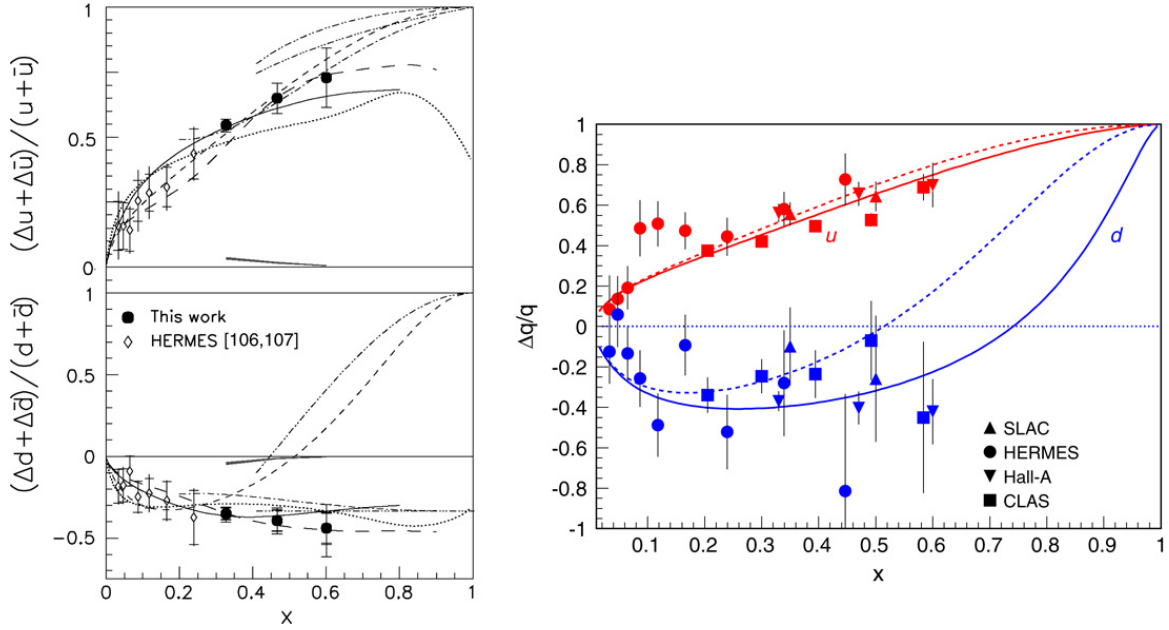
Fig. 22. $\Delta u/u$ (upper side of both panels) and $\Delta d/d$ (lower side of both panels) results from JLab Hall A E99-117 [61,62] (left panel) and from CLAS EG1b [72] (right panel), compared with the world data and theoretical predictions (see text for details).

(1) *General properties of the parton densities*

- In DIS, one can only obtain information on the combinations $\Delta q(x, Q^2) + \Delta \bar{q}(x, Q^2)$, i.e., there is no information at all about the $\Delta \bar{u}$ and $\Delta \bar{d}$ sea quarks, though $\Delta s + \Delta \bar{s}$ is determined. Nonetheless, in presenting results, some authors use conventions such as $\Delta \bar{u} = \Delta \bar{d} = \Delta \bar{s}$, or variants thereof, in order to show results for the valence quarks. It is important to bear in mind that these results are not physical and are entirely convention-dependent.

- To determine $\Delta \bar{u}$ and $\Delta \bar{d}$ one needs to study semi-inclusive deep inelastic scattering or semi-inclusive hadron–hadron reactions, where, however, one also needs information about fragmentation functions.

- Because the gluon has zero electric charge it does not couple directly to the photon, so it contributes in Eq. (58) only in NLO. However, as shown in Eq. (54), it also plays a role in the evolution of the parton densities, but since the evolution is only logarithmic and the lever arm in Q^2 of present day experiments is relatively small (*much* smaller than in the unpolarized case), there is considerable uncertainty about the form and magnitude of $\Delta G(x, Q^2)$.

- The parametrizations assumed for the $\Delta q(x)$ at some value of Q^2 follow general intuition based on the parton model. In particular, if the $q_{+,-}(x)$ are regarded as positive number densities then, via Eqs. (36) and (37) one imposes the *positivity* condition

$$|\Delta q(x)| \leq q(x). \tag{67}$$

It can be shown that if positivity holds at some Q_0^2, then it is preserved under evolution to larger values of Q^2 [117, 15], but care must be taken since there are fits to the *unpolarized* data with parton densities which are *negative* at $Q^2 = 1$ GeV/c^2 [118]! This is possible because in the unpolarized case one has the luxury of using only data typically with $Q^2 \geq 4$ GeV/c^2, by which point the density has evolved into a positive one.

- There is some guidance as to the behavior as $x \to 1$. Perturbative QCD arguments [112] suggest that quark densities vanish like a power of $(1 - x)$ which depends on the helicity; see the discussion in Section 2.4. In practice the exponents of $(1 - x)$ are left as free parameters to be determined in the fit to the data, and tend to come out close to the expected values.

- What the behavior should be as $x \to 0$ is not very clear. Based on the correspondence between $x \to 0$ in the structure functions, and energy $\nu \to \infty$ in virtual-photon Compton scattering, one would expect the power of x to be controlled by the leading Regge intercept i.e.

$$g_1(x) \sim x^{-\alpha} \tag{68}$$

where α is the intercept of the $a_1(1260)$ meson Regge trajectory in the isovector channel, and the $f_1(1285)$ meson trajectory in the isoscalar channel [119]. These intercepts are not well known (see discussion in [13]). Roughly

$$-0.4 \leq \alpha_{a_1} \approx \alpha_{f_1} \leq -0.18.$$

However, we know that for unpolarized DIS the effective power α increases with Q^2 for the range of x explored thus far, contrary to the Regge picture, and this is explained as due to QCD evolution (soft Pomeron vs. hard Pomeron). Bass [120] suggests that something similar might be expected for the polarized case.
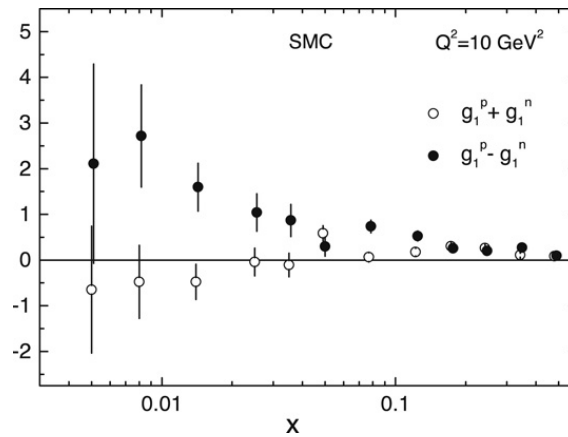
Fig. 23. Comparison of $g_1^p \pm g_1^n$.

Study of the small x behavior of the DGLAP evolution equations [121] yields parton densities that grow more rapidly than any power of $\ln(x_0/x)$ (where x_0 is the upper limit where the treatment is valid), and the growth rate increases with Q^2. On the other hand summation of double logarithmic terms at small x, which are not included in DGLAP, leads to the expectation $C_s x^{-a_s}$ and $C_{ns} x^{-a_{ns}}$ for the singlet and non-singlet contributions to g_1 respectively (The coefficients C are sensitive to the structure of the parton densities). This was originally studied in [122,123] using a constant, non-running value of α_s and later by Ermolaev, Greco and Troyan [124] using a running coupling. Both approaches give the same structure with $a_s > a_{ns}$, but with somewhat different numerical values of the powers of x. In [124] the intercepts are

$$a_s \approx 2\, a_{ns} \approx 0.86,$$

implying that the singlet flavor combination $(g_1^p + g_1^n)$ should diverge more rapidly than the non-singlet combination $(g_1^p - g_1^n)$ as x goes to zero. Thus one would expect

$$|g_1^p + g_1^n| \geq |g_1^p - g_1^n| \quad \text{as } x \to 0. \tag{69}$$

The only data on both flavor combinations at extremely small x values *and* $Q^2 \geq 1$ GeV^2 are from the SMC experiment [125] shown in Fig. 23, where precisely the opposite trend is visible. COMPASS data on the deuteron further confirm the smallness of the flavor singlet (see Fig. 17). Further information will become available when COMPASS publish their new data on g_1^p. However, as experiments probe smaller and smaller x, there ought to be a dramatic change in the trend of the data, or else the theoretical arguments are incomplete. Indeed Blümlein and Vogt [126] suggest that corrections for sub-leading terms could significantly change these results. (A more detailed discussion can be found in Section 11.8 of [93]; for possible connections to the infrared renormalon model see the work of Kataev [127]).

It is also argued [110] that

$$\frac{\Delta G(x)}{G(x)} \propto x \quad \text{as } x \to 0. \tag{70}$$

Again, in practice, the power of x is taken as a parameter to be determined by the fit to the data.

- As explained in Section 2.2 there is, alas, no absolute physical meaning to parton densities in QCD. One has to specify in what factorization scheme they are determined. Although the differences between densities in different schemes are proportional to $\alpha_s(Q^2)$, these differences can be surprisingly large for the smaller densities e.g. $\Delta s(x)|_{\overline{MS}} \approx 2\,\Delta s(x)|_{JET}$ at $Q^2 = 1$ GeV/c^2 [94].
- Although there has been a tremendous increase in the amount and quality of polarized data in the past few years, it is still usual to impose, rather than test, the various sum rules (Bjorken, $SU(3)_{flavour}$) which should be satisfied by the quark densities. For a discussion of sum rule tests, see Section 3.2.
- It is important to appreciate that the QCD formula for $g_1(x, Q^2)$, Eq. (58), is a *leading twist* (LT) expression, i.e. it neglects terms of order M^2/Q^2. For experiments at relatively low values of Q^2 the expression Eq. (58) must be supplemented by *higher twist* (HT) terms. There are two types of HT terms: target mass corrections, which are purely kinematical, and dynamical corrections. The target mass corrections can be calculated exactly and were first given in a closed form for g_1 by Piccione and Ridolfi [128]. For a new approach, see also [129]. The details and Q^2 evolution of the dynamical HT terms are not known, so they are simply parametrized in the form $h(x)/Q^2$, with $h(x)$ determined, after applying the target mass corrections, from experiment at a few values of x. For access to the literature see [130].
- It is well known that parton densities extracted in LO and NLO sometimes differ significantly, and one may therefore worry about the effect of NNLO etc. corrections. Some indication of the reliability of the NLO approximation can be obtained via the LSS Transformation Test [94]. In each order of perturbative QCD there exist transformation formulae relating parton densities in different factorization schemes. Let us indicate this symbolically for two schemes, A and B:

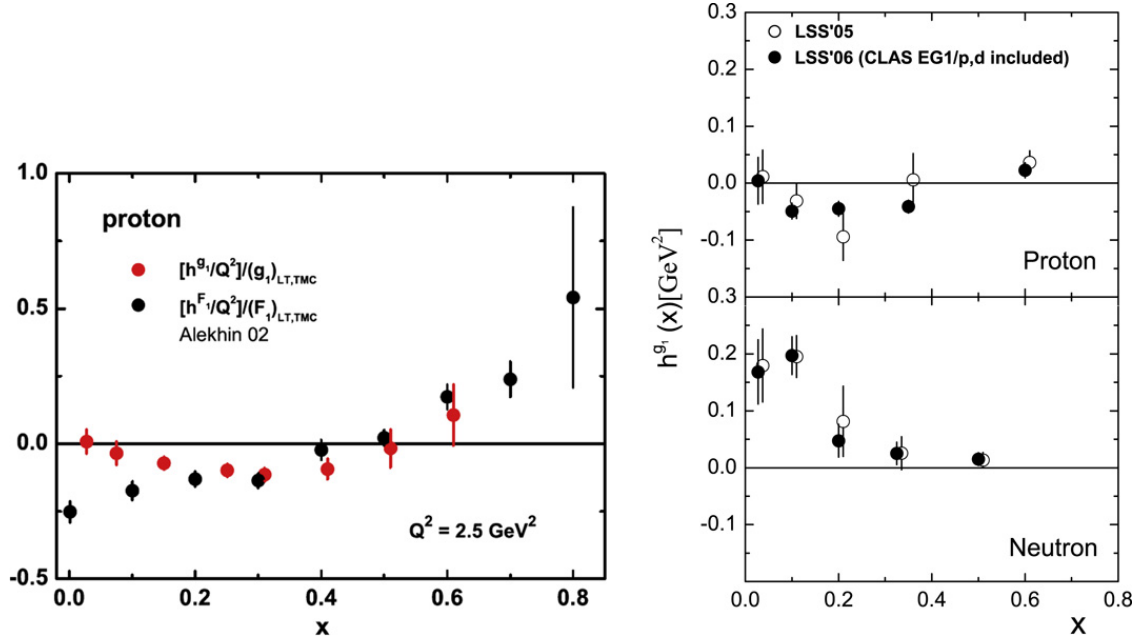$$\Delta q(x)|_B = T_{B \leftarrow A}\, \Delta q(x)|_A. \tag{71}$$

Fig. 24. Comparison of HT terms in g_1 and F_1 (left panel) and higher twist terms for protons and neutrons extracted from data (right panel).

Suppose now that $T_{B \leftarrow A}$ is known to NLO accuracy, and the parton densities are extracted from the data, *independently*, in NLO, using schemes A and B, with results $\Delta q(x)|_{A,B}^{data}$, respectively. If the densities can be extracted reliably in NLO i.e. NNLO effects are unimportant, then one should find

$$\Delta q(x)|_B^{data} = T_{B \leftarrow A} \, \Delta q(x)|_A^{data} . \tag{72}$$

Any failure of this equality is a measure of the importance of NNLO effects. Thus the ratio

$$\frac{\Delta q(x)|_B^{data} - T_{B \leftarrow A} \, \Delta q(x)|_A^{data}}{\Delta q(x)|_B^{data} + T_{B \leftarrow A} \, \Delta q(x)|_A^{data}}$$

gives some indication of the reliability of the parton densities.

A detailed discussion of many of the above issues can be found in [131].

(2) Extraction of parton densities from DIS

Following upon the remarkable EMC experiment in 1988, there have been many new data on polarized DIS and many QCD analyses. We shall only be concerned with the recent analyses which have included all or most of the present world data, namely, Leader, Sidorov and Stamenov (LSS'05 and LSS'06) [7,130], Alexakhin et al. (COMPASS'06) [49], Hirai, Kumano and Saito (AAC'03) [132], Blümlein and Böttcher (BB) [133] and Glück, Reya, Stratmann and Vogelsang (GRSV2000) [108]. We shall also comment on the ground-breaking paper of de Florian, Sassot, Stratmann and Vogelsang (DSSV) [104] which analyzed simultaneously data on DIS, SIDIS and pion production in polarized pp collisions at RHIC, and on the work of Hirai and Kumano (AAC'08) [134] who analyzed data on DIS and on pion production at RHIC. Details of the parametrizations etc. can be found in the papers cited and also on the Durham HEP databases website [135].

One of the problems in any analysis is to decide whether to use the lowest twist (LT) expression Eq. (58) or to include higher twist (HT) terms. This is not just a question of the kinematic region in a given experiment, but also of what quantity one fits. Thus long ago we discovered empirically that HT terms cancelled out in the ratio $\frac{g_1}{F_1}$. Put

$$g_1^{EXP} = g_1^{LT} + g_1^{HT} \qquad F_1^{EXP} = F_1^{LT} + F_1^{HT} .$$

Then

$$\left[\frac{g_1}{F_1}\right]^{EXP} \approx \frac{g_1^{LT}}{F_1^{LT}} \left[1 + \frac{g_1^{HT}}{g_1^{LT}} - \frac{F_1^{HT}}{F_1^{LT}}\right]$$

$$\approx \frac{g_1^{LT}}{F_1^{LT}} \tag{73}$$

provided there is a cancellation between $\frac{g_1^{HT}}{g_1^{LT}}$ and $\frac{F_1^{HT}}{F_1^{LT}}$.

The left panel of Fig. 24 which compares HT terms for g_1 [130] and for F_1 [136] demonstrates the validity of this for $x \geq 0.15$, but clearly indicates that ignoring HT terms in the ratio $\frac{g_1}{F_1}$ below $x = 0.15$ is incorrect. The HT terms for g_1
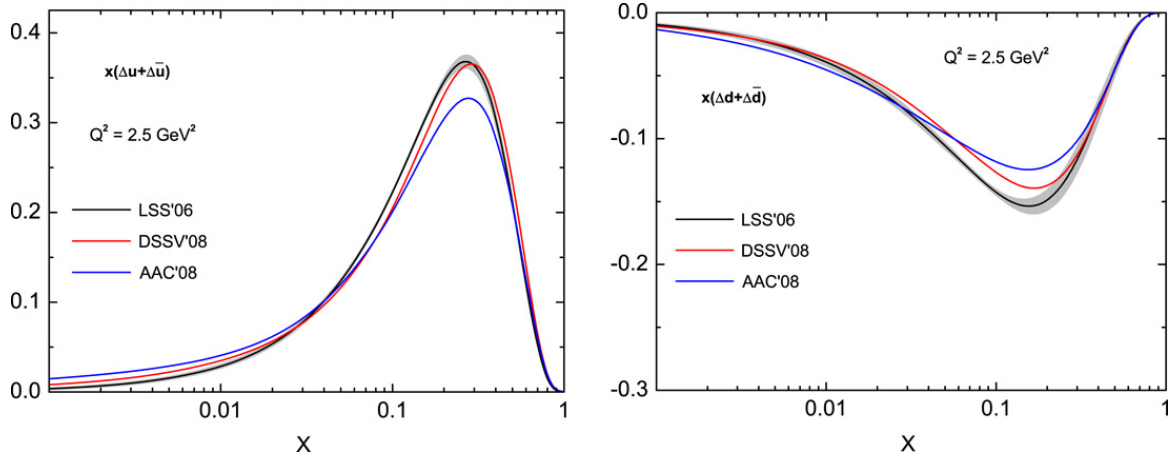
Fig. 25. Comparison of LSS'06 (with shaded error band), DSSV and AAC'08 ($\overline{MS}$) $x(\Delta u + \Delta \bar{u})$ and $x(\Delta d + \Delta \bar{d})$ densities.
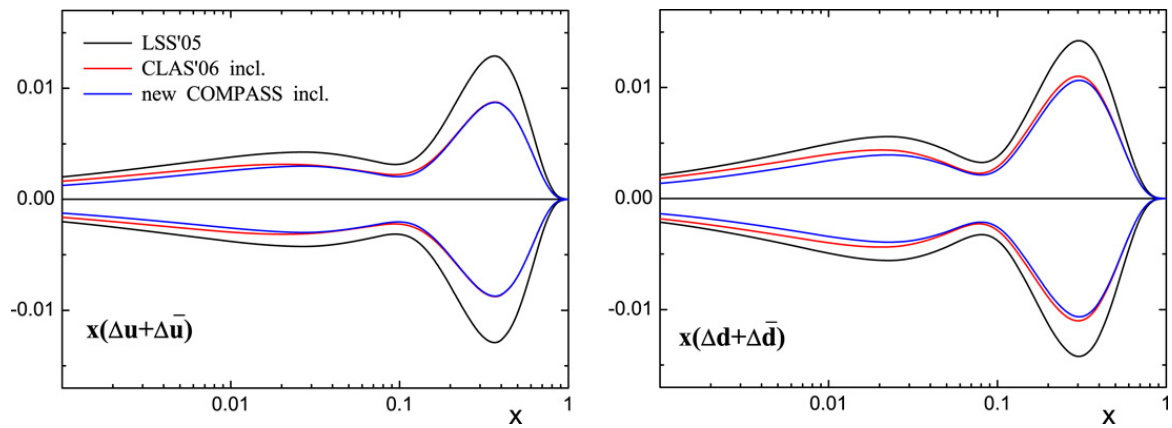

Fig. 26. Impact of CLAS'06 and COMPASS'06 data on the uncertainties in $x(\Delta u + \Delta \bar{u})$ and $x(\Delta d + \Delta \bar{d})$ of the LSS'05 analysis.

determined in [130] are shown in the right panel of Fig. 24 using 5 bins in x. (The results change negligibly if 7 bins are utilized.)

A more subtle problem relates to the kinematic relations between various quantities. The exact relations between $A_\parallel$, A_1 and g_1 include HT terms involving γ^2, both in Eq. (32) and in the expression for D, Eq. (26). If it is safe to ignore HT terms in g_1, F_1 is it safe to ignore them in these kinematic relations as well? DSSV assume it is, whereas LSS insist that if γ^2 is significant such terms must be kept in the kinematic relations. The validity of the latter viewpoint is borne out by the empirical fact (accidental?) that HT terms can be ignored in $\frac{g_1}{F_1}$ in the region $x \geq 0.15$, where, in some cases, γ^2 is non-negligible. Thus the DSSV analysis, which treats $\frac{g_1}{F_1}$ in LT, but ignores γ^2, may be unreliable in those regions where γ^2 is important. This issue is particularly important for data from HERMES and JLab.

- *The light quark densities.* There is broad agreement between the various analyses for the $\Delta u(x) + \Delta \bar{u}(x)$ and $\Delta d(x) + \Delta \bar{d}(x)$ parton densities. Generally the constraint Eq. (66) has not been enforced in the parametrizations used for the d quark. Early data demanded negative values of $\Delta d(x) + \Delta \bar{d}(x)$ and continued to do so even when the measured region was extended to $x = 0.6$ at Jefferson Laboratory [61,72]. These data are discussed in detail in Section 2.4. Note that a fit [137] using the Brodsky, Burkardt and Schmidt type parametrization [110], which respects Eq. (66), led to a $\Delta d(x) + \Delta \bar{d}(x)$ which became positive just beyond $x = 0.6$. With the 12 GeV upgrade at Jefferson it should be possible to explore out to $x = 0.8$ and to settle the matter. Fig. 25 shows a comparison between the LSS'06, DSSV and AAC'08 $\Delta u + \Delta \bar{u}$ and $\Delta d + \Delta \bar{d}$ densities. It is seen that the agreement is impressive, although the d-quark polarization $\Delta d(x)/d(x)$ is still rather uncertain at high x (see also Section 2.4).

  In Fig. 26 we show the impact of the CLAS'06 and COMPASS'06 data on the uncertainties in $x(\Delta u + \Delta \bar{u})$ and $x(\Delta d + \Delta \bar{d})$ which had been found in the LSS'05 analysis. The uncertainties are estimated by the usual Hessian method, utilizing $\Delta \chi^2 = 1$. It should be borne in mind that these uncertainties, and all those to follow, must be treated with caution. They are calculated relative to a chosen analytical form for the parametrization of the parton density and do not at all reflect possible uncertainties in the form of parametrization.

- *The polarized strange quark density.* This is a highly controversial issue at present. All analyses of purely DIS data have found negative values for $\Delta s(x) + \Delta \bar{s}(x)$. Fig. 27 shows the impact of the CLAS'06 and COMPASS'06 data on the uncertainty in the LSS'05 determination of $x(\Delta s(x) + \Delta \bar{s}(x))$.
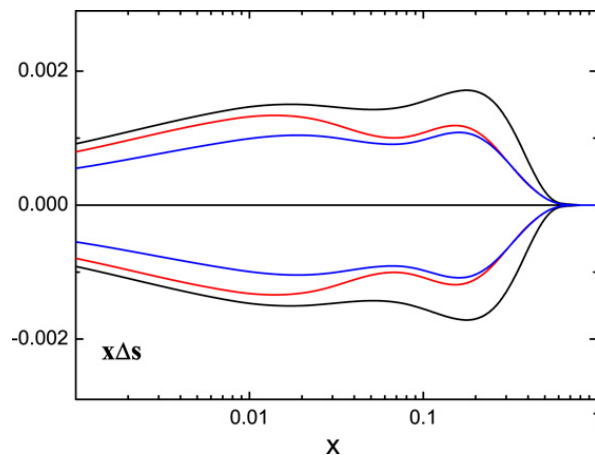
Fig. 27. Impact of CLAS'06 and COMPASS'06 data on uncertainties in the LSS'05 determination of $x(\Delta s(x) + \Delta \bar{s}(x))$. For curve labels see Fig. 26.

An important quantity is the first moment

$$\Delta S \equiv \int_0^1 dx [\Delta s(x) + \Delta \bar{s}(x)]. \tag{74}$$

LSS'06 [130] give for its value

$$\Delta S_{\overline{MS}} = -0.126 \pm 0.010 \qquad \text{at } Q^2 = 1 \text{ GeV}^2 \tag{75}$$

and in [138] it was shown that a positive value for the first moment would imply a huge breaking of $SU(3)_F$ invariance, far greater than the $\pm 10\%$ breaking estimated by Ratcliffe [139]. Nonetheless analyses of SIDIS data for kaon production have suggested positive values of $\Delta s(x) + \Delta \bar{s}(x)$ for $x \geq 0.03$. A hint of this first emerged in the HERMES analysis of 2004/5 [140] and was confirmed by the more precise data reported in [102] where the first moment for the measured range $0.02 \leq x \leq 0.6$ was given as

$$\Delta S = 0.037 \pm 0.019(stat.) \pm 0.027(sys.). \tag{76}$$

One could argue that the HERMES results should not be taken too seriously, since the analyses were carried out in LO and relied on derived quantities called *purities*, whose accuracy may have been overestimated. However, the recent combined analysis of DIS, SIDIS and $pp \rightarrow \pi^0$ or jet $+X$ by the DSSV group [104], which is an $\overline{MS}$ NLO, LT analysis, also finds positive values for $\Delta s(x) + \Delta \bar{s}(x)$ for $x \geq 0.03$, yet ends up with a negative first moment $\Delta S = -0.114$ at $Q^2 = 10 \text{ GeV}^2$. This is achieved by $\Delta s(x) + \Delta \bar{s}(x)$ becoming negative below roughly $x = 0.02$. But there are essentially no data in the latter region, which suggests this must be caused by the need to satisfy the $SU(3)_F$ symmetry condition Eq. (46). DSSV state that they do *not* impose $SU(3)_F$ symmetry, and they multiply the RHS of Eq. (46) by $(1 + \epsilon_{SU(3)})$ where $\epsilon_{SU(3)}$ is a free parameter. However, a χ^2 bias against large values of $\epsilon_{SU(3)}$ is built into the minimization procedure[1] which explains the turning negative of $\Delta s(x) + \Delta \bar{s}(x)$, although this is not stated in the quoted paper.

The recent AAC'08 analysis [134], based on the world data on DIS plus the π^0 production data from RHIC (incorporated at LO), also finds a negative strange quark density. Fig. 28 compares the LSS'06 version of $\Delta s + \Delta \bar{s}$ with that of DSSV and AAC'08. Note that the shape appears somewhat different in the various DIS analyses. The origin of this has been traced to the different choices of unpolarized densities used in the imposition of positivity [141], as can be seen in the figure.

It is thus clear that the origin of the positive values for $\Delta s(x) + \Delta \bar{s}(x)$ lies entirely in the SIDIS data. It may be significant that both the HERMES and DSSV analyses utilize the recent de Florian, Sassot and Stratmann [142] set of fragmentation functions, which are surprisingly different from earlier sets of fragmentation functions, especially for kaons. COMPASS are studying the dependence of $\Delta s(x) + \Delta \bar{s}(x)$ on the choice of fragmentation functions. A preliminary report can be found in the talk of R. Windmolders at the SPIN2008 Conference.

Finally, there is an intriguing question as to whether the standard collinear analysis should be applied to the SIDIS data. The point is the following. What we mean by any $q(x, Q^2)$ or $\Delta q(x, Q^2)$ actually involves an integral over the intrinsic transverse momentum k_t of the quark up to a maximum $k_t^2 \approx Q^2$. If, as is the case for some of the SIDIS data, the magnitude of the transverse momentum of the detected hadron is less than Q, then it is perhaps incorrect to analyze the data using the conventional collinear densities. Indeed, Bass [143] has shown that for that part of the strange quark density generated via photon–gluon fusion the *sign* of ΔS is sensitive to the upper limit in the k_t^2 integration, but the overall effect is much too small to be relevant.

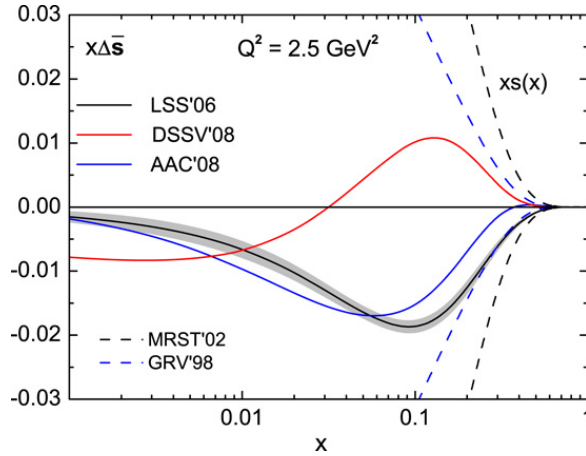[1] Private communication from Werner Vogelsang.

Fig. 28. LSS'06, DSSV and AAC'08 ($\overline{MS}$) versions of $x(\Delta s + \Delta \bar{s})$.

- *The flavor singlet first moment* $\Delta \Sigma$. All the modern global analyses obtain compatible values for $\Delta \Sigma$. In the $\overline{MS}$ scheme, where $a_0(Q^2) = \Delta \Sigma (Q^2)$ they find at $Q^2 = 4 \, \text{GeV}^2$:

LSS'06	COMPASS'06	AAC'08	DSSV
0.24 ± 0.04	0.29 ± 0.01	0.25 ± 0.05	0.24

For reasons which are not understood these values are somewhat lower than the values obtained directly from Γ_1^d as discussed in Section 3.2.

- *The polarized gluon density.* In Section 2.2 we explained how the "spin crisis in the parton model" could be alleviated by generating the experimentally small value of a_0 through a cancellation between relatively large values of $\Delta \Sigma$ and ΔG (see Eq. (62)). Present day estimates are $a_0 \approx 0.2$. Thus demanding $\Delta \Sigma \approx 0.6$ requires, for the first moment,

$$\Delta G \approx 1.7 \quad \text{at } Q^2 = 1 \, \text{GeV}^2. \tag{77}$$

The question is whether this is compatible with what we know about the polarized gluon density.

There are three ways to access $\Delta G(x)$: via polarized DIS, and via the measurement of the asymmetry A_{LL} both in SIDIS production of charmed quarks or high p_T jets, and in semi-inclusive polarized pp reactions at RHIC. Here we will only discuss DIS. The latter approaches have been treated in Section 2.3.

In determining the parameters of the polarized gluon density from fits to the data on $g_1(x, Q^2)$, it should be remembered, as already mentioned, that the main role of the gluon is in the evolution with Q^2, but that the range of Q^2 is very limited, so the determination of $\Delta G(x)$ is imprecise.

For a long time all analyses seemed to indicate that $\Delta G(x)$ was a positive function of x. LSS used a very simple parametrization

$$x\Delta G(x) = \eta_g A_g x^{a_g} [xG(x)] \tag{78}$$

where A_g is fixed so that the first moment of ΔG is given by η_g. In the minimization procedure there was nothing to stop η_g from being negative. Yet the best χ^2 values always corresponded to positive $\Delta G(x)$. With the inclusion of recent
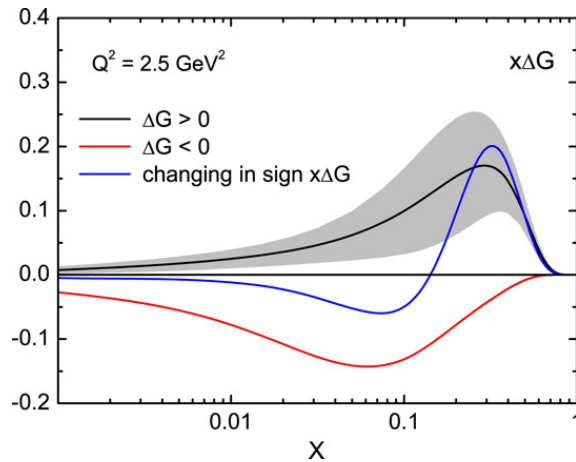

Fig. 29. Comparison of the three types of LSS'06 ($\overline{MS}$) $x\Delta G(x)$.
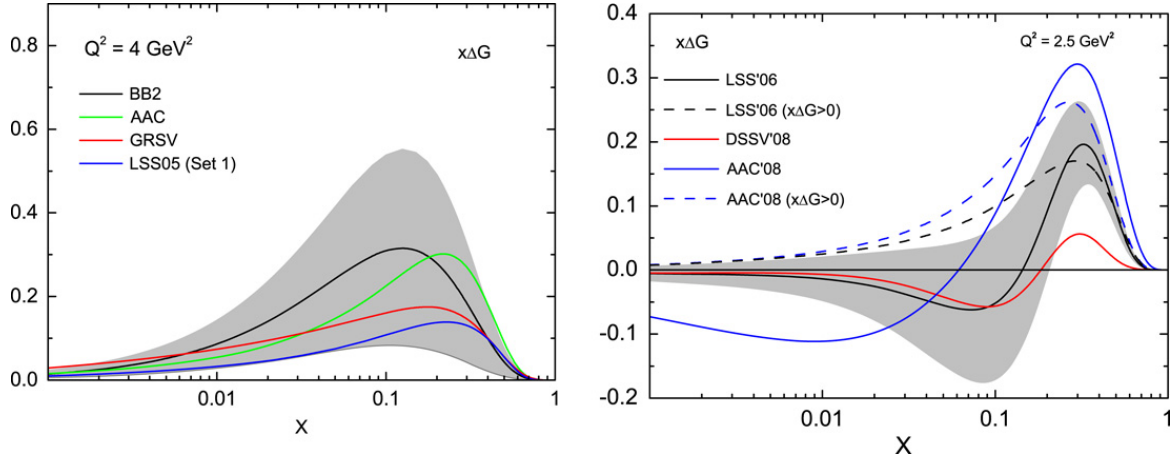
Fig. 30. Left: a compilation of earlier results for $x\Delta G(x)$; right: present situation.
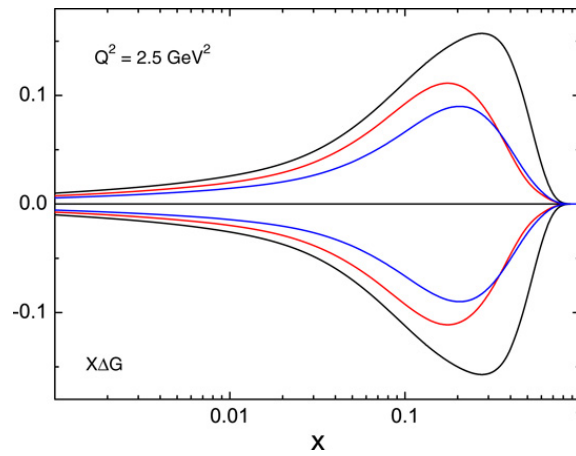
Fig. 31. Impact of CLAS'06 and COMPASS'06 data on uncertainties in the LSS'05 determination of $x\Delta G(x)$. For curve labels see Fig. 26.

data, LSS'06 [130] find equally good fits with positive, negative and sign-changing $\Delta G(x)$, *provided* higher twist terms are included. The latter are particularly demanded by the CLAS'06 data [72]. Fig. 29 compares the LSS'06 positive, negative and sign-changing versions of $\Delta G(x)$.

Also the COMPASS'06 analysis [49], even though HT terms are not included, finds acceptable negative $\Delta G(x)$ fits, but has some peculiarities (linked to the fact that the flavor combinations $\Delta q_{3,8}$ and $\Delta \Sigma$ are parametrized, rather than the individual quark densities), which suggest it may not be very physical. The DSSV analysis finds a sign-changing $\Delta G(x)$, while the AAC'08 analysis finds both positive and sign-changing densities. In the left hand panel of Fig. 30 we show various results for $\Delta G(x)$ as of a couple of years ago. The right panel shows the present situation. In Fig. 31 we show the impact of the CLAS'06 and COMPASS'06 data on the uncertainty in the LSS'05 determination of $x\Delta G(x)$.

Regarding the present data, in all fits, and irrespective of the form of the gluon density, the magnitude is always found to be very small. Typically one has $|\Delta G| \approx 0.29 \pm 0.32$, *much* smaller than the desired 1.7 ! As discussed in Section 2.3, all the present data on SIDIS and pp reactions are perfectly compatible with this very small magnitude for ΔG and cannot distinguish between the various sign possibilities.

2.6. The spin structure function g_2

The spin structure function g_2, unlike g_1 and F_1, does not have an intuitive interpretation in the simple quark–parton model. To understand g_2 properly, it is best to start with the operator product expansion (OPE) method (see also Sections 2.1, 2.5, 3.1 and 3.4). In the OPE, neglecting quark masses, g_2 can be cleanly separated into a twist-2 and a higher twist term:

$$g_2(x, Q^2) = g_2^{WW}(x, Q^2) + g_2^{H.T.}(x, Q^2) . \tag{79}$$

The leading-twist term can be determined from g_1 as [9]

$$g_2^{WW}(x, Q^2) = -g_1(x, Q^2) + \int_x^1 \frac{g_1(y, Q^2)}{y} dy \tag{80}$$

Fig. 32. Results for g_2 of the proton and the deuteron (top-left panel) and the neutron (top-right panel) as a function of x from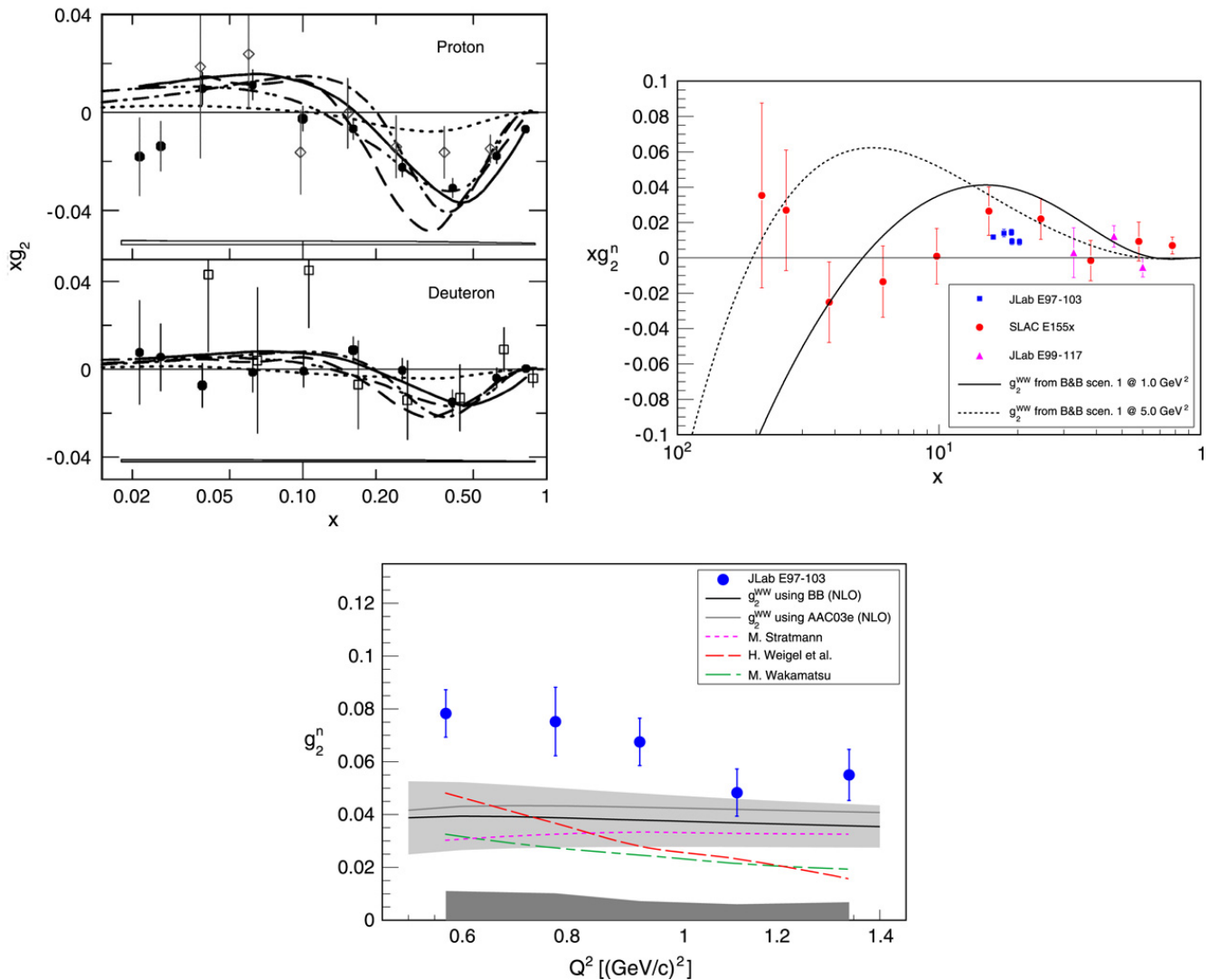 SLAC [41] and JLab Hall A [62,63], in comparison with g_2^{WW} (solid curves). The left panel also shows bag model calculations of Stratmann [147] (dash-dot-dot) and Song [148] (dot) and the chiral soliton models of Weigel [149,150] (dash dot) and Wakamatsu [151] (dash). The bottom plot shows results for g_2^n from JLab Hall A [63] as a function of Q^2 at an x value around 0.2, in comparison with g_2^{WW} and models.

(this holds also with the inclusion of TM corrections [144]), and the higher-twist term $g_2^{H.T.}(x, Q^2)$ arises from quark–gluon correlations. Therefore, g_2 provides a clean way to study higher-twist effects.

Experimentally, g_2 can be extracted from combined measurements of both the longitudinal and the transverse target spin cross section differences (Eqs. (14) and (15) in Section 1.1), or the corresponding asymmetries $A_\parallel$, $A_\perp$. These measurements demand high precision and large luminosity, since the factors multiplying g_2 tend to be relatively small in DIS kinematics. Several experiments [31,40,145,146] therefore took only enough statistics on the transverse target configuration to reduce the systematic error on g_1 due to the unknown contribution from g_2 below the statistical error, yielding only crude information on g_2 itself.

Two experiments at SLAC, E143 and E155 [34,41] took dedicated data to measure g_2 and the virtual photon asymmetry A_2 (see Eq. (23)) with more precision. The most extensive data set in the DIS region comes from the second run of E155, both for the proton and the deuteron, with g_2 for the neutron extracted from the difference. The general trend of these data follows the Wandzura–Wilczek form (Eq. (80)), but some deviations are seen for the proton, especially at small x. The data on A_2 show that this asymmetry is indeed rather small, well below the limit given in Eq. (30).

Fig. 32 shows the SLAC results on the proton, deuteron (top-left panel) and neutron (top-right panel) as a function of x. Also shown on the top-right panel of Fig. 32 are recent JLab neutron results with polarized ^{3}He from Hall A E99-117 [62] and E97-103 [63]. E97-103 is a dedicated precision measurement of g_2^n in the DIS region at low Q^2 to study its Q^2 dependence. It covered five different Q^2 values from 0.58 to 1.36 GeV^2 at $x \approx 0.2$. Results on the Q^2 dependence of g_2^n are given in the bottom panel of Fig. 32. The light-shaded area in the plot gives the leading-twist contribution, obtained by fitting world data [133] and evolving to the Q^2 values of this experiment. The systematic errors are shown as the dark-shaded area near the

horizontal axis. The precision reached is more than an order of magnitude improvement over that of the SLAC data [41]. The difference of g_2 from the leading twist part (g_2^{WW}) is due to higher-twist effects and is sensitive to quark–gluon correlations. The measured g_2^n values are consistently higher than g_2^{WW}. For the first time, there is a clear indication that higher-twist effects become significantly positive at Q^2 below 1 GeV^2, while the bag model [147] and Chiral Soliton model [150,151] predictions of higher-twist effects are negative or close to zero. The g_1^n data obtained from the same experiment agree with the leading-twist calculations within the uncertainties.

2.7. Spin structure in the resonance region

While most measurements of spin structure functions initially focused on the deep-inelastic region, more recently experiments have also collected a truly massive data set on g_1 and g_2 in the region $W < 2$ GeV, the nucleon resonance region, over a wide range in Q^2. Because the (resonant) final state in this kinematic region can have a strong influence on scattering matrix elements, these data are less suitable for a direct interpretation within the framework of perturbative QCD (Section 2.2). On the other hand, they can reveal new and important information on the internal structure of nucleon resonances and their excitation by the electromagnetic probe. Combining proton, deuteron and neutron targets, one can separate the various spin–isospin channels that lead to the excitation of overlapping resonances as well as non-resonant (multi-) meson production.

For a given resonance, the (electro- or) photo-excitation strength can, in general, be given in terms of three helicity amplitudes, namely $A_{3/2}(Q^2)$ (transverse photons leading to final state helicity 3/2), $A_{1/2}(Q^2)$ (transverse photons leading to final state helicity 1/2) and $S_{1/2}(Q^2)$ (longitudinal photons). These amplitudes are directly related to the photon asymmetries,
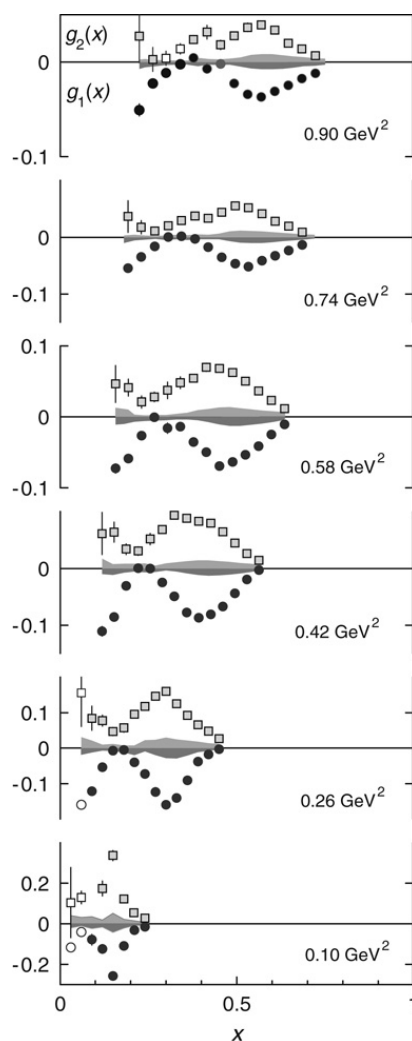
Fig. 33. Data on the spin structure functions g_1 (filled circles) and g_2 (open squares) vs. x in the resonance region, for ^{3}He (approximately a neutron target), from Jefferson Lab's Hall A. Statistical errors are shown as error bars, while the systematic errors are indicated by the shaded bands. The average Q^2 for each data set is indicated in the figure.
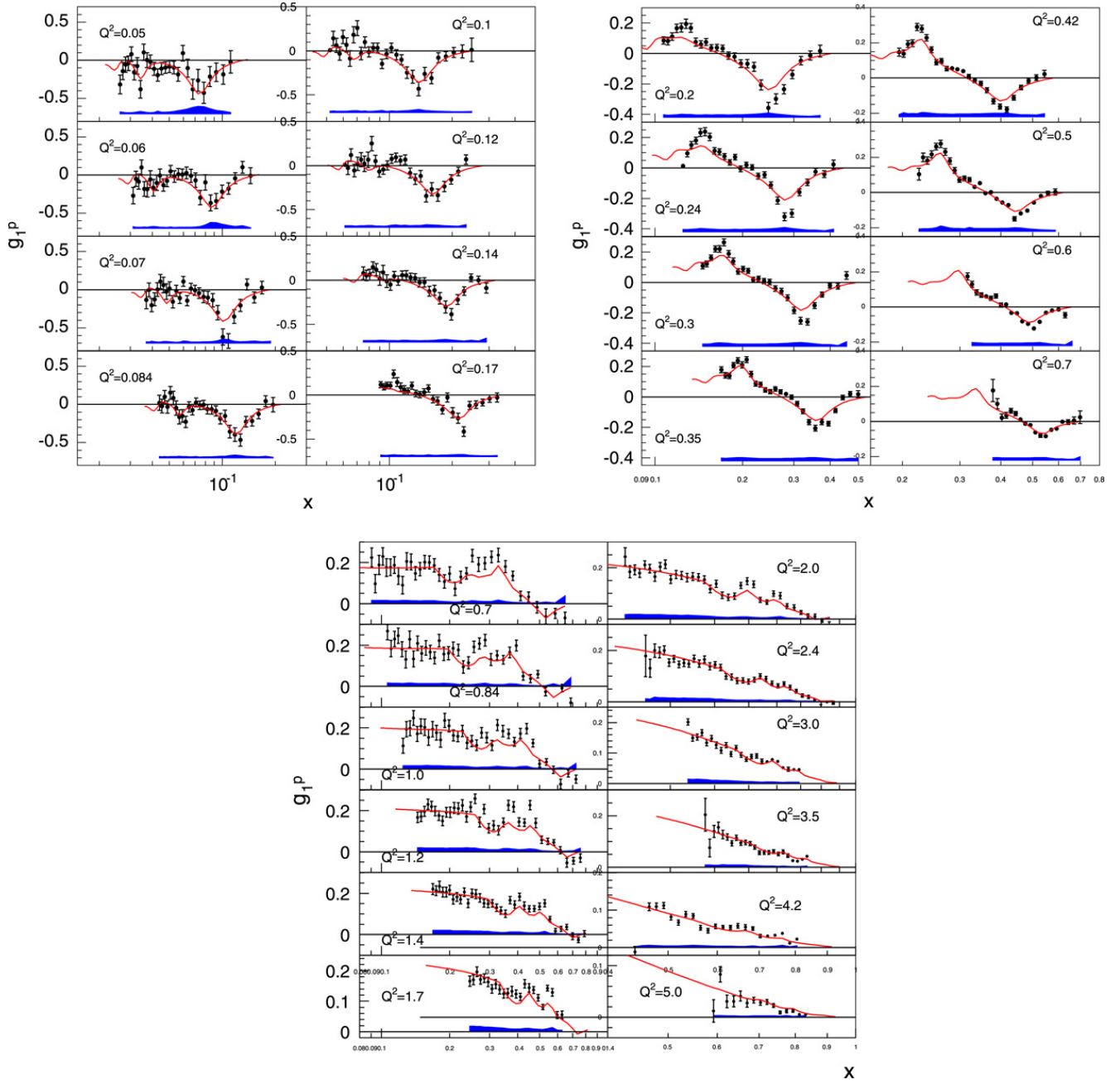
Fig. 34. Data on the spin structure functions g_1 of the proton vs. x in the resonance region and beyond, from Jefferson Lab's Hall B. Statistical errors are shown as error bars, while the systematic errors are indicated by the shaded bands. The average Q^2 for each data set is indicated in the figure. The curves are from a phenomenological parametrization of the data. A similarly complete data set exists also for the deuteron.

viz.

$$A_1 = \frac{|A_{1/2}|^2 - |A_{3/2}|^2}{|A_{1/2}|^2 + |A_{3/2}|^2}$$ (81)

$$A_2 = \sqrt{2}\frac{Q}{q^*}\frac{S_{1/2}^* A_{1/2}}{|A_{1/2}|^2 + |A_{3/2}|^2}.$$

Here, q^* is the (virtual) photon 3-momentum in the rest frame of the resonance. As a consequence, electromagnetic excitation of spin-1/2 resonances will have an asymmetry $A_1 = 1$ since the amplitude $A_{3/2}$ cannot contribute. Vice versa, for resonances like the delta (with spin 3/2) that are predominantly excited via $M1$ transitions, one has $A_{3/2} \approx \sqrt{3}A_{1/2}$ and therefore $A_1 \approx -0.5$. By studying the Q^2 dependence of these asymmetries for a given mass range, one can gain information on the relative strength of overlapping resonances (and non-resonant background) as well as, for spin-3/2 resonances, the transition from $A_{3/2}$ dominance at low Q^2 to the asymptotic $A_{1/2}$ dominance expected from helicity conservation in collinear pQCD.

Fig. 35. Data on the spin structure functions g_1 and g_2 of the proton versus x in the resonance region, for an average Q^2 of 1.3 GeV^2, from Jefferson Lab's Hall C (dark filled symbols) and other experiments (as indicated). Statistical errors are shown as error bars, while the systematic errors are indicated by the shaded bands.

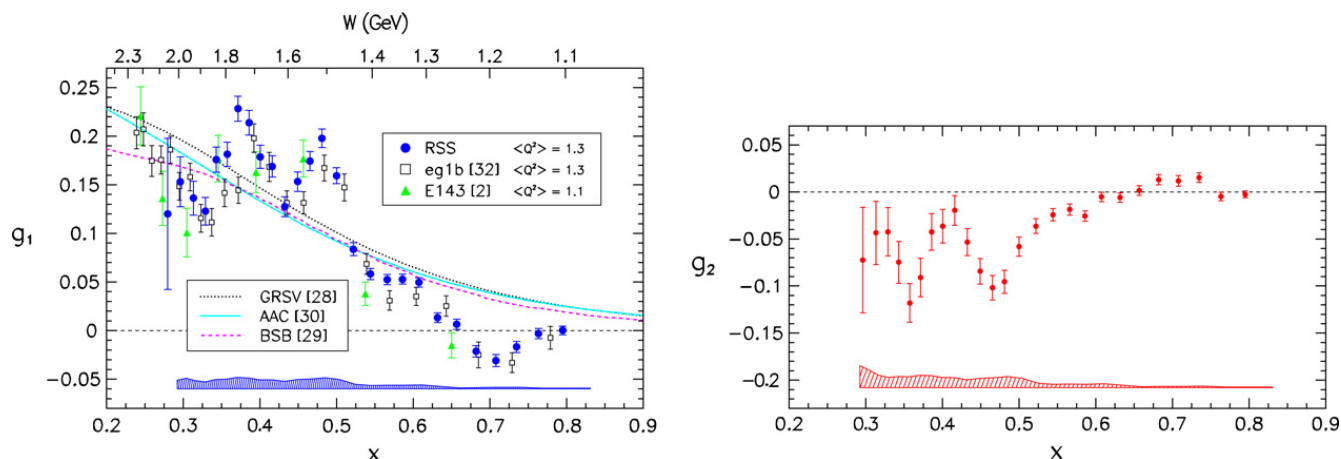Measurements of spin structure functions in the resonance region are also required for the evaluations of moments (Section 3), since in most cases the integrals must be evaluated up to $x = 1$, which includes the resonance and elastic region, particularly at more moderate Q^2. As an example, for $Q^2 = 3$ GeV^2, half of the x range, $0.5 < x < 1$, lies in the resonance region. These measurements are also very important to study the onset of duality for spin structure functions, see Section 4. Finally, higher order QED radiative corrections to all measurements (even in the DIS region) have contributions from the resonance region, making good knowledge of spin structure functions at low W imperative for accurate interpretation.

The first experiment to measure double spin observables at SLAC was also the first to take data in the resonance region [20]. The next dedicated measurement was by the E143 collaboration [39], who used a lower beam energy of 9.7 GeV to cover the resonance region at $Q^2 = 0.5$ GeV^2 and 1.2 GeV^2. These data showed that the asymmetry A_1 is indeed negative in the Δ region at moderate Q^2, while it rises rapidly to rather large values in the second resonance region (dominated by the S_{11} and D_{13} resonances).

Since then, experiments in all three halls at Jefferson Lab have collected a vast data set on all inclusive spin structure functions throughout the resonance region, for proton, deuteron and ^{3}He targets, spanning several orders of magnitude in Q^2 (from 0.015 to 5 GeV^2). Figs. 33–35 show some samples from this data set. Double spin asymmetries in the resonance region were also measured at MIT Bates with the BLAST detector [152] on the proton and the deuteron at 0.85 GeV beam energy. The kinematic region covered ranges from $Q^2 = 0.08 - 0.38$ GeV^2 and from the elastic peak to $W = 1.33$ GeV. More data in the region of the $\Delta(1232)$ resonance were also obtained at NIKHEF for $Q^2 = 0.11$ GeV^2 [153].

The data in Fig. 33 are from experiment E94-010 in Jefferson Lab's Hall A [57]. Both spin structure functions g_1 and g_2 were extracted directly from cross section differences for polarized electrons scattering off a ^{3}He target polarized both along and transverse to the beam (see Eqs. (14) and (15)). These data approximate the spin structure functions for a free neutron, although nuclear corrections were not applied. One can clearly see the strongly negative response of g_1 in the $\Delta(1232)$ resonance region (high x). The structure function g_2 is close to the negative of g_1, which implies that A_2, which is proportional to $g_1 + g_2$, is close to zero.

Fig. 34 shows a sample from the vast data set collected with CLAS during the EG1 experiment [72] on the spin structure function g_1 for the proton and the deuteron. g_1 was extracted from measurements of the asymmetry $A_\parallel$ (see Eq. (31)) over a range in x covering both the resonance and deep inelastic regions, for over 25 bins in Q^2. As Q^2 increases over 2 orders in magnitude, the asymmetry (and therefore g_1) changes from a predominantly negative value ($A_{3/2}$-dominance) to the strongly positive DIS limit for nearly all x except in the region of the $\Delta(1232)$ resonance.

Finally, we show in Fig. 35 the data from the "RSS" experiment in Hall C [80]. This experiment measured g_1 and g_2 in the resonance region for one bin in Q^2, centered around 1.3 GeV^2, for both proton and deuteron, using transversely and longitudinally polarized targets. The g_1 data "oscillate" around the deep inelastic curves (from various NLO fits), while g_2 is in rough agreement with the Wandzura–Wilczek form (not shown).

3. Sum rules and spin polarizabilities

3.1. Moments of spin structure functions

Moments of structure functions are a powerful tool to study fundamental properties of nucleon structure, like the total momentum fraction carried by quarks or the total contribution of quark helicities to the spin of the nucleon. While a complete description of structure functions based on fundamental QCD principles may be unattainable for now, moments

of structure functions can be directly compared to rigorous theoretical results, like sum rules, lattice QCD calculations and chiral perturbation theory. The original "spin crisis" was directly due to a discrepancy between the data and an approximate "sum rule" by Ellis and Jaffe [3]. On the other hand, a detailed measurement of the Q^2-evolution of the Bjorken sum rule [5] provides a significant test of pQCD in the spin sector.

As mentioned in Section 2.1, via the Operator Product Expansion (OPE) the moments of $g_{1,2}$ can be related to hadronic matrix elements of current operators. The moments are given as a sum, ordered according to the *twist* $\tau =$ (dimension − spin) of the current operators, beginning with the lowest twist $\tau = 2$. Each additional unit of τ produces a factor of order $\frac{\Lambda_{QCD}}{Q}$, and is thus less important in the high Q^2 regime. Strictly speaking, the higher twist terms are mixed up with correction terms of order $\frac{M^2}{Q^2}$, of purely kinematic origin (target mass corrections), which can be calculated exactly, so as to expose the HT terms of dynamic origin. Some of the twist 2 terms are directly *measurable* in *other* processes. Twist 3 and higher terms can sometimes be determined from combinations of measured quantities.[2]

After a long series of manipulations one finds expressions for the nth moment $\int_0^1 dx\, x^{n-1} g_1(x, Q^2)$ for $n = 1, 3, 5, \ldots$ of g_1 and the nth moment $\int_0^1 dx\, x^{n-1} g_2(x, Q^2)$ for $n = 3, 5, 7, \ldots$ of g_2, in terms of hadronic matrix elements of certain local operators. (For details see Section 22.2 of [156]).

The most important case is the first moment, $n = 1$, of g_1, where the operators involved are the octet of well known axial-vector currents which control neutron and hyperon β-decay:

$$J_{5\mu}^i = \bar{\psi} \gamma_\mu \gamma_5 \left(\frac{\lambda_i}{2} \right) \psi \quad (i = 1, 2, \ldots, 8), \tag{82}$$

where the λ_j are the usual Gell-Mann matrices and ψ is a column vector in flavor space

$$\psi = \begin{pmatrix} \psi_u \\ \psi_d \\ \psi_s \end{pmatrix}. \tag{83}$$

The flavor singlet current, which does not play a role in β-decay, is

$$J_{5\mu}^0 = \bar{\psi} \gamma_\mu \gamma_5 \psi. \tag{84}$$

The relation of the hadronic matrix elements to the first moments $a_3 \equiv g_A$, a_8, a_0 of the flavor combinations of quark densities introduced in Eqs. (44) is

$$\langle P, S | J_{5\mu}^3 | P, S \rangle = M a_3 S_\mu$$

$$\langle P, S | J_{5\mu}^8 | P, S \rangle = \frac{M}{\sqrt{3}} a_8 S_\mu$$

$$\langle P, S | J_{5\mu}^0 | P, S \rangle = 2 M a_0(Q^2) S_\mu. \tag{85}$$

The Q^2 dependence of a_0 arises because the singlet current has to be renormalized and it is customary and convenient to choose Q^2 as the renormalization scale.

At leading twist the expression for $\Gamma_1^{p,n}$, valid for $Q^2 \gg M^2$, can be written

$$\Gamma_1^{p,n} = \frac{1}{12} \left[\left(\pm a_3 + \frac{1}{3} a_8 \right) E_{NS}(Q^2) + \frac{4}{3} a_0(Q^2) E_S(Q^2) \right], \tag{86}$$

where the coefficient functions are given, for 3 active flavors, by

$$E_{NS}(Q^2) = 1 - \left(\frac{\alpha_s}{\pi} \right) - 3.58 \left(\frac{\alpha_s}{\pi} \right)^2 - 20.22 \left(\frac{\alpha_s}{\pi} \right)^3 \cdots \tag{87}$$

and in the $\overline{MS}$ scheme

$$E_S(Q^2) = 1 - \left(\frac{\alpha_s}{\pi} \right) - 1.096 \left(\frac{\alpha_s}{\pi} \right)^2 \cdots. \tag{88}$$

Note that the singlet coefficient here multiplies $a_0(Q^2)$ and not the invariant quantity referred to in various papers as $\hat{a}_0$, $g_A^{(0)}|_{inv}$ and $\Delta\Sigma|_{invariant}$, which are the value of $a_0(Q^2)$ as $Q^2 \to \infty$.

There exist important sum rules for the moments of $g_{1,2}$ which we now discuss.

---

[2] The reader is warned that the notation in the literature on this subject is in a state of anarchy, with identical symbols often being used for significantly different quantities in different papers. Thus $G_{1,2}$ sometimes means M^3 times our $G_{1,2}$, but perhaps more bizarre is the use of the symbol ν for $P \cdot q$ in [154,155].

- *The Bjorken sum rule.* Using only isospin invariance Bjorken [5] showed that as $Q^2 \to \infty$,

$$\int_0^1 \mathrm{d}x \, [g_1^p(x, Q^2) - g_1^n(x, Q^2)] = \frac{g_A}{6} \left[1 - \left(\frac{\alpha_s}{\pi}\right) - 3.58 \left(\frac{\alpha_s}{\pi}\right)^2 - 20.22 \left(\frac{\alpha_s}{\pi}\right)^3 \cdots \right], \tag{89}$$

where the square bracket on the RHS contains the perturbative corrections Eq. (87), for 3 active flavors, to Bjorken's original result $g_A/6$. The sum rule is quite rigorous, involving only the assumption of isospin invariance, and inspired Feynman to say that its failure would signal the demise of QCD.

- *The Efremov, Leader, Teryaev sum rule.* The ELT sum rule [11] is also a rigorous result, following from the OPE, and states that

$$\int_0^1 \mathrm{d}x \, x \, [g_{1,f}^V(x) + 2g_{2,f}^V(x)] = 0, \tag{90}$$

where V implies *valence* contribution and the result holds for each flavor f. It was originally thought reasonable to assume that the sea-quark densities are the same in protons and neutrons, in which case Eq. (90) can be written as a kind of analogue to the Bjorken sum rule

$$\int_0^1 \mathrm{d}x \, x \, [g_2^p(x) - g_2^n(x)] = \frac{1}{2} \int_0^1 \mathrm{d}x \, x \, [g_1^n(x) - g_1^p(x)]. \tag{91}$$

However, the above assumption is tantamount to assuming $\Delta \bar{u} = \Delta \bar{d}$ in a proton, which, at least for the *unpolarized* antiquark densities, is not a good approximation. For further interesting sum rules of this type see [144,157].

- *The Burkhardt–Cottingham sum rule.* The BC sum rule [10]

$$\int_0^1 \mathrm{d}x \, g_2(x) = 0 \tag{92}$$

does *not* follow from the OPE, although it looks as if it does, because the nth moment of g_2 is proportional to $(n-1)$; but, as mentioned, the OPE result for g_2 only holds for $n \geq 3$.

The BC sum rule is based on an assumption about the asymptotic behavior of a particular virtual Compton amplitude (see discussion below). The argument is not watertight and it may be that

$$g_2(x) \to \frac{1}{x^2} \quad \text{as } x \to 0, \tag{93}$$

thus making the integral in Eq. (92) diverge. For a detailed discussion of this issue, see Section 5.2 of [12]. Note that the Wandzura–Wilczek approximation to g_2, Eq. (38) automatically satisfies the BC sum rule

$$\int_0^1 \mathrm{d}x \, g_2^{WW}(x) = 0. \tag{94}$$

- *Higher twist corrections.*

At lower values of Q^2 higher twist contributions become important. Of particular interest is $\Gamma_1(Q^2)$, which can be expanded, for $Q^2 > \Lambda_{QCD}^2$, in inverse powers of Q^2 (twist expansion)

$$\Gamma_1(Q^2) = \mu_2(Q^2) + \frac{\mu_4(Q^2)}{Q^2} + \frac{\mu_6(Q^2)}{Q^4} + \cdots \tag{95}$$

with μ_2, the leading twist term, given by Eq. (86).

The evolution in Q^2 of the $\mu_n(Q^2)$ can, in principle, be calculated in perturbative QCD, but results are known only for μ_2, and it is usual, therefore, to ignore the Q^2 dependence of $\mu_{4,6}$. The functions μ_n are related to matrix elements of operators of twist $\tau \leq n$; the occurrence of operators with twist lower than n is a kinematic effect, a consequence of target mass corrections.

We consider now the structure of the higher twist (i.e., $1/Q^2$) corrections to $\Gamma_1(Q^2)$ as defined in Eq. (95). As mentioned $\mu_4(Q^2)$ contains both target mass (TM) corrections and genuine dynamical higher twist contributions. The TM corrections for $g_{1,2}(x, Q^2)$ were given in [128]. For the first moment they yield

$$\mu_4^{TM}(Q^2) = \frac{2M^2}{9} \int_0^1 \mathrm{d}x \, x^2 \, [5g_1(x, Q^2) + 6g_2(x, Q^2)] \tag{96}$$

g_2, as discussed in Section 2.6, contains a twist-2 (and kinematic twist-3) part, g_2^{WW}, given in Eq. (80), and a dynamic twist-3 part given by $g_2 - g_2^{WW}$. Writing

$$g_2 = g_2^{WW} + (g_2 - g_2^{WW}) \tag{97}$$

one finds, after a little algebra, that

$$\mu_4^{TM}(Q^2) = \frac{2M^2}{9}\left\{\int_0^1 dx\, x^2\, g_1(x, Q^2) + 6\int_0^1 dx\, x^2\, [g_2(x, Q^2) - g_2^{WW}(x, Q^2)]\right\}. \tag{98}$$

The twist-2 combination of moments is usually referred to as a_2 and the twist-3 as d_2. More precisely

$$a_2(Q^2) \equiv 2\int_0^1 dx\, x^2\, g_1(x, Q^2) \qquad d_2(Q^2) \equiv 3\int_0^1 dx\, x^2\, [g_2(x, Q^2) - g_2^{WW}(x, Q^2)]. \tag{99}$$

There is also a genuine twist-4 contribution to μ_4, written as $\frac{4M^2}{9}f_2$, so that finally

$$\mu_4(Q^2) = \frac{M^2}{9}[a_2(Q^2) + 4d_2(Q^2) + 4f_2(Q^2)]. \tag{100}$$

The twist-4 part f_2 cannot be written in terms of moments of the standard scaling functions. In terms of operator matrix elements it is defined by

$$f_2(Q^2)M^3 S^\mu = \frac{1}{2}\sum_{flavors} e_f^2 \langle P, S \mid g\bar{\psi}_f\, \tilde{G}^{\mu\nu}\, \gamma_\nu\, \psi_f \mid P, S \rangle \tag{101}$$

where $\tilde{G}^{\mu\nu} = (1/2)\epsilon^{\mu\nu\alpha\beta}G_{\alpha\beta}$ with the sign convention $\epsilon^{0123} = +1$. (Note that in some papers the normalization of the covariant spin vector is taken to be $S^2 = -M^2$, in which case M^2 will appear on the LHS of Eq. (101).)

The first correct expressions for d_2 and f_2 were given by Ji and Unrau [155] and by Ehrnsperger, Mankiewicz and Schäfer [158]. (Note that in Ji's paper the twist-4 term in Eq. (100) appears with a minus sign. This is because his coupling g in the operator in Eq. (101) has the opposite sign to the usual convention i.e. he uses for the covariant derivative acting on quark fields $D^\mu = \partial^\mu + igA^\mu$.)

Since μ_4, a_2 and d_2 can be measured, Eq. (100) yields a measurement of the twist-4 matrix element f_2. Both d_2 and f_2 can then be compared to non-perturbative QCD calculations.

Finally, it is of some interest to consider the color electric and color magnetic polarizabilities of the nucleon [159]. They are defined by

$$\chi_E 2M^3 \boldsymbol{S} = \langle N, \boldsymbol{S} \mid \boldsymbol{j}_a \times \boldsymbol{E}_a \mid N, \boldsymbol{S}\rangle \qquad \chi_B 2M^3 \boldsymbol{S} = \langle N, \boldsymbol{S} \mid j_a^0 \boldsymbol{B}_a \mid N, \boldsymbol{S}\rangle \tag{102}$$

where $\boldsymbol{S}$ is the rest frame spin vector of the nucleon and j_a^μ is the quark current. $\boldsymbol{E}_a$ and $\boldsymbol{B}_a$ are the color electric and magnetic fields respectively. The color polarizabilities can be expressed in terms of d_2 and f_2 as

$$\chi_E = \frac{2}{3}(2d_2 + f_2) \qquad \chi_M = \frac{1}{3}(4d_2 - f_2). \tag{103}$$

- *Extrapolation to low Q^2: the Gerasimov, Drell, Hearn sum rule.* The twist expansion does not converge for very small Q^2. Thus to study polarized structure functions in the low Q^2 region it is necessary to make contact with soft, non-perturbative physics i.e. to study the relation to Compton scattering with *real*, or almost real photons. In this region care must be exercised in defining moments of structure functions. As already mentioned in Section 2.1 relations between moments of structure functions and matrix elements of operators are only valid if the moments include the elastic contributions located at $x = 1$. In the *deep* inelastic region the elastic contributions are negligible and are not included in experimental estimates of the moments, but at low Q^2, in the resonance region, the distinction is important. Thus moments in the latter region, *without* an elastic contribution will be labeled $\bar{\Gamma}$.

The GDH sum rule [160,161] concerns Compton scattering with *real* photons, i.e., with $Q^2 = 0$, and follows from the fact that the value of the forward spin-flip amplitude, $f_2(\nu)$, at $\nu = 0$, calculated to order e^2, is given by low energy theorems, and from the assumption that the dispersion relation for it does not require subtractions. This leads to

$$\int_0^\infty \frac{d\nu}{\nu}[\sigma_A(\nu) - \sigma_P(\nu)] = -\frac{2\pi^2\alpha}{M^2}\kappa^2 \tag{104}$$

where κ is the anomalous magnetic moment of the nucleon. The $\sigma_{A,P}$ are the total cross-sections for the absorption of a circularly polarized photon by a proton polarized with spin antiparallel/parallel to the photon spin.

Since, to order e^2, the cross-sections are zero below the pion production threshold ν_0 (see below), and following the convention used by experimentalists, we write Eq. (104) in the form

$$I(0) \equiv \int_{\nu_0}^\infty \frac{d\nu}{\nu}[\sigma_A(\nu) - \sigma_P(\nu)] = -\frac{2\pi^2\alpha}{M^2}\kappa^2. \tag{105}$$

In the language of DIS the above cross-section difference is referred to as σ_{TT} and Eq. (105), generalized to non-zero Q^2, is usually written

$$\lim_{Q^2 \to 0} \bar{I}_{TT}(Q^2) = -\kappa^2/4 \tag{106}$$

where

$$\bar{I}_{TT}(Q^2) = M^2 \int_{\nu_0(Q^2)}^{\infty} \frac{d\nu}{\nu^2} [\nu M G_1(\nu, Q^2) - Q^2 G_2(\nu, Q^2)] \tag{107}$$

$$= \frac{2M^2}{Q^2} \bar{\Gamma}_{TT}(Q^2) \tag{108}$$

with

$$\nu_0(Q^2) = \frac{Q^2 + m_\pi(2M + m_\pi)}{2M} \tag{109}$$

and where $\bar{\Gamma}_{TT}(Q^2)$ is the *inelastic* portion of the first moment

$$\bar{\Gamma}_{TT}(Q^2) \equiv \int_0^{x_0(Q^2)} dx \left[g_1(x, Q^2) - \frac{4M^2 x^2}{Q^2} g_2(x, Q^2) \right] \tag{110}$$

and $x_0(Q^2)$ is the threshold for pion production,

$$x_0 = \frac{Q^2}{Q^2 + m_\pi(2M + m_\pi)}. \tag{111}$$

Note that the generalization of $I(0)$ in Eq. (105) to arbitrary Q^2 is then given by

$$I(Q^2) = \frac{8\pi^2 \alpha}{M^2} \bar{I}_{TT}(Q^2). \tag{112}$$

The relevance of Eqs. (106) and (108) to deep inelastic scattering was first pointed out by Anselmino, Ioffe and Leader [162], who noted that the first moment $\bar{\Gamma}_{TT}^p(Q^2)$, which is a slowly (logarithmically) varying, positive function in the DIS region, would have to change drastically in order to satisfy Eq. (106) at small Q^2. However [162] failed to distinguish between the full moment $\Gamma_{TT}^p(Q^2)$ and its inelastic version $\bar{\Gamma}_{TT}^p(Q^2)$, and Ji [154] pointed out that there is a significant difference between the extrapolation to $Q^2 = 0$ of the full and the inelastic moments. The reason is a non-uniformity of the limits $\nu \to 0$ and $Q^2 \to 0$ in the generalization of $f_2(\nu)$ to $Q^2 \neq 0$, namely,

$$\lim_{Q^2 \to 0} \lim_{\nu \to 0} f_2(\nu, Q^2) \neq \lim_{\nu \to 0} \lim_{Q^2 \to 0} f_2(\nu, Q^2). \tag{113}$$

Thus whereas the RH limit does not inherit an elastic contribution from the Born terms in Compton scattering the LH one does. And since the integrals involved in the moments above correspond to $\nu = 0$ in $f_2(\nu, Q^2)$, it is the LH limit which must be used in the extrapolation to $Q^2 = 0$. Thus for the *full* moment Eq. (106) is altered to

$$\lim_{Q^2 \to 0} I_{TT}(Q^2) = \frac{M^2}{Q^2} [F_1^{el}(Q^2) + F_2^{el}(Q^2)]^2 - \kappa^2/4 \tag{114}$$

where $F_{1,2}^{el}$ are the Dirac and Pauli *elastic* form factors normalized to

$$F_{1p}^{el}(0) = 1 \qquad F_{1n}^{el}(0) = 0 \qquad F_{2p,n}^{el}(0) = \kappa_{p,n}. \tag{115}$$

In a similar way one can generalize to arbitrary Q^2 [154] the spin-dependent Compton amplitudes $S_{1,2}$, normalized so that

$$Im S_{1,2}(\nu, Q^2) = 2\pi \, G_{1,2}(\nu, Q^2). \tag{116}$$

For S_1 one obtains the dispersion relation

$$S_1(\nu, Q^2) = 4 \int_{\nu_0(Q^2)}^{\infty} \frac{G_1(\nu', Q^2)\nu' d\nu'}{\nu'^2 - \nu^2}. \tag{117}$$

Then

$$\frac{M^3}{4} S_1(0, Q^2) = \bar{I}_1(Q^2) \equiv M^2 \int_{\nu_0(Q^2)}^{\infty} \frac{d\nu}{\nu} M G_1(\nu, Q^2) \tag{118}$$

$$= \frac{2M^2}{Q^2} \bar{\Gamma}_1(Q^2) \tag{119}$$

where $\bar{\Gamma}_1(Q^2)$ is the *inelastic* portion of the first moment $\Gamma_1(Q^2)$

$$\bar{\Gamma}_1(Q^2) \equiv \int_0^{x_0(Q^2)} dx \, g_1(x, Q^2) \tag{120}$$

and

$$\lim_{Q^2 \to 0} \bar{I}_1(Q^2) = -\kappa^2/4. \tag{121}$$

For the full moment,

$$\lim_{Q^2 \to 0} I_1(Q^2) = \frac{M^2}{Q^2} F_1^{el}(Q^2) \, [F_1^{el}(Q^2) + F_2^{el}(Q^2)] - \kappa^2/4. \tag{122}$$

In the DIS region the elastic contribution to the moments is totally negligible. However in the extrapolation down through the resonance region towards $Q^2 = 0$ it is vitally important to distinguish between the two cases.

We turn now to the Compton amplitude $S_2(\nu)$ which underlies the BC sum rule. If one assumes that $S_2(\nu, Q^2)$ satisfies a superconvergence relation, i.e., that it vanishes as $\nu \to \infty$ fast enough so that both S_2 and νS_2 satisfy unsubtracted dispersion relations, then one can show that

$$\int_0^\infty Im S_2(\nu, Q^2) \mathrm{d}\nu = 2\pi \int_0^\infty G_2(\nu, Q^2) \mathrm{d}\nu = 0 \tag{123}$$

which leads to Eq. (92) for the full moment. From a knowledge of the elastic terms in $S_2(0, Q^2)$ one obtains an expression for the inelastic integral

$$\bar{I}_2(Q^2) \equiv \frac{2M}{Q^2} \int_0^{x_0(Q^2)} g_2(x, Q^2) \mathrm{d}x = \frac{1}{4} F_2^{el}(Q^2)[F_1^{el}(Q^2) + F_2^{el}(Q^2)]. \tag{124}$$

For a discussion of the convergence properties of the amplitudes see Section 2.10 of [163].

- *Generalization of the GDH approach.* The above type of analysis, based on the dispersion relations for $f_2(\nu, Q^2)$, $S_{1,2}(\nu Q^2)$, has been generalized to all the amplitudes in virtual Compton scattering by Drechsel, Pasquini and Vanderhaeghen [164]. For very small energies, $\nu < \nu_0(Q^2)$, the amplitudes can be expanded in powers of ν^2. The coefficients of the next-to-leading terms are called *generalized forward spin polarizabilities* of the nucleon. They can be expressed in terms of moments of the structure functions and can thus be measured. They are important because they reflect soft, non-perturbative aspects of nucleon structure, and can be calculated, at least approximately, using various forms of chiral perturbation theory and lattice methods. They thus provide benchmark tests for these theories. Here we shall simply give the expressions for experimentally relevant polarizabilities. For details of the amplitudes etc, see [164].

$$\gamma_0(Q^2) \equiv \gamma_{TT}(Q^2) = 2\alpha \int_{\nu_0}^\infty \frac{\mathrm{d}\nu}{\nu^4} \Big[\nu M G_1(\nu, Q^2) - Q^2 G_2(\nu, Q^2)\Big] \tag{125}$$

$$= \frac{16\alpha M^2}{Q^6} \int_0^{x_0} x^2 \Big[g_1(x, Q^2) - \frac{4M^2 x^2}{Q^2} g_2(x, Q^2)\Big] \mathrm{d}x \tag{126}$$

$$\delta_0(Q^2) \equiv \delta_{LT}(Q^2) = 2\alpha \int_{\nu_0}^\infty \frac{\mathrm{d}\nu}{\nu^3} \Big[M G_1(\nu, Q^2) + \nu G_2(\nu, Q^2)\Big] \tag{127}$$

$$= \frac{16\alpha M^2}{Q^6} \int_0^{x_0} x^2 \Big[g_1(x, Q^2) + g_2(x, Q^2)\Big] \mathrm{d}x. \tag{128}$$

The comparison between theory and experiment is discussed in the next few sections.

3.2. First moment of g_1 at high Q^2 and sum rules

After the EMC announced their surprising result [2], the next round of experiments at SLAC, CERN and DESY was focused on the goal to measure the first moments of g_1 for the proton, deuteron and neutron (^{3}He) in the DIS region with increasing precision. The main interest was to gain information on the contribution of quark helicities to the nucleon spin and to test the Bjorken sum rule [5].

Experimentally, these integrals can only be measured over some finite range in x, since the limit $x \to 0$ for finite Q^2 requires infinitely high energy transfers ν. In practice, all existing experiments accessing g_1 are fixed target experiments, with a lower limit of x of the order $x = 0.004 - 0.01$ (if $Q^2 \geq 1$ GeV^2). Experimental results for the moments Γ_1 therefore include some extrapolation to $x = 0$, typically based on Regge phenomenology [120,165,166], NLO fits or some other assumption about the functional form of the underlying quark densities. This extrapolation to the lower integral limit is the largest source of theoretical uncertainty for the results obtained so far. Most experiments also use an extrapolation at high x, since small statistics and limited momentum resolution prevent an accurate measurement in this kinematic region. However, at sufficiently large Q^2, the contribution from this extrapolation is very small and well defined.

Table 1 lists the final results for the first moments measured at $Q^2 \geq 1$ and evolved to a fixed Q^2 (as indicated) for the more recent experiments. The quoted uncertainties include both statistical and systematic errors added in quadrature.

Table 1

Results for the first moments of the spin structure functions g_1 from different experiments. Each experiment evolved its data to a fixed value of Q^2 which is indicated. The results for the deuteron are *not* corrected for its D-state, but are "per nucleon".

Q^2 (GeV^2)	Γ_1^p	Γ_1^n	Γ_1^d	$\Gamma_1^p - \Gamma_1^n$	Ref.
10	0.120 ± 0.016	–	0.019 ± 0.015	0.198 ± 0.023	SMC [28]
3	–	-0.033 ± 0.011	–	–	E142 [31]
3	0.133 ± 0.010	-0.032 ± 0.018	0.047 ± 0.007	0.164 ± 0.023	E143 [34]
5	–	-0.056 ± 0.009	–	0.168 ± 0.010	E154[a] [38]
5	0.118 ± 0.008	-0.058 ± 0.009	–	0.176 ± 0.008	E155[a] [36]
2.5	0.120 ± 0.009	-0.028 ± 0.009	0.043 ± 0.004	0.148 ± 0.017	HERMES[b] [44]
3	–	–	0.046 ± 0.006	–	COMPASS [49]
5	Bjorken sum rule			0.182 ± 0.002	

[a] From an NLO analysis.
[b] Over measured region $x > 0.021$ only.

The results from different experiments are in agreement within uncertainties, after taking Q^2-evolution into account. The possible exception is the deuteron result of SMC [28] which is significantly lower than all others; this is due to a strongly negative contribution from the unmeasured low-x region which has since been ruled out by COMPASS data. In particular, the Bjorken sum rule is confirmed to within 7%–15% of its value 0.182 ± 0.002 (evolved to the average $Q^2 = 5$ GeV^2 of the data listed in Table 1); by far the largest remaining uncertainty stems from the low-x convergence of the integral. This agreement can be considered a successful test of Q^2-evolution and the value of the strong coupling constant α_s.

COMPASS and HERMES used their most recent result on the deuteron to extract an "experimental estimate" of the singlet axial charge a_0 (which equals $\Delta\Sigma$ in the $\overline{MS}$ scheme), yielding $\Delta\Sigma \approx 0.35 \pm 0.06$ for COMPASS (at $Q^2 = 3$ GeV^2) and $\Delta\Sigma \approx 0.33 \pm 0.04$ for HERMES (evaluated at $Q^2 = 5$ GeV^2). These numbers are somewhat higher than most recent NLO analyses (see Section 2.5), but in agreement with similar analyses by other experiments. All results on Γ_1 point towards a negative contribution to the integral from strange quarks and antiquarks of order ≈ -0.1, while semi-inclusive results from HERMES [45,102] are consistent with $\Delta s \geq 0$ in their measured range, see Sections 2.3 and 2.5.

3.3. The BC and ELT sum rules

While the first moment of g_1 depends on Q^2 and changes significantly from the DIS region to the real photon point, the Burkhardt–Cottingham sum rule for the first moment of g_2 should apply at all values of $Q^2 > 0$, as long as the elastic contribution is included in the integral. It can therefore be tested both by DIS data and at lower Q^2, where a significant contribution to the integral comes from the nucleon resonance region.

The SLAC E155 data discussed in Section 2.6 yielded a first test of the sum rule for the proton and the deuteron. The data were integrated over the measured region, $0.02 < x < 0.8$ at $Q^2 = 5$ GeV^2. The contribution from the unmeasured large-x region is negligible. For the low-x expansion, one can use the assumption that g_2 follows the Wandzura–Wilczek form (Eq. (80)) which yields a result independent of our knowledge of g_1 below $x = 0.02$. Under these assumptions, E155 found the integral for the proton to be -0.022 ± 0.008 and that for the deuteron as -0.002 ± 0.011, after averaging with the data from E143. While the proton result appears to be inconsistent with the BC sum rule at the 2.75σ level, any firm conclusion depends strongly on the behavior of g_2 at small x which is not known with enough precision and may not follow the Wandzura–Wilczek form.

The same data were also used to estimate the value for the ELT integral (Eq. (90)) using the approximation given in Eq. (91), with the neutron structure functions inferred from the measured proton and deuteron ones. The integral over the measured region is consistent with the expected value of zero, within errors of ± 0.008. Here, the extrapolation to small x is less critical because of the extra factor of x in the integral.

The most extensive measurement of the BC sum rule at smaller Q^2 comes from an experiment using a longitudinally and transversely polarized ^{3}He target in Hall A. The integral of $\Gamma_2^{^3\text{He}} = \int g_2^{^3\text{He}}(Q^2)dx$ is plotted in the left panel of Fig. 36 for the measured region (from break-up threshold on up and covering the resonance region; solid circles). For comparison, we also show a calculation using the MAID code [168] which is a unitary isobar model describing the nucleon resonance region, with parameters fit to meson photo- and electro-production data. Added to the MAID result is an estimate of the pd and ppn breakup contributions via a calculation of quasi-elastic single-proton knockout in the impulse approximation. The open circles show the experimental results after adding an estimated DIS contribution. The solid squares correspond to the results obtained after adding the elastic contributions for ^{3}He and are in good agreement with the expected value of zero within the systematic errors (indicated by the error bands for the experimental systematic error and the uncertainty on the low-x extrapolation).

After applying some nuclear corrections, results for the neutron can be extracted from the ^{3}He data. The result for Γ_2^n is plotted in the right panel of Fig. 36 in the measured region (solid circles), while the open circles include the elastic contribution and the open diamonds correspond to the results obtained after adding an estimated DIS contribution assuming $g_2 = g_2^{WW}$ for the neutron. Taking the difference between proton and deuteron data from E155, one can estimate the result for the neutron at high Q^2 (open square), which is consistent with zero but with a rather large error bar. The results from
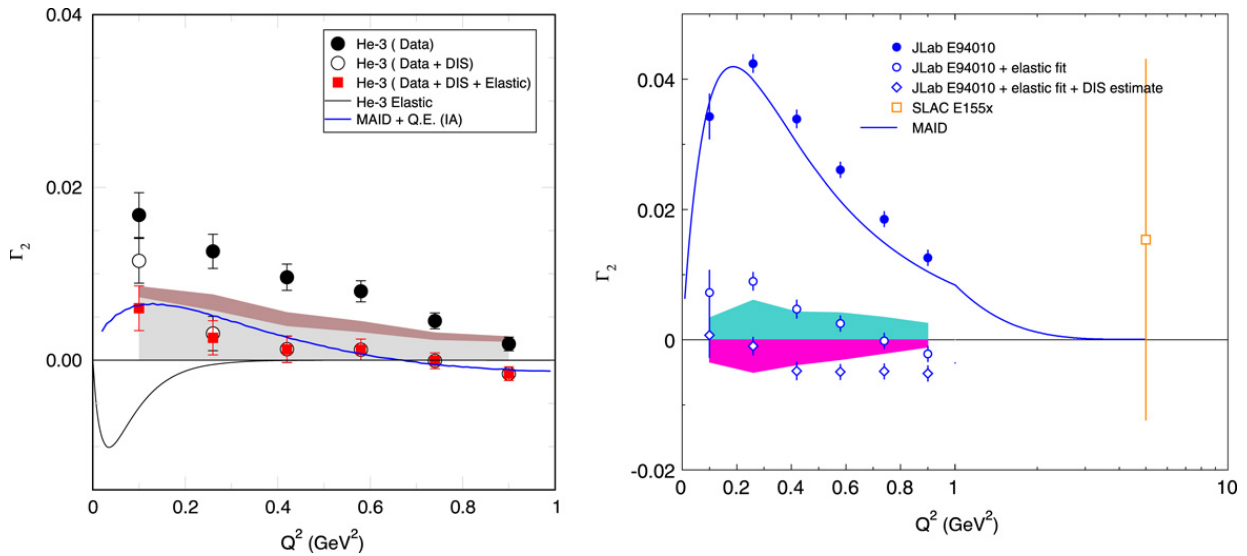
Fig. 36. Results for the BC sum $\Gamma_2(Q^2)$ for ^{3}He [167] and the neutron [57]. The integrals over the measured region (filled circles) are compared with MAID model calculations. Light (dark) shaded bands indicate experimental (extrapolation) systematic errors.

the Hall-A experiment for the neutron integral are the most precise data on the BC sum rule and are consistent with the expectation of zero, within systematic errors. The MAID parametrization agrees with the general trend but is slightly lower than the data in the measured (resonance) region, presumably because multi-pion final states are not included in the MAID code.

The RSS experiment in Hall C [80] also took data on g_2 for the proton and the deuteron, at an average Q^2 of about 1.3 GeV^2. For the proton, they find a negative integral over the measured region (1 GeV $< W <$ 2 GeV), but after adding the elastic contribution and an estimate for the small-x part, they find a (preliminary) result for the BC sum very close to zero, with (small) statistical and (dominant) systematical errors of about ± 0.005. This result is in disagreement with the SLAC result, but the unmeasured region ($x < 0.29$) is rather large and Q^2 is significantly lower. Preliminary results on the deuteron are slightly negative but consistent with zero within an error of about ± 0.015.

3.4. Higher moments and higher twist

While the moments of the structure function g_1 provide information on the parton densities, the moments of g_2 are related to higher twist effects and provide information on quark–gluon interactions (correlations). The x^2 moment of the spin-structure functions given in Eq. (99),

$$d_2 = 3 \int_0^1 x^2 [g_2(x) - g_2^{WW}(x)] \mathrm{d}x, \tag{129}$$

is of special interest: at high Q^2 it is a twist-3 matrix element and is related to the color polarizabilities [169], see Section 3.1. It can be calculated in lattice QCD [170] and a number of theoretical models [147,150,151].

Experimentally, due to the x^2 weighting, the contributions are dominated by the high-x region and the problem of low-x extrapolation is avoided. The SLAC E155 data [41] allowed the first extraction of $\bar{d}_2^p$ and $\bar{d}_2^n$ (excluding the elastic contribution). Combining E155 results with earlier SLAC data, at an average Q^2 of 5 GeV^2, $\bar{d}_2^p = 0.0032 \pm 0.0017$ and $\bar{d}_2^n = 0.0079 \pm 0.0048$. Combining these data with the JLab g_2 from Hall A E99-117 [62] a new value for the third moment $\bar{d}_2^n$ was extracted at an average Q^2 of 5 GeV^2. Compared to the previously published SLAC result [41], the uncertainty on $\bar{d}_2^n$ has been improved by about a factor of 2 (see Fig. 37). While a negative or near-zero value was predicted by lattice QCD and most models, the new result for $\bar{d}_2^n$ is positive. Also shown in Fig. 37 are the low Q^2 (0.1–1 GeV^2) results for $\bar{d}_2^n$ from another Hall A experiment, E94-010 [57], which were compared to a Chiral Perturbation Theory calculation [171] and a prediction based on MAID [172]. The elastic part, while negligible at high Q^2, is significant at low Q^2 (<1 GeV^2) and was subtracted from both theoretical calculations. The MAID calculation represents the low-Q^2 data rather well, probably due to the x^2-weighting which suppresses the contribution of higher mass final states.

A new precision experiment to measure d_2^n at an average Q^2 of 3 GeV^2 is planned in Hall A in early 2009 [173]. Further measurements [174] of d_2^n at constant Q^2 ranging from 3 to 5 GeV^2 are planned at JLab after the 12 GeV energy upgrade.

The Hall C RSS experiment [80] measured g_2 on the proton and the deuteron and extracted $\bar{d}_2^p = 0.0072 \pm 0.0017$ at a Q^2 value of 1.3 GeV^2. A more comprehensive measurement of g_2^p and d_2^p is scheduled in Hall C [175]. It will cover a wide Q^2 range from 2.5 to 6.5 GeV^2.
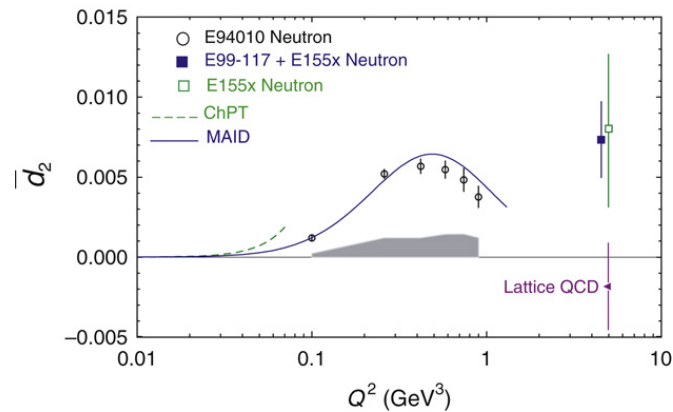
Fig. 37. Results for $\bar{d}_2^n(Q^2)$ from JLab Hall A [57,62] and SLAC [41], together with lattice QCD calculations [170].

Table 2

Results of μ_4, μ_6 and μ_8 at $Q^2 = 1$ GeV^2 for proton, neutron and p–n. The uncertainties are first statistical then systematic.

Target	Q^2 (GeV^2)	μ_4/M^2	μ_6/M^4	μ_8/M^6
Proton [176]	0.6–10.0	$-0.065 \pm 0.012 \pm 0.048$	$0.143 \pm 0.021 \pm 0.056$	$-0.026 \pm 0.008 \pm 0.016$
Neutron [59]	0.5–10.0	$0.019 \pm 0.002 \pm 0.024$	$-0.019 \pm 0.002 \pm 0.017$	$0.00 \pm 0.00 \pm 0.03$
p–n [179]	0.5–10.0	$-0.060 \pm 0.045 \pm 0.018$	$0.086 \pm 0.077 \pm 0.032$	$0.011 \pm 0.031 \pm 0.019$
p–n [180]	0.66–10.0	$-0.039 \pm 0.010 \pm 0.026$	$0.084 \pm 0.011 \pm 0.024$	0.047 ± 0.026

Table 3

Results of f_2, χ_E and χ_B at $Q^2 = 1$ GeV^2 for proton, neutron and p–n. The uncertainties are first statistical then systematic.

Target	f_2	χ_E	χ_B
p [176]	$-0.160 \pm 0.028 \pm 0.109$	$-0.082 \pm 0.016 \pm 0.071$	$0.056 \pm 0.008 \pm 0.036$
n [59]	$0.034 \pm 0.005 \pm 0.043$	$0.031 \pm 0.005 \pm 0.028$	$-0.003 \pm 0.004 \pm 0.014$
p–n [179]	$-0.136 \pm 0.102 \pm 0.039$	$-0.100 \pm 0.068 \pm 0.028$	$0.036 \pm 0.034 \pm 0.017$
p–n [180]	$-0.101 \pm 0.027 \pm 0.067$	-0.077 ± 0.050	0.024 ± 0.028

The higher-twist contributions to Γ_1 can be obtained by a fit with an OPE series, Eq. (95), truncated to an order appropriate for the precision of the data. The goal is to determine the twist-4 matrix element f_2. Once μ_4 is obtained, f_2 is extracted by subtracting the leading-twist contributions of a_2 and d_2 following Eq. (100). To have an idea how the higher-twist terms (twist-6 and above) affect the twist-4 term extraction, it is necessary to study the convergence of the expansion and to choose the Q^2 range in a region where the μ_8 term is not significant. This study is made possible only with the availability of the new low-Q^2 data from JLab.

Higher-twist analyses have been performed on the proton [176–178], the neutron [59] and the Bjorken sum (p–n) [179, 180]. Γ_1 at moderate Q^2 was obtained from the JLab g_1 data with details described in Section 3.5. For consistency, the unmeasured low-x parts of the JLab and the world data on Γ_1 were re-evaluated using the same prescription [59]. The elastic contribution, negligible above Q^2 of 2 GeV^2 but significant (especially for the proton) at lower values of Q^2, was added using the parametrization of Ref. [181]. The leading-twist term μ_2 was determined by fitting the data at $Q^2 \geq 5$ GeV^2 assuming that higher twists in this Q^2 region are negligible. Using the proton (neutron) data alone, and with input of $a_3(=g_A)$ from the neutron beta decay and a_8 from hyperon decay (assuming SU(3) flavor symmetry), $\Delta \Sigma = 0.15 \pm 0.07$ for the proton analysis [176] and $\Delta \Sigma = 0.35 \pm 0.08$ for the neutron analysis [59] were obtained. Note that there is a difference of nearly two standard deviations between these two results; this difference presumably comes from the different data sets used for the two analyses.

The fit results using an expansion up to $(1/Q^6)$ in determining μ_4 are summarized in Table 2. The extraction on p–n was performed twice: first [179] with the combined Hall A E94-010 neutron and Hall B EG1A proton data and then the second time [180] with the EG1B proton and deuteron data. In order to extract f_2, shown in Table 3, the target-mass corrections a_2 were evaluated using the Blümlein–Böttcher NLO fit to the world data [133] for the proton and a JLab fit to the world neutron data, which includes the recent high precision neutron results at large x [61,62]. The d_2 values used are from SLAC E155 [41] (proton) and JLab E99-117 [62] (neutron).

The fits were repeated varying the minimum Q^2 threshold to study the convergence of the OPE series. The extracted quantities have large uncertainties (dominated by the systematic uncertainty) but are stable with respect to the minimal Q^2 threshold when it is below 1 GeV^2. The results do not vary significantly when the μ_8 term is added, which justifies *a posteriori* the use of the truncated OPE series in the chosen Q^2 range. In the proton case, the elastic contribution makes a significant contribution to the μ_6 term at low Q^2 but this does not invalidate *a priori* the validity of the series since the elastic contribution affects mainly μ_6 and μ_8 remains small compared to μ_4. We notice the alternation of signs between
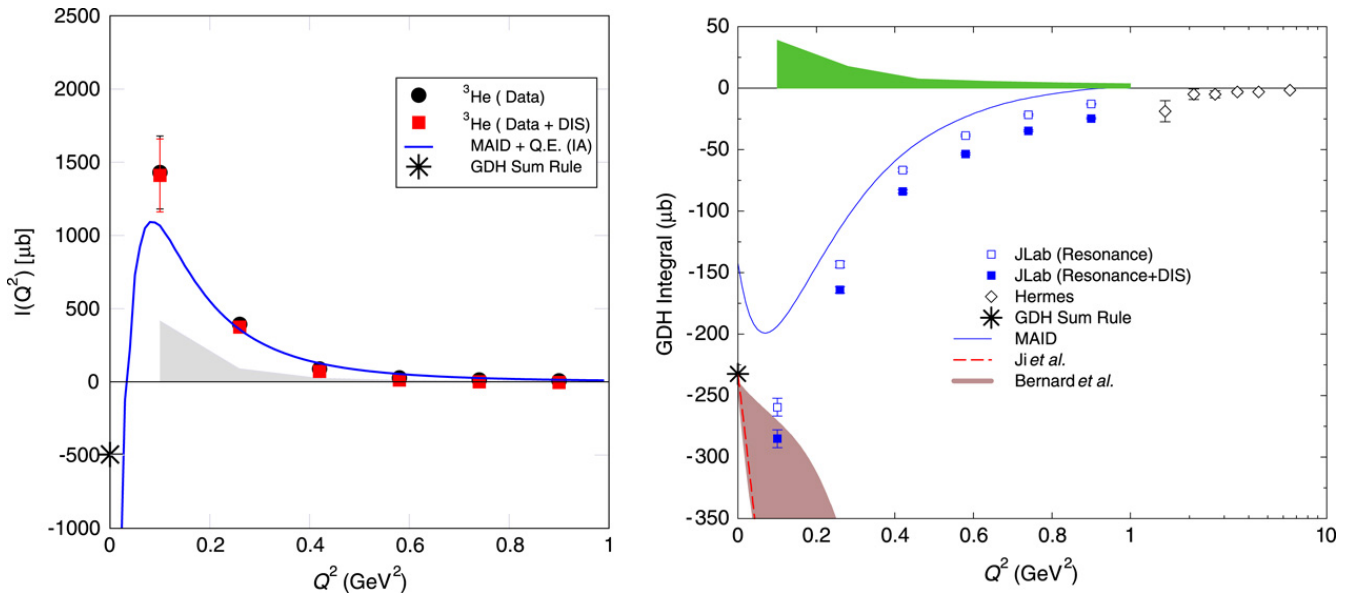
Fig. 38. Results of the GDH sum $I(Q^2)$ for ^{3}He [167] (left) and for the neutron [56] (right). The ^{3}He GDH results are compared with the MAID model plus a contribution from quasi-elastic nucleon knock-out. The neutron GDH results are compared with χPT calculations of Ji [171] (dashed line) and Bernard et al. [189] (shaded area). The MAID model calculation [172] is represented by a solid line. Data from HERMES [190] are also shown.

the coefficients. This leads to a partial suppression of the higher-twist effects and may be a reason for quark–hadron duality in the spin sector (see Section 4). We also note that the sign alternation is opposite for the proton and neutron. Following Eq. (103), the electric and magnetic color polarizabilities were determined, see Table 3. We observe a sign change in the electric color polarizability between the proton and the neutron. We also expect a sign change in the color magnetic polarizability. However, with the large uncertainty and the small negative value of the neutron χ_B, it is difficult to confirm this expectation.

Additional data from JLab experiment EG1 are presently under analysis and will significantly improve the precision of the first moments Γ_1^p and Γ_1^d around $Q^2 = 1\,\text{GeV}^2$, which is the crucial region for the extraction of higher-twist contributions. These data should therefore allow a more precise extraction of quantities like f_2 and the color polarizabilities.

3.5. GDH sum rule and chiral expansion

In recent years the Gerasimov, Drell and Hearn (GDH) sum rule [160,161] at $Q^2 = 0$ has attracted much experimental and theoretical [60,182] effort that has provided us with rich information. Experimental measurements of the GDH sum on the proton and deuteron were performed at Mainz [183] and Bonn [184,185], and the contribution from the first resonance region and below was also measured at LEGS [186]. The results show that the GDH sum rule is satisfied for the proton, assuming a model [182] for the unmeasured regions. A review on the overall status of the GDH sum rule for real photons has been published recently in this journal [187].

A generalized sum rule [188] connects the GDH sum rule with the Bjorken sum rule and provides a clean way to compare theories with experimental data over the entire Q^2 range. The (generalized) GDH sum rule and similar spin sum rules relate the moments of the spin-structure functions to the nucleon's static properties (e.g., its anomalous magnetic moment) and to real or virtual Compton amplitudes (see Eqs. (116)–(122) and (125)–(127)), which can be calculated theoretically. Several papers [60,164,182] provide comprehensive reviews on this subject.

Fig. 38 shows the extended GDH integrals $I(Q^2) = \int_{\nu_0}^{\infty} [\sigma_{1/2}(Q^2) - \sigma_{3/2}(Q^2)] \mathrm{d}\nu/\nu$ for ^{3}He (left) and for the neutron (right), which were extracted from Hall A experiment E94-010 [167,56], from break-up threshold for ^{3}He and from pion threshold for the neutron to $W = 2$ GeV. The uncertainties, when visible, represent statistics only; the systematics are shown by the shaded bands. The solid squares include an estimate of the unmeasured high-energy part. The corresponding uncertainty is included in the systematic uncertainty band.

The ^{3}He results rise with decreasing Q^2. Since the GDH sum rule at $Q^2 = 0$ predicts a large negative value, a drastic turnaround should happen at Q^2 lower than 0.1 GeV^2. A simple model using MAID [172] plus quasi-elastic contributions estimated from a PWIA model [191] indeed shows the expected turnaround. The data at low Q^2 should be a good testing ground for few-body Chiral Perturbation Theory calculations.

The ^{3}He results indicate a smooth variation of $I(Q^2)$ to increasingly negative values as Q^2 varies from 0.9 GeV^2 towards zero. The data are more negative than the MAID model calculation [172], again presumably due to the contribution from multi-pion final states. (Since the calculation only includes contributions to $I(Q^2)$ for $W \le 2$ GeV, it should be compared with the open circles.) The GDH sum rule prediction, $I(0) = -232.8\,\mu$b, is indicated in Fig. 38, along with extensions to $Q^2 > 0$ using two next-to-leading order χPT calculations, one using the Heavy Baryon approximation
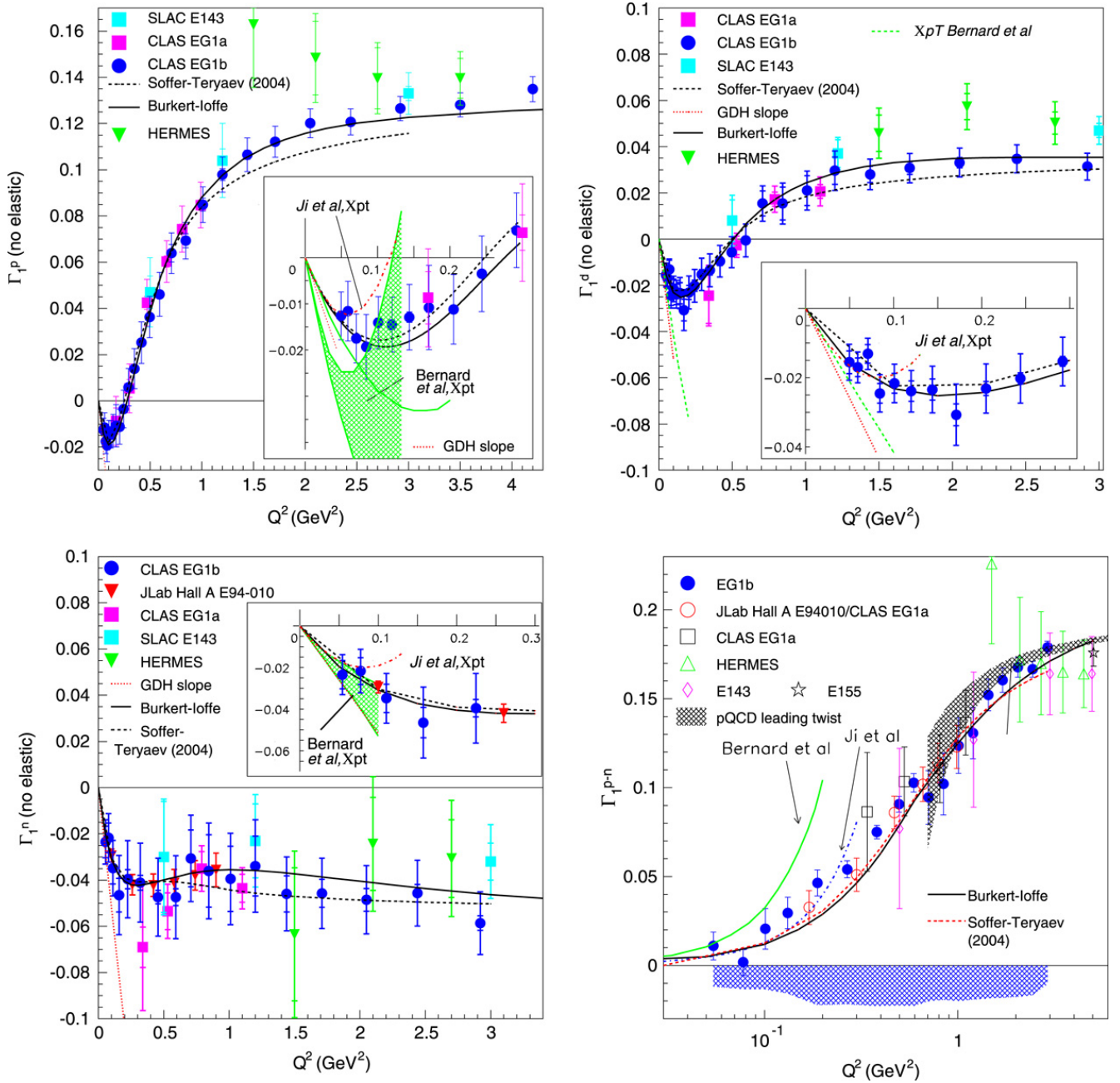
Fig. 39. Results on $\overline{\Gamma}_1(Q^2)$ for p, d, n and p–n from JLab Hall A [57], CLAS EG1a [71] and EG1b [192], together with data from SLAC and HERMES. The slopes at $Q^2 = 0$ predicted by the GDH sum rule are given by the red dotted lines. The solid (short-dashed) lines are the predictions from the Burkert–Ioffe (Soffer–Teryaev) parametrizations [194,193]. The leading twist Q^2-evolution of the p–n moment is given by the grey band. The insets show comparisons with χPT calculations. The dot-dashed lines (green lines and bands) at low Q^2 are the next-to-leading order χPT predictions by Ji et al. [171] (Bernard et al. [189]) (For interpretation of the references to colour in this figure legend, the reader is referred to the web version of this article.).

(HBχPT) [171] (dashed line) and the other based on Relativistic Baryon χPT (RBχPT) [189]. The shaded band shows the RBχPT calculation including resonance effects [189], which have an associated large uncertainty due to the resonance parameters used.

In Fig. 39 we present the existing data set on the related quantity $\bar{\Gamma}_1(Q^2)$ (Eq. (120)) at low to moderate Q^2. The upper two panels show the data on the proton and the deuteron from EG1a [71] together with new results from the Hall B EG1b experiment [192]. The bottom row shows published results for the neutron from Hall A [57] and for the proton–neutron difference obtained by combining all of these data sets. Also shown are data from SLAC E143 [34] and E155 [36] as well as from HERMES [44]. The inner error bars indicate the statistical uncertainties while the outer ones are the quadratic sums of the statistical and systematic uncertainties, except for the lower-right panel where the systematic errors are indicated by a shaded band.

As $Q^2 \to 0$, the slopes of $\bar{\Gamma}_1$ (shown as dotted lines in Fig. 39) and of $\bar{\Gamma}_{TT}$ are the same, both given by the GDH sum rule (see Eqs. (106)–(110), (120) and (121)). The behavior at low Q^2 can be calculated with χPT. We show results of calculations by
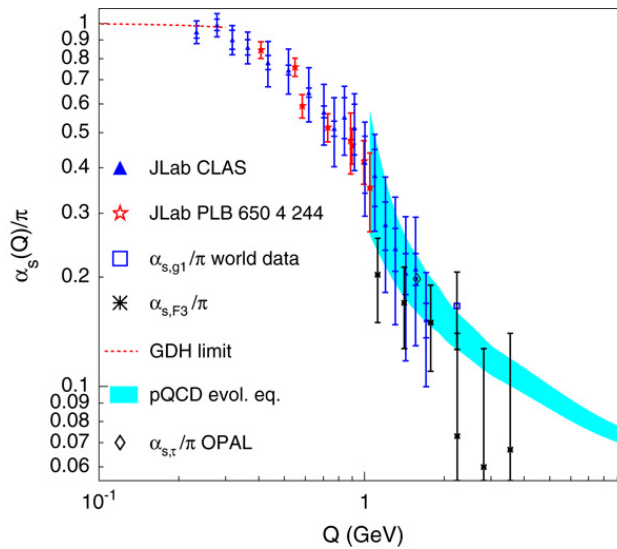
Fig. 40. Results for α_{s,g_1} [196] extracted from the generalized Bjorken sum, together with other world data on effective strong couplings.

Ji et al. [171] using HBχPT and by Bernard et al. [189] without and with the inclusion of vector mesons and Δ degrees of freedom. The calculations are in reasonable agreement with the data at the lowest Q^2 values of 0.05–0.1 GeV^2. At moderate and large Q^2 data are compared with two phenomenological model calculations [193,194]. The model by Soffer and Teryaev [193] assumes a smooth variation with Q^2 of the integral $\int [g_1(x) + g_2(x)]\mathrm{d}x$ (which is constrained by DIS data at large Q^2 and by sum rules at the photon point) and subtract the contribution from $\bar{\Gamma}_2$ (using the BC sum rule) to extract $\bar{\Gamma}_1(Q^2)$. The curve by Burkert and Ioffe [194] uses a parametrization of the resonance region (similar to MAID) and adds a Vector Meson Dominance-inspired ansatz to connect the GDH sum rule at the photon point with the DIS data for $\bar{\Gamma}_1$. Both models describe the data well.

The lower-right panel in Fig. 39 shows the moment of $g_1^p - g_1^n$, the Bjorken integral. This is of special interest because it contains contributions only from the flavor non-singlet (or isovector) part, and the contribution from the $\Delta(1232)$ resonance cancels [195]. The data at high Q^2 were used to test the Bjorken sum rule as described in Section 3.2. They were also used to extract a value of the strong coupling constant, α_s, assuming the validity of the sum rule. The leading-twist pQCD evolution of the Bjorken sum rule is shown by the grey band. It tracks the data down to surprisingly low Q^2, which indicates an overall suppression of higher-twist effects (see Section 3.4). The new JLab data at low Q^2 provide interesting information in the low energy region, where the strong interaction is truly strong and non-perturbative.

A new attempt [196,197] was made to extract an effective strong coupling, α_{s,g_1} in the low Q^2 region (Fig. 40). The extracted α_{s,g_1}, which by definition must converge towards a finite value as $Q^2 \to 0$, shows a clear trend of weakening Q^2 dependence with decreasing Q^2. With the GDH sum rule as a constraint at $Q^2 = 0$, a model fit to the extracted α_{s,g_1} shows a small Q^2 slope at the origin. This is consistent with a conformal behavior, which may be important for any attempt to apply AdS/CFT [198] for the strong interaction in the low-energy region.

The generalized spin polarizabilities provide additional benchmark tests of χPT calculations, and their measurement is an important step in understanding the dynamics of QCD in the low Q^2 region. Since they have an extra $1/\nu^2$ weighting compared to the first moments, these integrals have less contributions from the large-ν region and converge much faster, which minimizes the uncertainty due to the unmeasured region at large ν.

Generalized spin polarizabilities have been evaluated with next-to-leading order χPT calculations [199,189]. One issue in the χPT calculations is how to properly include the nucleon resonance contributions, especially the $\Delta(1232)$ resonance. As was pointed out in [199,189], while γ_0 is sensitive to resonances, δ_{LT} is insensitive to the Δ resonance.

The first results for the neutron generalized forward spin polarizabilities $\gamma_0(Q^2)$ and $\delta_{LT}(Q^2)$ were obtained at Jefferson Lab Hall A [58]. The results for $\gamma_0^n(Q^2)$ are shown in the top panel of Fig. 41. The statistical uncertainties are smaller than the size of the symbols. The data are compared with a next-to-leading order ($O(p^4)$) HBχPT calculation [199], a next-to-leading order RBχPT calculation and the same calculation explicitly including both the Δ resonance and vector meson contributions [189]. Predictions from the MAID model [172] are also shown. At the lowest Q^2 point, the RBχPT calculation including the resonance contributions is in good agreement with the experimental result. For the HBχPT calculation without explicit resonance contributions, discrepancies are large even at $Q^2 = 0.1$ GeV^2. This might indicate the significance of the resonance contributions or a problem with the heavy baryon approximation at this Q^2. The higher Q^2 data point is in good agreement with the MAID prediction, but the lowest data point at $Q^2 = 0.1$ GeV^2 is significantly lower.

Results for γ_0 on the proton have been recently submitted for publication [192]. They show significant disagreement with both χPT calculations [199,189]. An isospin separation of γ_0 was performed and discussed in Ref. [180]. The isoscalar (γ_0^{p+n})
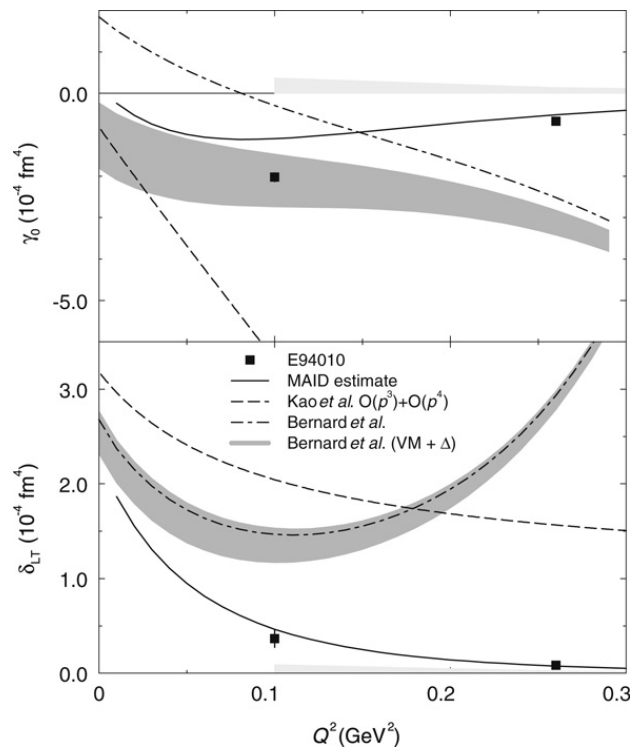
Fig. 41. Results for the neutron spin polarizabilities γ_0 (top panel) and δ_{LT} (bottom panel). Solid squares represent the results with statistical uncertainties. The light bands represent the systematic uncertainties. The dashed curves represent the heavy baryon χPT calculation [199]. The dot-dashed curves and the dark bands represent the relativistic baryon χPT calculation without and with [189] the Δ and vector meson contributions, respectively. Solid curves represent the MAID model [172].

and isovector (γ_0^{p-n}) combinations also disagree with χPT, in spite of the fact that for the latter the contribution from the $\Delta(1232)$ resonance cancels.

Since δ_{LT} is insensitive to this resonance contribution for each nucleon individually, it was believed that δ_{LT} should be more suitable than γ_0 to serve as a testing ground for the chiral dynamics of QCD [199,189]. The bottom panel of Fig. 41 shows δ_{LT} compared to χPT calculations and the MAID predictions. While the MAID predictions are in good agreement with the results, it is surprising to see that the data are in significant disagreement with the χPT calculations even at the lowest Q^2, 0.1 GeV^2. This disagreement ("δ_{LT} puzzle") presents a significant challenge to the present Chiral Perturbation Theory.

New experimental data have been taken at very low Q^2, down to 0.02 GeV^2 for the neutron (^{3}He) [65] for both longitudinal and transverse target polarizations, but only for longitudinal target polarization for the proton and the deuteron [200]. Preliminary results just became available for the neutron. Analysis is underway for the proton and deuteron data. These results will provide benchmark tests of χPT calculations at the kinematics where they are expected to work. A new proposal [201] was recently approved to measure g_2^p with a transversely polarized proton target in the low Q^2 region. It will provide an isospin separation of the spin polarizabilities to shed light on the "δ_{LT}" puzzle.

4. Quark–hadron duality in spin structure

In the previous sections, we have interpreted spin structure function data and their integrals either in terms of quark and gluon degrees of freedom (Sections 2.1–2.6 and 3.1–3.4) or in terms of low-energy effective theories (Sections 2.7 and 3.5). While quarks and gluons are the fundamental degrees of freedom for the theory of strong interactions, QCD, a description in terms of their hadronic composites (nucleon, nucleon resonances and light mesons) is often more economical at lower resolution Q^2, where perturbative QCD is not applicable and calculations are extremely difficult. At intermediate resolution, models like the constituent quark model may be able to describe some of the observed phenomena.

Both from a theoretical and a practical point of view, it is interesting to investigate where and how these different pictures of the nucleon connect and overlap. In particular, if we can find a kinematic region where both the quark–parton description and the hadronic description are found to be valid to some degree, we can potentially expand the kinematic range of experiments that attempt to extract information on quarks in the nucleon. At the same time, we could gain new insights on the transition from quasi-free quarks at short length scales to their confinement at larger distances.

Such "dual" descriptions of experimental data have been successful in cases including e^+e^- annihilation, semi-leptonic heavy meson decays and lepton scattering; for a review see [202]. In particular, in the 1970s Bloom and Gilman [203] found that the unpolarized structure function $F_2(x, Q^2)$ in the nucleon resonance region ($W < 2$ GeV) at moderate Q^2, when averaged over suitable intervals in x, was quite close to the deep inelastic, scaling structure function $F_2(x)$ measured at
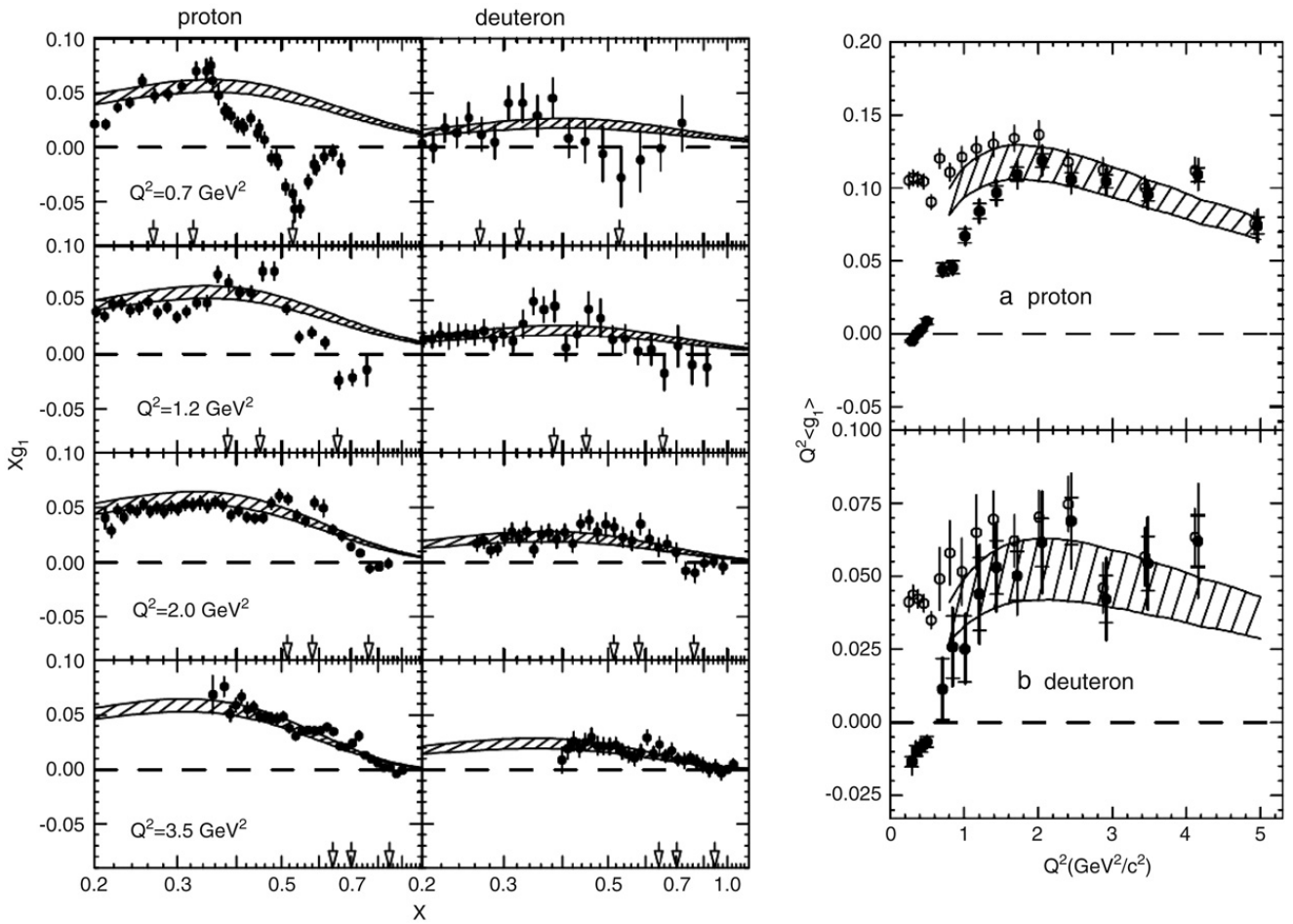
Fig. 42. Data on the spin structure functions $g_1(x, Q^2)$ of the proton and the deuteron from Jefferson Lab's Hall B (left panel) and its average over the resonance region (right panel). Prominent resonances are indicated by arrows in the left panel. The hatched curves represent the range of extrapolated DIS results from modern NLO fits (GRSV and AAC, see Section 2.5), evolved to the Q^2 of the data and corrected for target mass effects. The open circles in the right panel include the elastic contribution, while the filled circles are only integrated over $W > 1.08$ GeV.

much higher Q^2 and W but the same average x. This finding has been confirmed and expanded in much greater detail by measurements at Jefferson Lab [204]. The agreement between resonance region and high-Q^2 data is typically improved if one accounts for target mass effects and the logarithmic Q^2 evolution of deep inelastic structure functions. Nachtmann [205] has shown how to handle the finite mass of the nucleon target exactly; an approximate method simply employs the modified Nachtmann scaling variable $\xi = 2x/(1 + \sqrt{1 + 4M^2x^2/Q^2})$. This has been extended to the polarized case by Piccione and Ridolfi [128].

In the framework of the OPE, a quark–parton description of structure function *moments* at intermediate Q^2 should in principle be always possible if one includes contributions of sufficiently high twists. This so-called *global* duality then becomes simply the observation that these higher-twist contributions are either small or cancel in integrated observables [206]. Experimentally, this seems to be the case for unpolarized structure functions of the proton; however, it is non-trivial whether the same is true for polarized structure functions and for neutron structure functions. In particular, the polarized structure function g_1 might not necessarily exhibit *local* duality (for a restricted range in x), since at low Q^2 and W it is dominated by the $\Delta(1232)$ resonance, which should have a negative spin asymmetry $A_1 \approx -0.5$ (see Section 2.7), while at large Q^2 and x one expects this asymmetry to approach unity (see Section 2.4). Therefore, a detailed study of the limits of validity of duality for polarized structure functions is of great interest.

First measurements of spin structure functions in the resonance region [20,39] found that, with the exception of the $\Delta(1232)$ resonance, duality seemed to hold approximately within errors, especially for the higher Q^2 data of E143 [39]. Early data from the Jefferson Lab EG1 program with CLAS [70,71] confirmed that local duality does not work well at low Q^2, with significantly higher statistics. The paper by Yun et al. [70] explicitly looked at the approach of the structure function $g_1^d(\xi, Q^2)$ towards the scaling limit for increasing Q^2 and found that this limit had not been reached yet up to $Q^2 = 1$ GeV^2. The HERMES collaboration [207] averaged their measured asymmetry A_1^p over the resonance region 1 GeV $< W < 2$ GeV for 5 different bins in x and Q^2 and found the results in reasonable agreement with DIS results, within their relatively large errors.

By far the most detailed study of duality in the spin structure function g_1 has been published by the EG1 collaboration [73]. As shown in Fig. 42, one observes a clear trend of strong, resonant deviations from the scaling curve at lower Q^2, towards
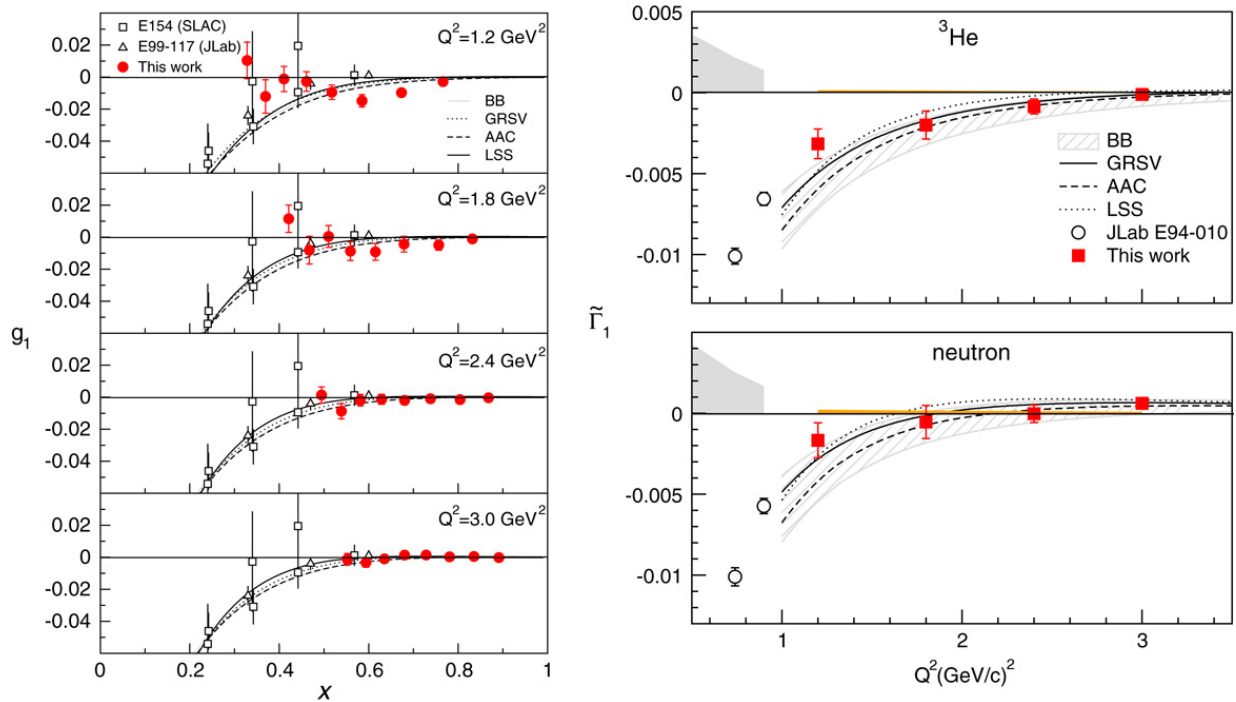
Fig. 43. New data on the spin structure functions $g_1(x, Q^2)$ of ^{3}He in the resonance region from Jefferson Lab's Hall A (solid circles, left panel), together with NLO curves for a combination of proton and neutron g_1 with proper polarization factors to mimic the nuclear spin structure function and evolved to the Q^2 of the data. The right panel show these data (solid squares) averaged over the resonance region for ^{3}He (top half) and corrected for nuclear effects to get the partial integrals for the neutron (bottom half). The NLO curves shown represent the range of extrapolated DIS results from modern NLO fits (Blümlein and Böttcher, GRSV, LSS and AAC, see Section 2.5), evolved to the Q^2 of the data and corrected for target mass effects.

a pretty good agreement at intermediate Q^2. The integral of g_1 over the whole resonance region begins to agree with the NLO results above $Q^2 \approx 1.7$ GeV^2. At lower Q^2, that integral rises above the NLO extrapolation if one includes the elastic contribution. This shows that the elastic peak somewhat overcompensates the negative contribution from the $\Delta(1232)$ resonance; however, leaving out the elastic part of the integral leads to integral values much below the NLO curves. The results on the proton and deuteron from EG1 [73] thus indicate a much slower approach to "global" duality for the polarized structure function g_1 than has been observed for unpolarized structure functions.

A more detailed examination shows that g_1 averaged over the first resonance region ($1.08 < W < 1.38$ GeV), which includes the $\Delta(1232)$ resonance, is substantially below the NLO expectations even to the highest Q^2 measured by EG1 (5 GeV^2). On the other hand, the three resonances ($P_{11}(1440)$, $S_{11}(1535)$, $D_{13}(1520)$) in the second resonance region ($1.38 < W < 1.58$ GeV) all have dominant $A_{1/2}$ transition amplitudes already at rather modest Q^2, so that the averaged g_1 in this region tends to overshoot the NLO limit. The cancellation of these two opposite effects, together with a rather quick approach to "local duality" for the higher resonance region ($W > 1.56$ GeV), leads to the approach to global duality seen in Fig. 42.

The data taken by the RSS collaboration in Hall C (see Section 2.7) corroborate these observations and add more precise data points for $Q^2 \approx 1.3$ GeV^2. They find that the integral over their measured region, 1.09 GeV $< W < 1.91$ GeV, is about $17\% \pm 8\%$ lower than the same integral over NLO evaluations of g_1^p evolved to $Q^2 = 1.3$ GeV^2, even after applying target mass corrections.

Very recently, new results have become available from a duality study in Hall A, using a ^{3}He target [64]. By combining NLO fits for the spin structure functions g_1^p and g_1^n with the proper polarization factors, one can directly compare these fits with the data on the nucleus ^{3}He (left panel of Fig. 43). Once again, at the lowest Q^2 point the data oscillate around the NLO curves and show a strong deviation in the region of the $\Delta(1232)$ resonance at least out to $Q^2 = 1.8$ GeV^2. At higher Q^2, both the data and the NLO fits are very close to zero, in contrast to g_1^p which is markedly positive for the extrapolated NLO fits. The partial integrals (up to $W = 1.91$ GeV) of these data are shown in the right panel of Fig. 43). Except for the lowest Q^2 point, good agreement with the integrals of NLO fits (both for ^{3}He and directly for the neutron) is seen, confirming the onset of duality around $Q^2 = 1.7$ GeV^2 for both protons and neutrons.

5. Summary and outlook

After 30 years of dedicated experiments, we are beginning to accumulate a rather detailed picture of a fundamental aspect of the nucleon, namely its spin structure. In spite of early worries (after the initial "spin crisis"), it appears that quark helicities *do* contribute a small but significant fraction of the (longitudinal) spin of the nucleon, up to one third. Most

importantly, the fundamental Bjorken sum rule [5] and its perturbative QCD evolution seem to be at least consistent with the data. In fact, none of the existing experiments show any features that would contradict pQCD in its realm of applicability.

Most pQCD-based analyses of the data agree fairly well on the contribution of various quark flavors to the proton spin, although there is still some controversy on the role played by strange sea quarks. We also don't know yet whether polarized up and down anti-quark densities show the same difference as the unpolarized ones. On the other hand, new high-precision data from Jefferson Lab constrain very nicely the polarized densities of valence up and down quarks at higher x. These data indicate that relativistic quark models, with one-gluon exchange corrections [109], and augmented by pion cloud contributions [208], yield a rather good description in the valence region where sea-quarks contribute little. The emergent picture (also from recent NLO analyses, see Section 2.5) is one where valence quarks ($\Delta q_V \equiv \Delta q - \Delta \bar{q}$) carry roughly the expected fraction ($\sim$60%) of the nucleon spin, while the (on average) negative helicity of sea quarks reduces this to about 30%–35%. Future experiments [209–211] at Jefferson Lab, after the approved energy upgrade to 11–12 GeV, will extend our knowledge of polarized quark densities out to $x > 0.8$ and will decisively test predictions from pQCD and QCD-inspired models. These same experiments, as well as presently scheduled 6 GeV ones [212,213], will further improve the precision with which we can study scaling violations and therefore extract polarized gluon and sea-quark densities. Additional information on individual quark and antiquark flavor contributions to the nucleon spin will come from future experiments at RHIC (in particular from direct $W^{\pm}$ production at 500 GeV center-of-mass energy) and the new FAIR facility in Darmstadt, Germany [214] as well as semi-inclusive measurements with COMPASS and at Jefferson Lab. Much additional information on the small-x behavior of quark- and antiquark polarization densities could be gotten from the electron–ion collider (EIC) that has recently been proposed [215], see below.

In addition to logarithmic violations of scaling, expected from pQCD, we also see some evidence for non-zero twist-3 and twist-4 matrix elements; however, the overall higher twist corrections to moments of spin structure functions seem rather modest even at fairly low Q^2, indicating a partial cancellation of contributions from different orders in the twist expansion. At these lower values of Q^2, we see a transition from partonic (quark and gluon) degrees of freedom to hadronic ones, without any dramatic break in the rather smooth transition region. Thanks to the vast data set in the nucleon resonance region, we can better constrain transition amplitudes and test this quark–hadron duality in detail. Averages over the resonance region seem to agree fairly well with extrapolations of deep inelastic data over the same range in x, albeit not to quite as low Q^2 as in the unpolarized case. Future measurements at Jefferson Lab with 6 GeV [175,173,216] and 12 GeV [174] beams will add to our knowledge of higher-twist matrix elements, and of the second spin structure function g_2 and its moments.

At the lower end of the Q^2 scale, the Gerasimov–Drell–Hearn sum rule at the real photon point seems to be well confirmed. However, it is too early to state with certainty whether the effective theory of QCD at low energies, χPT, yields a good description of the data very close to that point. Some tentative successes in describing the first moment Γ_1 of g_1 will be tested very soon, when the new data on the neutron (^{3}He), the proton and the deuteron collected in Halls A and B at Jefferson Lab become available [65,200]. For the polarizabilities like γ_0 and δ_{LT}, which are given by higher moments of $g_{1,2}$, the agreement at present is unsatisfactory; it may be necessary to go to a higher order in χPT before agreement is reached. New data on these quantities will also be collected at Jefferson Lab [201].

One of the most important remaining open questions is the provenance of the remaining 2/3 of the nucleon spin that is not carried by quark helicities. We know now that the gluon contribution cannot be very large, but its precise magnitude and shape are not known yet, and it could still be an important fraction of the total. Improved statistics from the direct measurements at RHIC and COMPASS will help, especially with expanded kinematics (higher and lower beam energies, different rapidity and p_T ranges, and new final state channels) which can begin to separate the low-x and high-x behavior of ΔG.

Additional information will come from future experiments of the spin structure functions at both extremes of the Q^2 scale, including the upcoming Jefferson Lab experiments with the future 11 GeV beam [209], and further COMPASS data. In this context, it is an interesting question whether future DIS measurements alone can distinguish between positive and negative $\Delta G(x)$. They can, indeed, but this requires a very high energy lepton–nucleon collider like the EIC proposal [215]. This can be seen in Fig. 44 which shows $g_1^p(x)$ at very small x for $1 < Q^2 < 1000$ GeV^2 for the two signs of $\Delta G(x)$. Clearly the behavior of $g_1^p(x)$ at small x and large Q^2 is quite different in the two cases.

A collider of the EIC type would also have a dramatic effect in reducing the uncertainties in the polarized parton densities. This is illustrated in Figs. 45 and 46 where it can be seen that the improvement even at moderate to large x, especially for Δs and ΔG, is remarkable.

Finally, the contribution from quark orbital angular momentum is also an important ingredient in the total spin balance of the nucleon. While a direct measurement is not available, one can learn much about the transverse distribution and motion of quarks from semi-inclusive measurements of single spin asymmetries. This is a fairly new field, with a very rich potential and a rapidly growing body of experimental data, but lies outside the scope of this article. It will be addressed by an upcoming review in this journal.

A second avenue towards a full accounting of the nucleon spin lies in measurements that are sensitive to Generalized Parton Distributions (GPDs), in particular Deeply Virtual Compton Scattering (DVCS). Moments of certain combinations of GPDs can be related to the total angular momentum (spin and orbital) carried by various quark flavors, as expressed in Ji's sum rule [8,218]. Again, seminal experiments in this area have already collected data that indicate that the necessary assumption of factorization (and the validity of the handbag diagram) seems to be fulfilled, and even give some model-dependent indication of the value of u- and d-quark angular momentum [219]. Future measurements at COMPASS and an
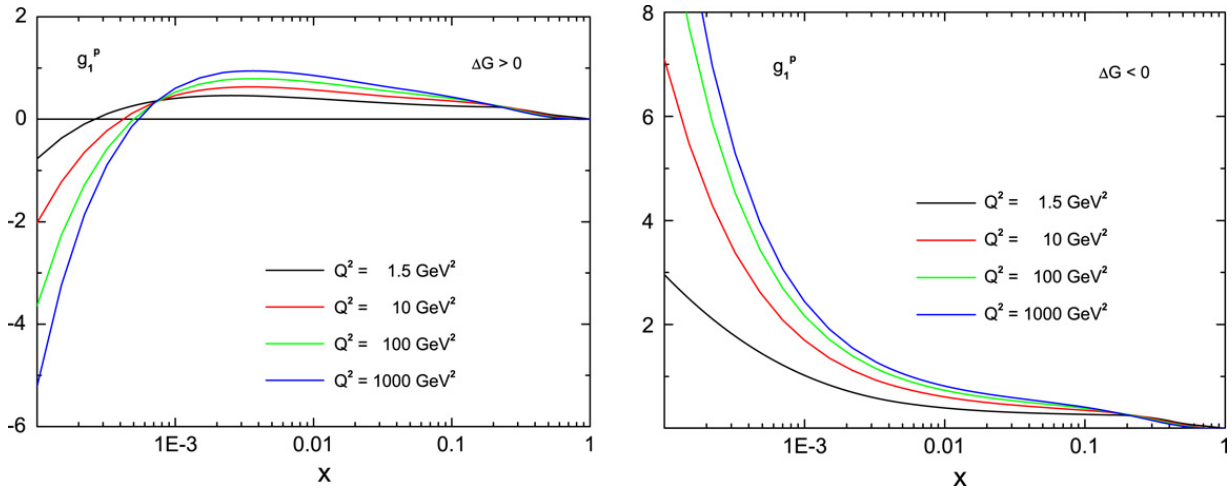
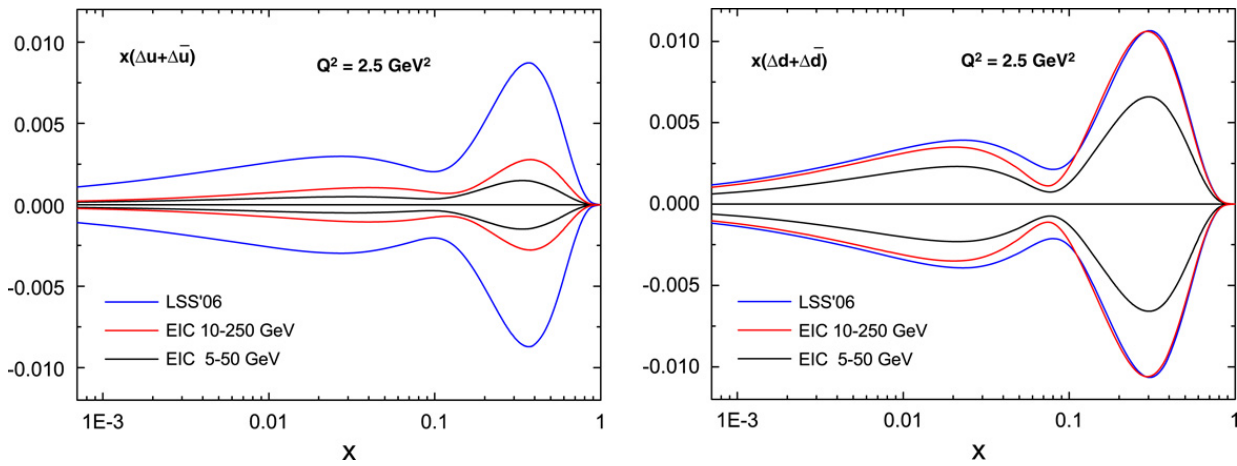**Fig. 44.** $g_1(x, Q^2)$ at various values of Q^2 attainable at EIC for positive and negative ΔG [217].

Fig. 45. Impact of two versions of EIC on the u and d uncertainties [217].
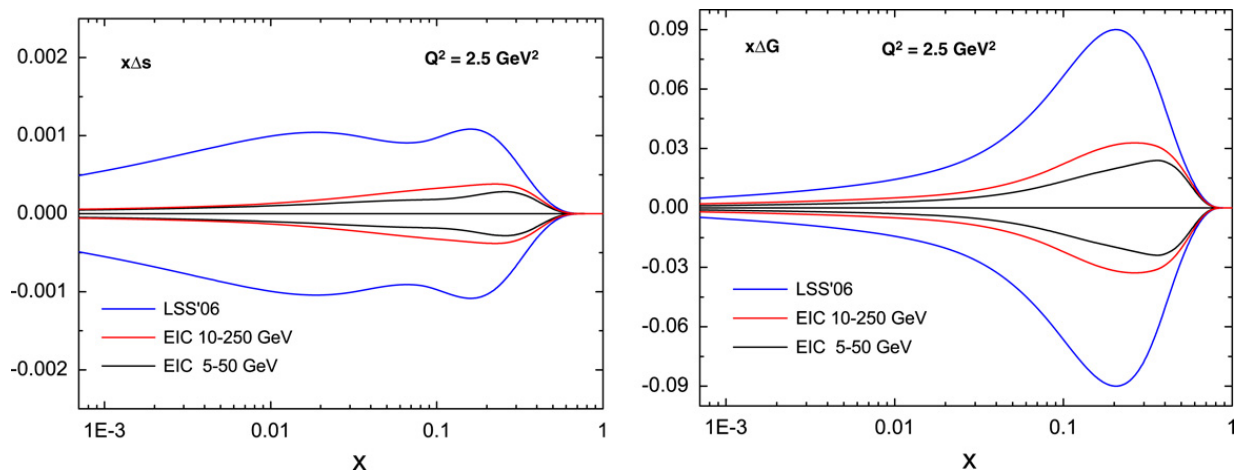

Fig. 46. Impact of two versions of EIC on the s and G uncertainties [217].

extensive program at the energy-upgraded Jefferson Lab will add substantially to this database. Ultimately, an electron–ion collider could map out GPDs in detail at significantly lower x than fixed-target experiments.

In summary, the interest in the nucleon spin structure continues unabated, with many novel experimental and theoretical approaches towards the ultimate understanding of all contributions to the nucleon's spin. An extensive and rich experimental program already lies ahead of us at existing facilities like CERN (COMPASS), RHIC and Jefferson Lab (both

during the remaining years of 6 GeV running and in the new era of 11–12 GeV beams). Ultimately, this field would benefit tremendously from a new collider of both polarized ions and polarized leptons, which is now in the planning stage.

Acknowledgments

References

[1] W.K.H. Panofsky, in: Proc. 14th Intl. Conf. on High Energy Physics, Vienna, p23: Geneva: CERN Information Service, 1968.
[2] J. Ashman, et al., [European Muon Collaboration], Phys. Lett. B 206 (1988) 364.
[3] J.R. Ellis, R.L. Jaffe, Phys. Rev. D 9 (1974) 1444;   Phys. Rev. D 10 (1974) 1669 (erratum).
[4] E. Leader, M. Anselmino, Z. Phys. C 41 (1988) 239.
[5] J.D. Bjorken, Phys. Rev. 179 (1969) 1547.
[6] E.S. Ageev, et al., [COMPASS Collaboration], Phys. Lett. B 633 (2006) 25. Preprint hep-ex/0511028.
[7] E. Leader, A.V. Sidorov, D.B. Stamenov, Phys. Rev. D 73 (2006) 034023. Preprint hep-ph/0512114.
[8] X. Ji, Internat J. Modern Phys. A 18 (2003) 1303.
[9] S. Wandzura, F. Wilczek, Phys. Lett. B 72 (1977) 195.
[10] H. Burkhardt, W.N. Cottingham, Ann. Phys. NY 56 (1970) 453.
[11] A.V. Efremov, O.V. Teryaev, E. Leader, Phys. Rev. D 55 (1997) 4307. Preprint hep-ph/9607217.
[12] M. Anselmino, A. Efremov, E. Leader, Phys. Rep. 261 (1995) 1;
     M. Anselmino, A. Efremov, E. Leader, Phys. Rep. 281 (1997) 399 (erratum). Preprint hep-ph/9501369.
[13] S.D. Bass, Rev. Modern Phys. 77 (2005) 1257. Preprint hep-ph/0411005.
[14] J. Soffer, O.V. Teryaev, Preprint hep-ph/9906455.
[15] X. Artru, M. Elchikh, J.M. Richard, J. Soffer, O.V. Teryaev, Preprint hep-ph/08020164.
[16] P. Hoodbhoy, R.L. Jaffe, A. Manohar, Nuclear. Phys. B 312 (1989) 571.
[17] L.L. Frankfurt, M.I. Strikman, Nucl. Phys. A 405 (1983) 557.
[18] M.J. Alguard, et al., Phys. Rev. Lett. 37 (1976) 1261.
[19] M.J. Alguard, et al., Phys. Rev. Lett. 41 (1978) 70.
[20] G. Baum, et al., Phys. Rev. Lett. 45 (1980) 2000.
[21] G. Baum, et al., Phys. Rev. Lett. 51 (1983) 1135.
[22] J. Ashman, et al., [European Muon Collaboration], Nuclear. Phys. B 328 (1989) 1.
[23] J. Alcorn, et al., Nucl. Instrum. Methods A 522 (2004) 294.
[24] Hall A Status Report - 2007.
[25] B. Adeva, et al., [Spin Muon Collaboration], Phys. Lett. B 302 (1993) 533.
[26] D. Adams, et al., [Spin Muon Collaboration (SMC)], Phys. Lett. B 329 (1994) 399.
[27] B. Adeva, et al., [Spin Muon Collaboration (SMC), Phys. Lett. B 369 (1996) 93.
[28] B. Adeva, et al., [Spin Muon Collaboration, Phys. Rev. D 58 (1998) 112001.
[29] B. Adeva, et al., [Spin Muon Collaboration], Phys. Rev. D 60 (1999) 072004;   Phys. Rev. D 62 (2000) 079902 (erratum).
[30] P.L. Anthony, et al., [E142 Collaboration], Phys. Rev. Lett. 71 (1993) 959.
[31] P.L. Anthony, et al., [E142 Collaboration], Phys. Rev. D 54 (1996) 6620.
[32] K. Abe, et al., [E143 Collaboration], Phys. Rev. Lett. 74 (1995) 346.
[33] K. Abe, et al., [E143 Collaboration], Phys. Rev. Lett. 75 (1995) 25.
[34] K. Abe, et al., [E143 collaboration], Phys. Rev. D 58 (1998) 112003.
[35] P.L. Anthony, et al., [E155 Collaboration], Phys. Lett. B 463 (1999) 339.
[36] P.L. Anthony, et al., [E155 Collaboration], Phys. Lett. B 493 (2000) 19.
[37] K. Abe, et al., [E154 Collaboration, Phys. Rev. Lett. 79 (1997) 26.
[38] K. Abe, et al., [E154 Collaboration], Phys. Lett. B 405 (1997) 180.
[39] K. Abe, et al., [E143 Collaboration], Phys. Rev. Lett. 78 (1997) 815.
[40] K. Abe, et al., [E154 Collaboration], Phys. Lett. B 404 (1997) 377.
[41] P.L. Anthony, et al., [E155 Collaboration], Phys. Lett. B 553 (2003) 18.
[42] K. Ackerstaff, et al., [HERMES Collaboration, Phys. Lett. B 404 (1997) 383.
[43] A. Airapetian, et al., [HERMES Collaboration], Phys. Lett. B 442 (1998) 484.
[44] A. Airapetian, et al., [HERMES Collaboration], Phys. Rev. D 75 (2007) 012007.
[45] A. Airapetian, et al., [HERMES Collaboration], Phys. Rev. D 71 (2005) 012003.
[46] A. Airapetian, et al., [HERMES Collaboration], Phys. Rev. D 75 (2007) 011103. Preprint hep-ex/0605108.
[47] A. Airapetian, et al., [HERMES Collaboration], Phys. Lett. B 648 (2007) 164. Preprint hep-ex/0612059.
[48] A. Airapetian, et al., [HERMES Collaboration], Phys. Rev. Lett. 84 (2000) 2584.
[49] V.Y. Alexakhin, et al., [COMPASS Collaboration], Phys. Lett. B 647 (2007) 8.
[50] E.S. Ageev, et al., [Compass Collaboration], Phys. Lett. B 647 (2007) 330.
[51] M. Alekseev, et al., [COMPASS Collaboration], Phys. Lett. B 660 (2008) 458. Preprint hep-ex/0707.4077.
[52] S.S. Adler, et al., [PHENIX Collaboration], Phys. Rev. D 73 (2006) 091102.
[53] B.I. Abelev, et al., [STAR Collaboration], Phys. Rev. Lett. 97 (2006) 252001.
[54] A. Adare, et al., [PHENIX Collaboration], Phys. Rev. D 76 (2007) 051106. Preprint hep-ex/0704.3599.
[55] B.I. Abelev, et al., [STAR Collaboration], Phys. Rev. Lett. 100 (2008) 232003. Preprint hep-ex/0710.2048.
[56] M. Amarian, et al., [Jefferson Lab E94-010 Collaboration], Phys. Rev. Lett. 89 (2002) 242301. Preprint nucl-ex/0205020.
[57] M. Amarian, et al., [Jefferson Lab E94-010 Collaboration], Phys. Rev. Lett. 92 (2004) 022301.
[58] M. Amarian, et al., [Jefferson Lab E94-010 Collaboration], Phys. Rev. Lett. 93 (2004) 152301.
[59] Z.E. Meziani, et al., Phys. Lett. B 613 (2005) 148. Preprint hep-ph/0404066.
[60] J.P. Chen, A. Deur, Z.E. Meziani, Modern Phys. Lett. A 20 (2005) 2745.
[61] X. Zheng, et al., [Jefferson Lab Hall A Collaboration], Phys. Rev. Lett. 92 (2004) 012004.
[62] X. Zheng, et al., [Jefferson Lab Hall A Collaboration], Phys. Rev. C 70 (2004) 065207.
[63] K. Kramer, et al., [Jefferson Lab E97-103 Collaboration], Phys. Rev. Lett. 95 (2005) 142002.
[64] P. Solvignon, et al., [Jefferson Lab E01-012 Collaboration], Preprint nucl-ex/0803.3845.

[65] JLab E97-110 Collaboration, The GDH Rule and the Spin Structure of ^{3}He and the Neutron Using Nearly Real Photons, J.P. Chen, A. Deur and F. Garibaldi, spokespersons.
[66] J.L. Friar, B.F. Gibson, G.L. Payne, A.M. Bernstein, T.E. Chupp, Phys. Rev. C 42 (1990) 2310.
[67] C. Ciofi degli Atti, S. Scopetta, Phys. Lett. B 404 (1997) 223. Preprint ucl-th/9606034.
[68] F.R.P. Bissey, V.A. Guzey, M. Strikman, A.W. Thomas, Phys. Rev. C 65 (2002) 064317. Preprint hep-ph/0109069.
[69] B.A. Mecking, et al., [CLAS Collaboration], Nucl. Instrum. Methods A 503 (2003) 513.
[70] J. Yun, et al., [CLAS Collaboration], Phys. Rev. C 67 (2003) 055204.
[71] R. Fatemi, et al., [CLAS Collaboration], Phys. Rev. Lett. 91 (2003) 222002.
[72] K.V. Dharmawardane, et al., [CLAS Collaboration], Phys. Lett. B 641 (2006) 11.
[73] P.E. Bosted, et al., [CLAS Collaboration], Phys. Rev. C 75 (2007) 035203.
[74] P.E. Bosted, M.E. Christy, preprint hep-ph/0711.0159.
[75] M.E. Christy, P.B. Bosted, preprint hep-ph/0712.3731.
[76] R. De Vita, et al., [CLAS Collaboration], Phys. Rev. Lett. 88 (2002) 082001;
     R. De Vita, et al., [CLAS Collaboration], Phys. Rev. Lett. 88 (2002) 189903 (erratum). Preprint hep-ex/0111074.
[77] A.S. Biselli, et al., [CLAS Collaboration], Phys. Rev. C 78 (2008) 045204. Preprint nucl-ex/0804.3079.
[78] S. Chen, et al., [CLAS Collaboration], Phys. Rev. Lett. 97 (2006) 072002. Preprint hep-ex/0605012.
[79] P.E. Bosted, H. Avakian (in preparation).
[80] F.R. Wesselmann, et al., [RSS Collaboration], Phys. Rev. Lett. 98 (2007) 132003.
[81] R.P. Feynman, Phys. Rev. Lett. 23 (1969) 1415.
[82] C.G. Callan, D.J. Gross, Phys. Rev. Lett. 21 (1968) 311.
[83] U. D'Alesio, E. Leader, F. Murgia (in preparation).
[84] L.M. Sehgal, Phys. Rev. D 10 (1974) 1663;
     L.M. Sehgal, Phys. Rev. D 11 (1975) 2016 (erratum).
[85] R.D. Young, D.B. Leinweber, A.W. Thomas, S.V. Wright, Nucl. Phys. Proc. Suppl. 109A (2002) 55.
[86] A.W. Thomas, Prog. Part. Nucl. Phys. 61 (2008) 219. Preprint hep-ph/0805.4437.
[87] W. Vogelsang, Phys. Rev. D 54 (1996) 2023. Preprint hep-ph/9512218.
[88] R. Mertig, W.L. van Neerven, Z. Phys. C 70 (1996) 637. Preprint hep-ph/9506451.
[89] R.D. Ball, S. Forte, G. Ridolfi, Phys. Lett. B 378 (1996) 255. Preprint hep-ph/9510449.
[90] R.D. Carlitz, J.C. Collins, A.H. Mueller, Phys. Lett. B 214 (1988) 229.
[91] D. Mueller, O.V. Teryaev, Phys. Rev. D 56 (1997) 2607. Preprint hep-ph/9701413.
[92] H.Y. Cheng, Phys. Lett. B 427 (1998) 371. Preprint hep-ph/9712473.
[93] E. Leader, Camb. Monogr. Part. Phys. Nucl. Phys. Cosmol. 15 (2001) 1.
[94] E. Leader, A.V. Sidorov, D.M. Stamenov, Phys. Lett. B 445 (1998) 232.
[95] S.L. Adler, Phys. Rev. 177 (1969) 2426.
[96] J.S. Bell, R. Jackiw, Nuovo Cimento A 60 (1969) 47.
[97] A.V. Efremov, O.V. Teryaev, JINR Report No. E2-88-287, 1988 (unpublished).
[98] G. Altarelli, G.G. Ross, Phys. Lett. B 212 (1988) 391.
[99] E. Leader, M. Anselmino, Santa Barbara Preprint NSF-ITP-88-142 and Proc. Workshop on Diquarks, Turin, Italy, 1988, World Scientific, 1989, p. 297.
[100] C. Amsler, et al., [Particle Data Group], Phys. Lett. B 667 (2008) 1.
[101] A. Deur, [EG1 Collaboration], private communication; Habilitation à diriger les recherches, PCCFT0802, Université Blaise Pascal, 2008.
[102] A. Airapetian, et al., [HERMES Collaboration], Preprint hep-ex/0803.2993.
[103] F. Robinet, [COMPASS Collaboration], in: Proceedings for DIS2008.
[104] D. de Florian, R. Sassot, M. Stratmann, W. Vogelsang, Preprint hep-ph/0804.0422.
[105] A. Adare, [PHENIX Collaboration], Preprint hep-ex/0810.0694.
[106] M. Sarsour, [STAR Collaboration], in: APS DNP meeting, Newport News, Virginia, October 2007, BAPS.2007.DNP.BB.10; D. Staszak [STAR Collaboration], in: Lake Louise Winter Institute, February 2008, Preprint hep-ex/0805.3004.
[107] B. Jager, A. Schafer, M. Stratmann, W. Vogelsang, Phys. Rev. D 67 (2003) 054005. Preprint hep-ph/0211007.
[108] M. Gluck, E. Reya, M. Stratmann, W. Vogelsang, Phys. Rev. D 63 (2001) 094005. Preprint hep-ph/0011215.
[109] N. Isgur, Phys. Rev. D 59 (1999) 034013. Preprint hep-ph/9809255.
[110] S.J. Brodsky, M. Burkardt, I. Schmidt, Nuclear. Phys. B 441 (1995) 197. Preprint hep-ph/9401328.
[111] F.E. Close, Nuclear. Phys. B 80 (1974) 269.
[112] G.R. Farrar, D.R. Jackson, Phys. Rev. Lett. 35 (1975) 1416.
[113] H. Avakian, S.J. Brodsky, A. Deur, F. Yuan, Phys. Rev. Lett. 99 (2007) 082001. Preprint hep-ph/0705.1553.
[114] E. Leader, A.V. Sidorov, D.B. Stamenov, Eur. Phys. J. C 23 (2002) 479. Preprint hep-ph/0111267.
[115] C. Bourrely, J. Soffer, F. Buccella, Eur. Phys. J. C 23 (2002) 487. Preprint hep-ph/0109160.
[116] F.E. Close, W. Melnitchouk, Phys. Rev. C 68 (2003) 035210. Preprint hep-ph/0302013.
[117] C. Bourrely, E. Leader, O.V. Teryaev, Preprint hep-ph/9803238.
[118] G. Watt, A.D. Martin, W.J. Stirling, R.S. Thorne, Preprint hep-ph/0806.4890.
[119] R.L. Heimann, Nuclear. Phys. B 64 (1973) 429.
[120] S.D. Bass, Modern Phys. Lett. A 22 (2007) 1005. Preprint hep-ph/0606067.
[121] R.D. Ball, S. Forte, G. Ridolfi, Nuclear. Phys. B 444 (1995) 287;   Nuclear. Phys. B 449 (1995) 680 (erratum).
[122] J. Bartels, B.I. Ermolaev, M.G. Ryskin, Z. Phys. C 70 (1996) 273. Preprint hep-ph/9507271.
[123] J. Bartels, B.I. Ermolaev, M.G. Ryskin, Z. Phys. C 70 (1996) 273;   Z. Phys. C 72 (1996) 627.
[124] B.I. Ermolaev, M. Greco, S.I. Troyan, Phys. Lett. B 579 (2004) 321. Preprint hep-ph/0307128.
[125] B. Adeva, et al., [Spin Muon Collaboration], Phys. Rev. D 58 (1998) 112002.
[126] J. Blumlein, A. Vogt, Phys. Lett. B 386 (1996) 350. Preprint hep-ph/9606254.
[127] A.L. Kataev, JETP Lett. 77 (2003) 458 [Pisma Zh. Eksp. Teor. Fiz. 77 (2003) 522]. Preprint hep-ph/0302101.
[128] A. Piccione, G. Ridolfi, Nuclear. Phys. B 513 (1998) 301. Preprint hep-ph/9707478.
[129] A. Accardi, W. Melnitchouk, Phys. Lett. B 670 (2008) 114. Preprint hep-ph/0808.2397.
[130] E. Leader, A.V. Sidorov, D.B. Stamenov, Phys. Rev. D 75 (2007) 074027. Preprint hep-ph/0612360.
[131] E. Leader, A.V. Sidorov, D.M. Stamenov, Phys. Rev. D 58 (1998) 114028.
[132] M. Hirai, S. Kumano, N. Saito, [Asymmetry Analysis Collaboration], Phys. Rev. D 69 (2004) 054021. Preprint hep-ph/0312112.
[133] J. Blümlein, H. Böttcher, Nuclear. Phys. B 636 (2002) 225. Preprint hep-ph/0203155.
[134] M. Hirai, S. Kumano, [Asymmetry Analysis Collaboration], Preprint hep-ph/0808.0413.
[135] http://durpdg.dur.ac.uk/HEPDATA/.
[136] S.I. Alekhin, Preprint hep-ph/0212370. See also S. Alekhin, Phys. Rev. D 68 (2003) 014002, Preprint hep-ph/0211096.
[137] E. Leader, A.V. Sidorov, D.B. Stamenov, Internat J. Modern Phys. A 13 (1998) 5573. Preprint hep-ph/9708335.
[138] E. Leader, D.B. Stamenov, Phys. Rev. D 67 (2003) 037503.
[139] P.G. Ratcliffe, Phys. Rev. D 59 (1999) 014038. Preprint hep-ph/9806381.
[140] A. Airapetian, et al., [HERMES Collaboration], Phys. Rev. Lett. 94 (2005) 012002. Preprint hep-ex/0408013.
[141] E. Leader, A.V. Sidorov, D.B. Stamenov, JHEP 0506 (2005) 033. Preprint hep-ph/0503140.

[142] D. de Florian, R. Sassot, M. Stratmann, Phys. Rev. D 76 (2007) 074033. Preprint hep-ph/0707.1506.
[143] S.D. Bass, Phys. Rev. D 67 (2003) 097502. Preprint hep-ph/0210214.
[144] J. Blümlein, A. Tkabladze, Nuclear. Phys. B 553 (1999) 427. Preprint hep-ph/9812478.
[145] D. Adams, et al., [Spin Muon Collaboration (SMC)], Phys. Lett. B 336 (1994) 125. Preprint hep-ex/9408001.
[146] D. Adams, et al., [Spin Muon Collaboration (SMC), Phys. Lett. B 396 (1997) 338.
[147] M. Stratmann, Z. Phys. C 60 (1993) 763.
[148] X. Song, Phys. Rev. D 54 (1996) 1955. Preprint hep-ph/9604264.
[149] H. Weigel, L.P. Gamberg, Nucl. Phys. A 680 (2000) 48. Preprint hep-ph/0004057.
[150] H. Weigel, Pramana 61 (2003) 921. Preprint hep-ph/0302212.
[151] M. Wakamatsu, Phys. Lett. B 487 (2000) 118. Preprint hep-ph/0006212.
[152] O.F. Filoti, Ph.D. Thesis, Univ. of New Hampshire, 2007.
[153] L.D. van Buuren, et al., Phys. Rev. Lett. 89 (2002) 012001.
[154] X.D. Ji, Phys. Lett. B 309 (1993) 187. Preprint hep-ph/9307303.
[155] X.D. Ji, P. Unrau, Phys. Lett. B 333 (1994) 228. Preprint hep-ph/9308263.
[156] E. Leader, E. Predazzi, Camb. Monogr. Part. Phys. Nucl. Phys. Cosmol. 4 (1996) 1.
[157] J. Blümlein, N. Kochelev, Nuclear. Phys. B 498 (1997) 285. Preprint hep-ph/9612318.
[158] B. Ehrnsperger, A. Schafer, L. Mankiewicz, Phys. Lett. B 323 (1994) 439. Preprint hep-ph/9311285.
[159] J.P. Chen, A. Deur, Z.E. Meziani, Modern Phys. Lett. A 20 (2005) 2745. Preprint nucl-ex/0509007.
[160] S.B. Gerasimov, Sov. J. Nucl. Phys. 2 (1966) 430 [Yad. Fiz. 2 (1966) 598].
[161] S.D. Drell, A.C. Hearn, Phys. Rev. Lett. 16 (1966) 908.
[162] M. Anselmino, B.L. Ioffe, E. Leader, Sov. J. Nucl. Phys. 49 (1989) 136. [Yad. Fiz. 49 (1989) 214].
[163] B.L. Ioffe, V.A. Khoze, L.N. Lipatov, Hard Processes. Vol. 1: Phenomenology, Quark Parton Model, North-Holland, Amsterdam, Netherlands, 1984,
       p. 340.
[164] D. Drechsel, B. Pasquini, M. Vanderhaeghen, Phys. Rep. 378 (2003) 99. Preprint hep-ph/0212124.
[165] N. Bianchi, E. Thomas, Phys. Lett. B 450 (1999) 439. Preprint hep-ph/9902266.
[166] S. Simula, M. Osipenko, G. Ricco, M. Taiuti, Phys. Rev. D 65 (2002) 034017. Preprint hep-ph/0107036.
[167] K. Slifer, et al., [E94010 Collaboration], Phys. Rev. Lett. 101 (2008) 022303. Preprint nucl-ex/0803.2267.
[168] D. Drechsel, O. Hanstein, S.S. Kamalov, L. Tiator, Nucl. Phys. A 645 (1999) 145.
[169] X.D. Ji, W. Melnitchouk, Phys. Rev. D 56 (1997) 1. Preprint hep-ph/9703363.
[170] M. Gockeler, et al., Phys. Rev. D 63 (2001) 074506. Preprint hep-lat/0011091.
[171] X.D. Ji, C.W. Kao, J. Osborne, Phys. Lett. B 472 (2000) 1. Preprint hep-ph/9910256.
[172] D. Drechsel, S.S. Kamalov, L. Tiator, Phys. Rev. D 63 (2001) 114010. Preprint hep-ph/0008306.
[173] JLab E06-014, Precision Measurements of the Neutron d_2: Towards the Electric χ_E and Magnetic χ_B Color Polarizabilities, S. Choi, X. Jiang,
       Z. E. Meziani, B. Sawatzky, spokespersons.
[174] JLab E12-06-121, A Path to 'Color Polarizabilities' in the Neutron: A Precision Measurement of the Neutron g_2 and d_2 at High Q^2 in Hall C, T. Averett,
       Z.E. Meziani, W. Korsch, B. Sawatzky, spokespersons.
[175] JLab E07-003, Spin Asymmetries on the Nucleon Experiment-SANE, S. Choi, Z.E. Meziani and O. Randon, spokespersons.
[176] A. Deur, Preprint nucl-ex/0508022.
[177] M. Osipenko, et al., Phys. Lett. B 609 (2005) 259. Preprint hep-ph/0404195.
[178] M. Osipenko, et al., Phys. Rev. D 71 (2005) 054007. Preprint hep-ph/0503018.
[179] A. Deur, et al., Phys. Rev. Lett. 93 (2004) 212001. Preprint hep-ex/0407007.
[180] A. Deur, et al., Phys. Rev. D 78 (2008) 032001. Preprint nucl-ex/0802.3198.
[181] P. Mergell, U.G. Meissner, D. Drechsel, Nucl. Phys. A 596 (1996) 367. Preprint hep-ph/9506375.
[182] D. Drechsel, L. Tiator, Ann. Rev. Nucl. Part. Sci. 54 (2004) 69. Preprint nucl-th/0406059.
[183] J. Ahrens, et al., [GDH Collaboration], Phys. Rev. Lett. 87 (2001) 022003.
[184] H. Dutz, et al., [GDH Collaboration], Phys. Rev. Lett. 91 (2003) 192001.
[185] H. Dutz, et al., [GDH Collaboration], Phys. Rev. Lett. 94 (2005) 162001.
[186] S. Hoblit, et al., [LSC Collaboration], Preprint hep-ex/0808.2183.
[187] K. Helbing, Prog. Part. Nucl. Phys. 57 (2006) 405. Preprint nucl-ex/0603021.
[188] X.D. Ji, J. Osborne, J. Phys. G 27 (2001) 127. Preprint hep-ph/9905410.
[189] V. Bernard, T.R. Hemmert, U.G. Meissner, Phys. Rev. D 67 (2003) 076008. Preprint hep-ph/0212033.
[190] A. Airapetian, et al., [HERMES Collaboration], Eur. Phys. J. C 26 (2003) 527. Preprint hep-ex/0210047.
[191] C. Ciofi degli Atti, E. Pace, G. Salme, Phys. Rev. C 51 (1995) 1108. Preprint nucl-th/9411006.
[192] Y. Prok, et al., [CLAS Collaboration], Preprint nucl-ex/0802.2232.
[193] J. Soffer, O. Teryaev, Phys. Rev. D 70 (2004) 116004. Preprint hep-ph/0410228.
[194] V.D. Burkert, B.L. Ioffe, Phys. Lett. B 296 (1992) 223.
[195] V.D. Burkert, Phys. Rev. D 63 (2001) 097904. Preprint nucl-th/0004001.
[196] A. Deur, V. Burkert, J.P. Chen, W. Korsch, Phys. Lett. B 665 (2008) 349. Preprint hep-ph/0803.4119.
[197] A. Deur, V. Burkert, J.P. Chen, W. Korsch, Phys. Lett. B 650 (2007) 244. Preprint hep-ph/0509113.
[198] S.J. Brodsky, G.F. de Teramond, Phys. Rev. Lett. 96 (2006) 201601. Preprint hep-ph/0602252.
[199] C.W. Kao, T. Spitzenberg, M. Vanderhaeghen, Phys. Rev. D 67 (2003) 016001. Preprint hep-ph/0209241.
[200] JLab E03-006, The GDH Sum Rule with nearly real photons and the proton g_1 structure function at low momentum transfer, M. Battaglieri, A. Deur,
       R. De Vita, M. Ripani, spokespersons.
[201] JLab E08-027, A Measurement of g_2^p and the Longitudinal–Transverse Spin Polarizability, J.P. Chen, A. Camsonne, K. Slifer, spokespersons.
[202] W. Melnitchouk, R. Ent, C. Keppel, Phys. Rep. 406 (2005) 127. Preprint hep-ph/0501217.
[203] E.D. Bloom, F.J. Gilman, Phys. Rev. Lett. 25 (1970) 1140.
[204] I. Niculescu, et al., Phys. Rev. Lett. 85 (2000) 1186.
[205] O. Nachtmann, Nuclear. Phys. B 63 (1973) 237.
[206] A. De Rujula, H. Georgi, H.D. Politzer, Phys. Lett. B 64 (1977) 428.
[207] A. Airapetian, et al., [HERMES Collaboration], Phys. Rev. Lett. 90 (2003) 092002. Preprint hep-ex/0209018.
[208] F. Myhrer, A.W. Thomas, Phys. Lett. B 663 (2008) 302. Preprint hep-ph/0709.4067.
[209] JLab E12-06-109, The Longitudinal spin Structure of the Nucleon, D. Crabb, A. Deur, K. Dharmawardane, T. Forest, K. Griffioen, M. Holtrop, S. Kuhn,
       Y. Prok, spokespersons.
[210] JLab E12-06-110, Measurement of Neutron Spin Asymmetry A_1^n in the Valence Quark Region Using an 11 GeV Beam and a Polarized ^{3}He Target in
       Hall C, G. Cates, J.P. Chen, Z.E. Meziani, X. Zheng, spokespersons.
[211] JLab E12-06-122, A measurement of neutron asymmetry A_1^n in the valence quark region using 8.8 GeV and 6.6 GeV beam energies and Bigbite
       spectrometer in Hall A, G. Cates, N. Liyanaga, Z.E. Meziani, G. Rosner, B. Wojtsekhowski, X. Zheng, spokespersons.
[212] JLab E-05-113, Semi-Inclusive Pion Production with a Longitudinally Polarized Target at 6 GeV, H. Avakian, P. Bosted, D. Crabb, K. Griffioen,
       spokespersons.
[213] JLab E07-011, A High Precision Measurement of the Deuteron Spin-Structure Function g_1^d/F_1^d, P. Bosted, F.R. Wesselmann, X. Jiang, spokespersons.
[214] B. Seitz, [PANDA Collaboration], Using anti-protons to measure nucleon structure: Prospects at PANDA, in: Prepared for 15th International Workshop
       on Deep-Inelastic Scattering and Related Subjects, DIS2007, Munich, Germany, 16–20 Apr., 2007.
[215] C.A. Aidala, [EIC Collaboration], Peering Into Hadronic Matter: The Electron–Ion Collider. Preprint nucl-ex/0806.4933.
[216] JLab E08-015, Transverse spin effects in SIDIS at 6 GeV with transversely polarized target using the CLAS Detector, H. Avakian, P. Bosted, K. Hafidi,
       N. Makins, P. Rossi, spokespersons.
[217] E. Leader, A.V. Sidorov, D.B. Stamenov (unpublished).
[218] X.D. Ji, Phys. Rev. Lett. 78 (1997) 610. Preprint hep-ph/9603249.
[219] M. Mazouz, et al., [Jefferson Lab Hall A Collaboration], Phys. Rev. Lett. 99 (2007) 242501. Preprint nucl-ex/0709.0450.